PRACA DOKTORSKA

Joanna Zapała

Structural study of self-assembled monolayers and thin layers of semi-conducting organic molecules

Ph.D. dissertation written under the supervision of
Dr hab. Robert Nowakowski, Assoc. Prof. (IChF PAN)
Dr hab. David Djurado (CNRS - CEA)

The presented dissertation was prepared within
the International Ph.D. Studies in Chemistry at the
Institute of Physical Chemistry of the Polish Academy of Sciences

Institute of Physical Chemistry
Polish Academy of Sciences
ul. Kasprzaka 44/52, 01-224 Warszawa

Commissariat à l'énergie atomique
et aux énergies alternatives
17 Rue des Martyrs, Grenoble, France

Warszawa, December 2015

Acknowledgments

Above all, I would like to thank my supervisor prof. Robert Nowakowski for his supervision, patience, imparted knowledge, and enthusiasm for scientific work. We can all hope for to eventually gain such a great knowledge in our fields.

I would like to especially thank dr David Djurado for introducing me to the mysteries of the X-ray measurements and for his invaluable guidance and support during one and a half year research work in wonderful Grenoble.

Thank you both for your trust and for choosing me for this project. It was the best time of my life.

I would like to thank all my former and current colleagues in the AFM/STM group for their help and friendliness: dr Agnieszka Maranda-Niedbała, Klaudyna Leniarska, Tomek Jaroch and dr Marek Knor. Thank you for providing the best work environment a person can hope for.

I would like to acknowledge prof. Adam Proń, prof. Małgorzata Zagórska, Renata Rybakiewicz and Kamil Kotwica from Warsaw University of technology for synthesis of studied material and for interesting scientific discussions throughout my PhD studies.

I would like to thank my mother, stepfather, grandparents and Marek Purzycki for their understanding, serenity and never ending emotional support, especially during my long-lasting stay far from home.

Financial support for this work was provided by the International PhD Projects Programme of the Foundation for Polish Science, co-financed from the European Regional Development Fund within the innovative Economy Operational Programme "Grants for Innovation".

Abbreviation	Meaning
A	acceptor
D	donor
DAD	donor-acceptor-donor
FWHM	full width at half maxima
HMDS	hexamethyldisilizane
HMWSC	high molecular weight semiconductors
HOMO	highest occupied molecular orbital
HOPG	highly oriented pyrolytic graphite
LMWSC	low molecular weight semiconductors
LUMO	lowest unoccupied molecular orbital
NDI	naphthalenebisimide
OFET	organic field-effect transistor
OLED	organic light emmiting diode
OTS	octadecyltrichlorosilane
P3AT	poly-3-alkylothiophene
PNDI	poly-naphthalenediimide
PTCDI	perylenetetracarboxilicdiimide
PTFE	poly(tetrafluoroethylene)
STM	scanning tunneling microscopy/microscope
TCB	1,3,5-trichlorobenzene
XRD	X-ray diffraction

Table of contents

1. Literature review 1

1.1. Introduction 1
1.1.1. Electronic world 1
1.1.2. History and future 1
1.2. Organic semiconductors 3
1.2.1. Division 3
1.2.2. Design 3
1.2.3. Tuning of electronic structure 4
1.3. Electrical conductivity of thin organic layers 8
1.3.1. Anisotropy of charge transport 8
1.3.2. Factors influencing charge transport in organic films 9
1.3.2.1. Molecular structure 9
1.3.2.2. Polymorphism 13
1.3.2.3. Molecular orientation at the interface and in the bulk 14
1.3.2.4. Spatial distribution of electron density in the molecule 18

2. Research goals 21

3. Experimental part 24

3.1. Investigated molecules 24
3.1.1. Arylene bisimides based DAD semiconductors 25
3.1.1.1. Names and chemical formulas 25
3.1.1.2. General information 25
3.1.2. Thiophene based DAD semiconductors 27
3.1.2.1. Names and chemical formulas 27
3.1.2.2. General information 27
3.2. Layers preparation 29
3.2.1. Monolayers preparation 29
3.2.2. Thin films preparation 29
3.2.3. Single crystals preparation 30
3.2.4. Powders preparation 30
3.3. Layers characterization methods 31
3.3.1. X-ray diffraction 31
3.3.1.1. Method description 31
3.3.1.2. Apparatus used and modes of measurements 33

3.3.2.STM 35
3.3.2.1. Method description 35
3.3.2.2. Apparatus used and modes of measurements 38

4. Results **39**

4.1. Arylene bisimides 39
4.1.1.Influence of the type of the conjugated unit 39
4.1.2.Influence of the molecular symmetry 54
4.1.3.Influence of the alkoxy chain length 60
4.2. Thiadiazole derivatives 72
4.2.1.The influence of the position of the substituent – XRD studies 72
4.2.1.1. Linear **T1** molecule 73
4.2.1.2. Linear **T4** molecule (chains in α position) 76
4.2.1.3. Non-linear **T2** molecule (chains in outer β position (C4)) 78
4.2.1.4. Non-linear **T5** molecule 79
4.2.1.5. Non-linear **T3** molecule (chains in inner β position (C2)) 81
4.2.2.The influence of the position of the substituent – STM studies 89
4.2.2.1. Non-linear **T2** molecule (chains in outer β position (C4)) 90
4.2.2.2. Non-linear **T3** molecule (chains in inner β position (C2)) 95
4.2.3.Effect of the central acceptor unit 101
4.2.4.Effect of the alkyl chain length 106

5. Conclusions **116**

6. References **123**

1. Literature review

1.1. Introduction

1.1.1. Electronic world

The number of electronic devices grows every year. According to the data from 2012,[1] an estimated number of 30-40 silicon based processors per person on average are used in the world. Healthcare, national security and economy are all unquestionably dependent on electronic technology and in many others areas of live electronic replacements of almost every possible objects used daily can be found. Still, electronic market is not yet saturated and new assignments and applications have been noted every year. The important and new direction in this field is organic electronics. Compared to traditional inorganic electronics, the benefits of electronic devices made from electroactive organic molecules are their low weight, easier processibility, flexibility and low cost. This makes organic electronic devices a desirable alternative in many actual applications. Also electroactive molecules in "soft electronics" create possibility of new applications that would be impossible using copper or silicon, for example in: skin-replacement, e-fibres and clothes, and in many others devices which have to be stretched, bent or adapted to surfaces of specific geometry.

1.1.2. History and future

It is therefore not surprising, that scientific interest in organic semiconductors can be traced back to the 50s of the past century.[2] However, evident and fast progress in the field has started from 1977, when Shirakawa, MacDiarmid, Heeger, et al. revealed[3] that doping of polyacetylene with halogens increases its electrical conductivity by 9 orders of magnitude to the level ~ 10^5 Sm^{-1} (i.e. close to conductivity of copper and silver ~ 10^8 Sm^{-1}). Authors were awarded The Nobel Prize in Chemistry in 2000 for discovery "*that plastic can, after certain modifications, be made electrically conductive"*.[4]

This milestone has initiated great interest in synthesis, physicochemical characterization and applications of organic semiconductors. It can be illustrated by tens of thousands scientific papers, including many full books and reviews that already have been published on various aspects of their chemistry, physics and electronics properties; describing (inter alia) their synthesis[5], architecture[6-8], functioning of devices[9] or applications in sensing[10]. As verified by the "Web of Science" citation reports, the number of papers following "organic semiconductors" topic published yearly is increasing incessantly (doubling every five years) from the beginning of the 21st century. The progress in this field is evident. Electroactive macromolecules developed in the 1980s were characterized by charge carriers mobility of 10^{-6} $cm^2V^{-1}s^{-1}$, whereas the materials actually used in optoelectronic devices exhibit mobilities around 1 $cm^2V^{-1}s^{-1}$ or higher (for example: 10^{-4} – 0.1 $cm^2V^{-1}s^{-1}$ for alkyl derivatives of terthiophene,[11-19] 2.7 $cm^2V^{-1}s^{-1}$ or higher for pentacene,[20-21] and ultra-high mobility of 43 $cm^2V^{-1}s^{-1}$ for 2,7-dioctyl[1]benzothieno[3,2-b][1]benzothiophene)[22]. Nowadays, the researches in the field are mainly focused on optoelectronic properties of organic semiconductors and four types of applications, in: transistors,[23] solar cells, displays[24-25] and lighting[26]. However, some other properties of these molecules are also a subject of interests and scientific investigations, including: electrochromism,[27] sensing,[28] anticorrosion,[29-30] as well as catalytic properties[31].

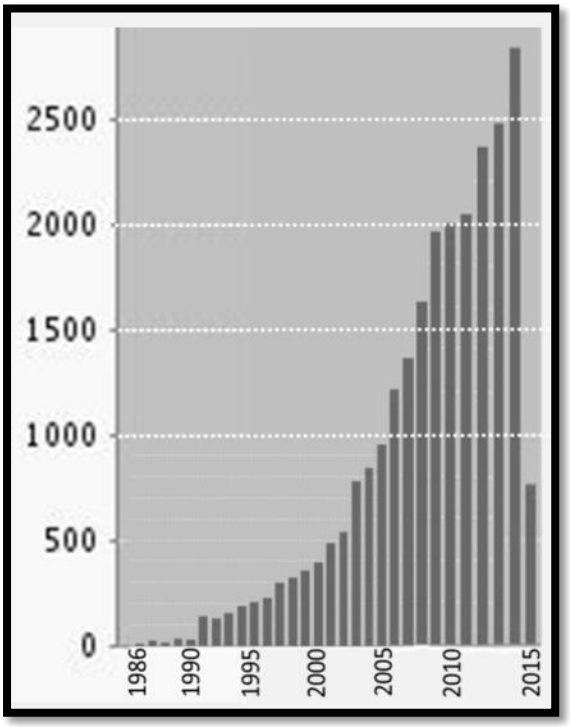

Figure 1.1.2.1 Web of science citation report of the number of papers published yearly following "organic semiconductor" topic (for day 01.05.2015).

1.2. Organic semiconductors

1.2.1. Division

In the simplest diversification, depending on molecular mass, two types of organic semiconductors can be distinguished: low and high molecular weight semiconductors (LMWSC and HMWSC, respectively). In the second case we are dealing with polymers – usually long chains which compose of many repeated subunits (mers). Some of LMWSC are shorter analogues (oligomers) of the corresponding semiconducting polymers. In general LMWSC are better defined than HMWSC since they are monodisperse. This is an important advantage of LMWSC leading to their easier and more straightforward processability in comparison to longer polymers. At this point it is important to remind that organic semiconductors are typically used in optoelectronic devices in the form of thin layers. The solution processability is therefore a crucial property of the molecule which determine its usefulness in organic electronics. For non-soluble compounds high-temperature or vacuum sublimation is usually required for fabrication of electronic devices. These techniques are no less sophisticated than photolithographic patterning involved in conventional silicon technology. Hence, keeping in mind the aim to create cheap, simple, and large electronic devices, the solution processability of electro-active materials is an important advantage of organic electronics. Basing on control solvent evaporation (dropcasting, spincoating, zonecasting or inkjet printing) it enables production of active layers over large areas by relatively easy and reproducible way.

1.2.2. Design

All organic semiconductors irrespective of their type are composed of chains of atoms linked by sigma bonds, with delocalized π-electron system which is considered to be "*conditio sine qua non"* of plastic conductivity. Nevertheless, the progress in LMWSC synthetic strategies enables synthesis of organic semiconductors of complex and sophisticated molecular structures designed to answer scientists specific needs. Using a strategy called "building block approach" new electro-active molecules can be fabricated by chemical assembly of different parts of classical semiconductors (molecular conjugated cores as well as terminal substituents). According this approach (see **Figure 1.2.1**) a base

semiconductor (central unit CU) is chemically bonded with one or more so called "intervening" units (IU) in order to modify electron density of the molecule. Then additional terminal units (TU), usually alkyl or alkoxy chains, are attached to molecular sides in the following step to improve solubility and, what goes with it, processability of the synthesized semiconductor. It is worth to emphasize, that terminal substituents, due to strong tendency for mutual interaction and interdigitation, also facilitate the formation of organized supramolecular structures in 2D monolayers as well as in 3D systems (crystals, thin layers and powders). Therefore, this procedure enables, as a final result, creation of new LMWSC of desired electronic and electrical properties (for example: energy levels and spatial distributions of HOMO and LUMO, type of conductivity etc.) and also required supramolecular abilities.

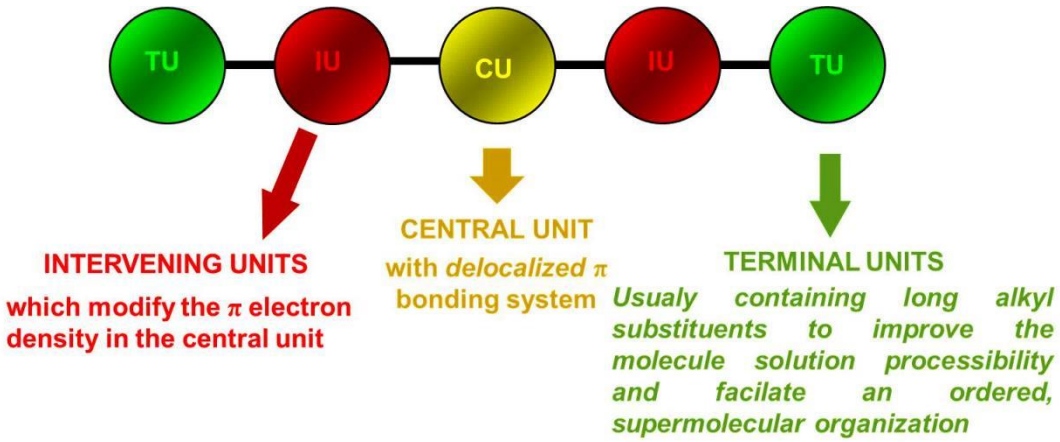

Figure 1.2.2.1 Model of LMWSC design.

1.2.3. Tuning of electronic structure

The next crucial parameters of organic semiconductors are their electronic properties which determine mechanism of conductivity. In general, electrical conductivity can be achieved among molecules by charge transport of holes (p-type semiconductors) or electrons (n-type). In practice charge transport depends on internal electronic structure of the molecule (for example: energy gap between HOMO and LUMO levels) as well as on its supramolecular abilities. The influence of the second factor is related to supramolecular organization in applied organic layers which frequently limits charge transport between one molecule to another.

From electronic point of view p-type semiconductors must be characterized by good injection and transport of hole carriers, while n-type semiconductors should enable the same properties for electrons. At this point it is important to emphasize that numbers of n-type organic semiconductors which can be practically useful for the preparation of n-channel transistors is much lower (fullerenes and arylenebisimides) in comparison to p-type analogs (for example: thiophene based molecules, tetrathiafulvalenes, pentacene based molecules, phthalocyanines, octaethylporphyrines). However, as n-type semiconductors can be theoretically synthesized by chemical modification of p-type molecules, the final effect of practical importance is a complex matter. There are at least two reasons of this situation. Firstly, n-type semiconductors contain polar groups which create problem with their solution processability. Secondly, these semiconductors are usually less stable when operating in ambient conditions since they are more sensitive to electron trapping by oxygen or water. This effect has been carefully investigated by several authors.[32-34] Using simplified approach it can be explained using band scheme presented in **Figure 1.2.3.1**.

The efficiency of charge carriers injection (holes or electrons) to electroactive layer depends on energy position of HOMO and LUMO of the molecule and energies of Fermi levels of both electrodes. The holes are injected to HOMO whereas the electrons to LUMO. Both processes are therefore modulated by energy barriers which are formed at the interfaces between active layer and electrodes (marked in the scheme by ΔEh and ΔEe).

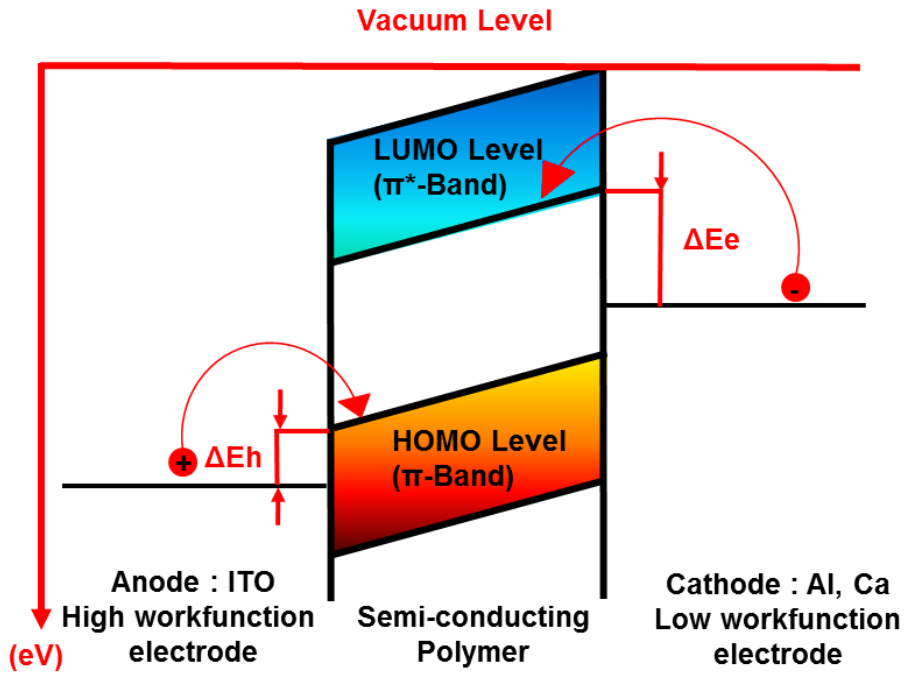

Figure 1.2.3.1
Band diagram.[35]

"Building block approach" enables to modify classical p-type semiconductor to obtain n-type derivative by introduction of side or peripheral electron withdrawing groups. This functionalization lowers LUMO level of the modified molecule and as a consequence decreases barrier for injection of electrons. However, crucial point concerns the position of HOMO which, at the same time, should not decrease since it keeps barrier for holes. In another words, it protects electrons from being trapped by oxygen and water. The appropriate functionalization of electronic levels is therefore a delicate matter which should lead to selectively performed decrease of barrier only for electron injection.

LUMO level might be tuned either by linear extension of molecular conjugated core or by the introduction of side or peripheral electron-withdrawing substituent into conjugated backbone of the molecule. It is known that cyano-, carbonyl- and the other middle-strength acceptor-like substituents affect (decrease) LUMO level in great manner, slightly influencing HOMO level. By contrast, usage of strong electron withdrawing groups can affect directly σ orbitals and lower electron density within whole conjugated core. By consequence, π-orbitals are less effectively screened which can lead to lowering of both HOMO and LUMO levels in comparable manner.

Let me recall a few examples of such modifications. Fluorine is the most electronegative element. Therefore, is no surprise that it is frequently used for tuning purpose. It is worth to emphasize that it does not only lower LUMO level but also was proved to additionally facilitate more dense packing of molecules (for example in perylene[36] and naphthalene[37-38] derivatives). The indirect important consequence of this change in supramolecular organization is better stability of the functionalized semiconductor. This is explained by the fact that fluorocarbons provide additional kinetic barrier for the diffusion of oxygen and moisture.

Other examples of widely used electron withdrawing groups are –CN, –Cl, –CF3 and heteroatoms of N, S. All these compounds lower LUMO level and have smaller impact on HOMO position. These modifications may give interesting effect, that base compounds which normally work as p-type semiconductor can be converted into n-type ones. Examples of such molecules are described by Ando et al. (thiazole derivative with trifluoromethylphenyl substituents)[39] and Yoon et al. (diperfluorohexyl functionalized quaterthiophene).[40] Both molecules exhibit n-type conductivity with good electron mobility of 1.83 $cm^2V^{-1}s^{-1}$ and 0.6 $cm^2V^{-1}s^{-1}$, respectively.

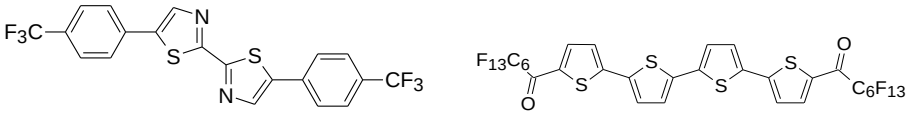

(a) **(b)**

Figure 1.2.3.2 N-type semiconductors prepared by chemical modification of typical p-type semiconductors synthesized by: **a)** Ando et al.,[39] **b)** Yoon et. al.[40]

"Building block approach" additionally creates new scope of synthesis of organic semiconductors exhibiting ambipolar behavior. Actually, this is a very attractive and novel material and subject of an extensive worldwide research effort. This interest is evidently confirmed by growing number of papers published yearly during last few years (**Figure 1.2.3.3**).

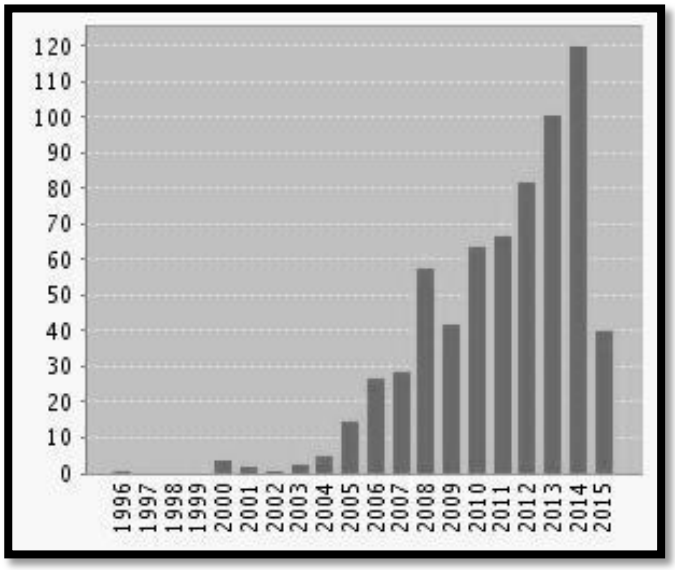

Figure 1.2.3.3 Web of science citation report of the number of papers published yearly following "ambipolar organic semiconductor" topic (for day 01.05.2015).

Molecules of this kind are either p- and n- type semiconductors depending on the operating conditions. This means that synthesis procedure should simultaneously tune both HOMO and LUMO levels in order to enable injection and good transport of both charge carriers (holes and electrons). Such effect can be obtained by coupling in a fixed stoichiometric ratio (often 1:1 or 2:1) of electron abundant and electron deficient chemical units (being electron-donor and electron-acceptor segments of the molecule). The very good base for functionalization are aromatic bisimides with naphthalene or perylene backbones since they exhibit n-type conductivity and combine several advantages like good charge carrier mobility, as well as chemical and thermal stability. According to various experts LUMO level of semiconductors appropriate for ambipolar transistors should be located below

-3.9 eV with respect to vacuum level, while HOMO slightly lower than -5.0 eV.[41-44] However, it should be yet again reminded that ambipolar behavior is a result of delicate balance between two different channels of conductivity and a final effect is a complicated matter which includes additional factors, like: mutual arrangement of electron-donor and electron acceptor segments in the molecule (leading to spatial separation or overlap of HOMO and LUMO) as well as supramolecular organization.

1.3. Electrical conductivity of thin organic layers

1.3.1. Anisotropy of charge transport

Electronic and optoelectronic properties of organic semiconductors are main factors which determine electrical conductivity of active layers in organic electronics devices. These properties can be broadly tuned by chemical modification of molecular structure of semiconductors used. This is a big advantage of organic electronics in comparison to traditional silicon technology. However, the another factor which seriously influences the final properties of organic electronic devices (including charge transport, etc.) is supramolecular organization of active material. Let me remind, that contrary to metals, the movement of charge carriers in organic molecules is strongly anisotropic, with preferential direction determined by their supramolecular organization. This can be, for example, long axis of a π-conjugated polymer chain or direction of π-stacking of aromatic low-molecular weight semiconductors. In both situations the effective mobility in the active layer is limited by the weakest point in conduction path which is a hoping of charge carriers between molecules. For example: the effective charge carrier mobility of several $cm^2V^{-1}s^{-1}$ can be obtained in the layer of well-ordered molecules when mobility inside molecular chain is two orders of magnitude higher (few hundreds $cm^2V^{-1}s^{-1}$).[45-46]

What is more, local areas of molecular disorder are another weak point lowering the mobility of charge carriers. The fundamental question in achieving good conductivity of the layer is therefore linked to supramolecular organization. The strategy is therefore to use optimally ordered layer whose structure minimizes negative effect of molecular disordering and determines good contact between sides of neighboring molecules.

In the next paragraph several selected literature examples showing different ways the supramolecular organization influences effective charge transport in organic layers are discussed.

1.3.2. Factors influencing charge transport in organic films

1.3.2.1. Molecular structure

This parameter is especially important for HMWSC as the charge transport can be influenced by various factors of their macromolecular structure e.g: regioregularity, molecular mass and polidispersity.

The importance of regioregularity has been demonstrated by Haihua Xu et al. who comparatively investigated two donor-acceptor conjugated copolymers, with either alternatively or randomly arranged D and A moieties (see **Figure 1.3.2.1.1**).[47] The polymer with well-reproduced D-A arrangement gave rise to a relatively high degree of crystallinity, resulting in a good charge-transport. Conversely, the polymer of randomly arranged D-A structure generated short-range ordered aggregates surrounded by amorphous regions leading, as a consequence, to much worse (ten times poorer) charge carrier mobility in the fabricated transistors.

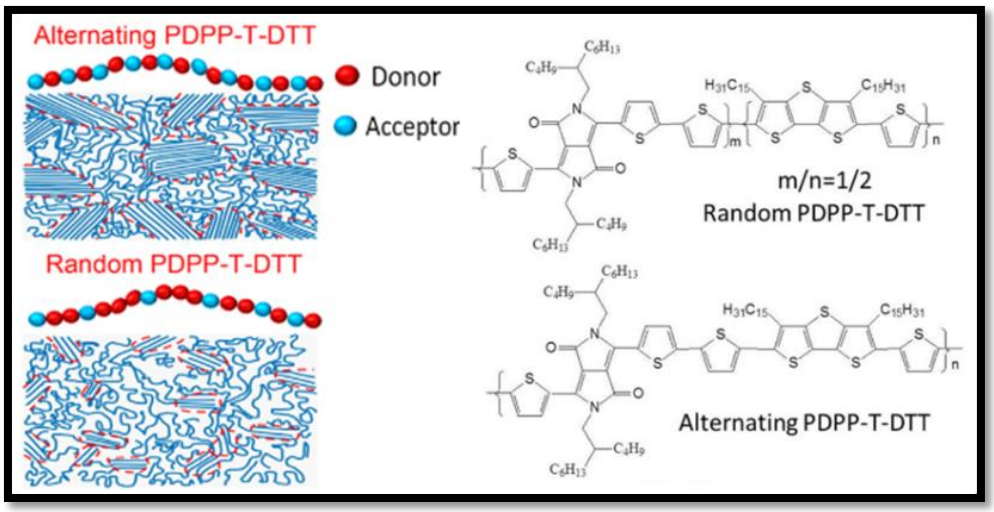

Figure 1.3.2.1.1 Molecular structures and proposed microstructures of thin films of alternating and random PDPP-T-DTT copolymers.[47]

Following this chain of thought, regioregular head-to tail poly-3-alkylothiophene (P3AT) are widely known to have considerably higher neutral and doping conductivities in transistors than those of regiorandom P3AT. The common explanation of this difference is in fact that worse molecular organization leading to larger disorder reduces the effective delocalization length.[48] The analogous effect is also observed in solar cells. The efficiencies of cells with regiorandom P3HT (of molecular weight ~11,000 g/mol) are much smaller (only 4%) than those obtained for cells with highly regioregular P3HT.[49] This huge difference is explained again by structural properties of the films due to stronger tendency of regioregular polymer to self-organize.

Kline et al investigated influence of molecular weight on charge-carrier mobility in thin layers of regioregular P3HT. [13-14] It was proved that molecular weight (polymer length) causes changes in the way of molecular packing. The combination of this effect with different contribution of disordered domains, which average area and boundaries are also changed with molecular weight, cause differences in charge carrier mobility in thin layer by at least four orders of magnitude.

Direct consequence of the molecular weight influence on supramolecular organization and charge carrier mobility is important role of polydispersity. This is important relation since in majority of cases HMWSC materials used in practice for optoelectronic devices are usually separated from post-reaction mixture by solvent extraction and are not strictly monodisperse. They consist of polymers (oligomers) of some range of molecular mass determined by the solvent used.

Jaroch et al. investigated effect of the chain length on the type and extent of the 2D supramolecular organization in oligomers of 4,4”-dioctyl-terthiophene.[19] STM investigations of the monolayers deposited on HOPG from polydispersed and corresponding series of monodispersed fractions confirmed that polydispersity can be considered as a key factor seriously limiting supramolecular ordering. It has been demonstrated that shorter molecules (consisting of 6 - 9 thiophene units) form well-defined two-dimensional islands, while the interactions between longer molecules (12 - 15 thiophene units) become strongly anisotropic. For higher molecular mass fractions, the supramolecular organization is one-dimensional and consists of more or less separated columns of ordered macromolecules. As a consequence of this evolution the polydispersed fractions show much less ordered organization because of the incompatibility of the supramolecular structures of molecules of different molecular masses. This example is a

strong argument that layers of well-ordered molecules can only be obtained by the deposition of very homogeneous and monodispersed material.

An interesting example of competition between effects of molecular electronic structure (LUMO level) and supramolecular organization on effective charge carrier mobility in thin films was presented by Durban et al.[50] Authors investigated a series of three naphthalenebisimide – thiophene copolymers (presented in **Figure 1.3.2.1.2**). The only difference in molecular structure between these macromolecules concerned the size of thiophene segment (thiophene, bithiophene or terthiophene). The consequence of structural dissimilarities were differences in molecular electronic properties. With increasing number of thiophene units, both, the ionization potential and electron affinity decreased which indicated raise of HOMO and LUMO levels. LUMO level was located at -3.85eV, -3.79eV and -3.76eV for **PNDI-1Th, PNDI-2Th** and **PNDI-3Ph,** respectively. Taking into account only this relation one can conclude that polymer containing one thiophene unit were supposed to be the best candidate for the application in n-channel FETs. In reality, the opposite relation was observed. The best performance was found for transistor with **PNDI-3Ph** (tenfold better than with **PNDI-1Ph** and a bit better than with **PNDI-2Ph**). Additional measurements performed by XRD showed different 3D supramolecular organization of these polymers. Ordering was found to improve significantly with increasing length of the thiophene segment. Supramolecular order, not electronic properties of individual molecule was a main factor determining the device performance in this polymer system.

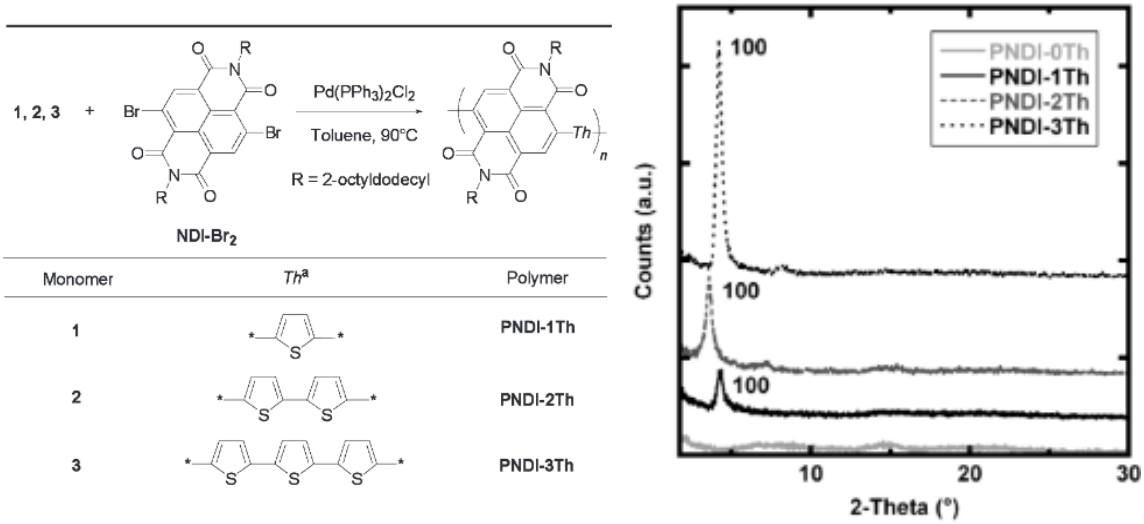

Figure 1.3.2.1.2 Chemical structures and X-ray diffraction profiles of thin films of copolymers studied by Duban et al.[50]

The same, dominant role of supramolecular organization was also observed in many systems of low molecular weight semiconductors. Various researchers reported mobility change (directly caused by the change of organization) with the substituent choice (among others, naphthalene[37-38] or perylene[51] bisimides and thiophene derivatives[51-56]). For example, Surin et al.[57] investigated conductivity of thin films of two semiconductors of donor-acceptor type mutually differing only by sequence of building blocks (**Figure 1.3.2.1.3**).

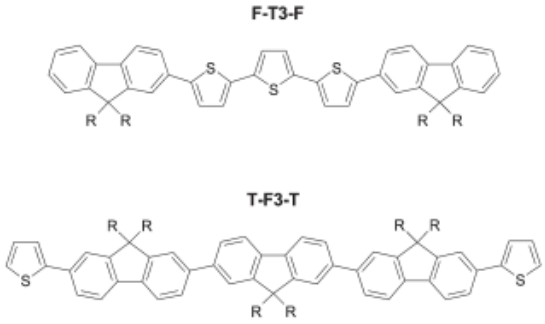

Figure 1.3.2.1.3
Chemical structures of F-T3-F and T-F3-T molecules synthesized by Surin et al.[57]

The obtained results indicated that molecule of A-DDD-A (T-F3-T) sequence was an insulator, while D-AAA-D (F-T3-F) was a good n-type semiconductor. Authors concluded that a main factor of this difference was related to supramolecular organization. The presence of alkyl chains in the central part of T-F3-T molecule was postulated to be a reason of weaker interactions between π systems of adjacent molecules in the layer resulting in microscopic scale in much worse electrical conductivity. The similar example of negative role of alkyl segments in not- optimal position was presented by Shuai et al.[58] In this research, conductivity of thin layers of different dithienonaphthothiadiazole derivatives, with and without alkyl substituents, was investigated. Non-substituted compound was organized into quasi-herringbone supramolecular structure exhibiting electrically attractive ambipolar behavior. Contrary to that, the layers of alkylated compounds were found to be insulating. Authors linked this difference to negative influence of alkyl chains being in bad position. They lead to increase of intermolecular separation in the layer lowering efficiency of the charge carriers transport.

In the view of those examples, it is important to emphasize that alkyl or alkoxy substituents play important role in initiation and control of molecular organization. However, their influence is frequently very sensitive and both the substituents position and their length are important factors which have to be optimized to obtain required effect.

1.3.2.2. Polymorphism

The next molecular feature frequently observed for organic semiconductors is polymorphism. This means that supramolecular organizations of these molecules in monolayer and three dimensional systems (thin layers, crystals and powders) are different. Direct consequence of polymorphism is dependence of supramolecular organization on one or several additional factors, like: substrate topology, thickness of the layer or method and conditions of the sample preparation. And once again, mobility change (directly caused by the change of supramolecular organization) are reported with connection to: thermal annealing (perylene[59,51] and thiophene[39] derivatives), substrate modification (perylene[60,51] and thiophene[39] derivatives) and deposition rate (thiophene derivatives[61]).

For example, several film morphologies of widely used LMWSC, namely N,N′-bis(1-ethylpropyl)-3,4:9,10-perylene-bis(dicarboximide), are reported in the literature, with dependence on applied processing parameters.[62-65] Brinkmann et al.[66] provides another striking example. Authors obtained and investigated films of an electron accepting polymer, poly{[N,N'-bis(2-octyldodecyl)-1,4,5,8-naphthalenedicarboximide-2,6-diyl]-alt-5,5'-(2,2'-bithiophene)} by means of two different methods, namely directional epitaxial crystallization on 1,3,5-trichlorobenzene (TCB) and epitaxy on friction transferred poly(tetrafluoroethylene) (PTFE) substrates. Both methods lead to highly ordered supramolecular organization, however with different π-stacking patterns. The films obtained by the first method were characterized by supramolecular organization in which the same segments of adjacent molecules, being in face-to-face position, formed stacking columns. The second method lead to supramolecular organization with additional shift between every second molecular row yelding stacking in which bithiophene segments π-overlaped with bisimide ones.

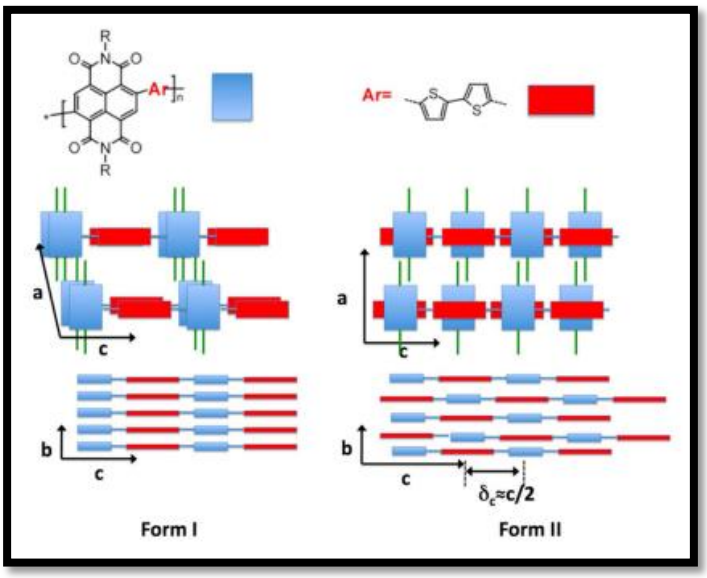

Figure 1.3.2.2.1 Schematic illustration of the stacking of NDI and T2 units in the layers prepared by two different deposition techniques.[66]

Form 1 - Epitaxy on crystallizable solvent (1,3,5-trichlorobenzene).

Form 2 - epitaxy on friction transferred poly(tetrafluoroethylene).

1.3.2.3. Molecular orientation at the interface and in the bulk

It is worth to emphasize that practical requirements concerning orientation of molecules at the electrode-semiconductor interface depend on the type of optoelectronic device. If all molecules lie flat on the electrode, i.e. with π-stacking axis in normal direction, charge transport preferentially occurs in the direction perpendicular to the substrate surface. Such arrangement is favorable for solar cells. If molecules adopt the edge-on position, with their longitudinal axis (100) in plane to the substrate surface, the π-stacking direction is parallel to the interface plane. In-plane conductivity is favorable for transistors.

Hence, the charge transport properties in organic devices can be substantially influenced by the orientation of molecules at electrode/semiconductor interface. This effect is especially important for some types and geometry of the devices. For example, as was proved for bottom-gated transistors, the effective region of active layer from a point of view of transistors efficiency is limited to approximately 5 nm (1–3 monolayers) from the gate surface.[67] Kline et al.[68] used X-ray diffraction to study the surface induced change of morphology and by consequence change of charge transport of popular semiconductor poly-3-hexylthiophene (P3HT) deposited on differently treated substrate surface by: (hexamethyldisilizane (HMDS) or octadecyltrichlorosilane (OTS)). P3HT films on OTS were characterized in majority by crystallites oriented at the interface with (010) and (001) faces (**Figure 1.3.2.3.1 (a)**). In contrast, the films formed on the substrate modified with

HDMS (**Figure 1.3.2.3.1 (b)**) consisted of large number of grain boundaries with the (100) face.

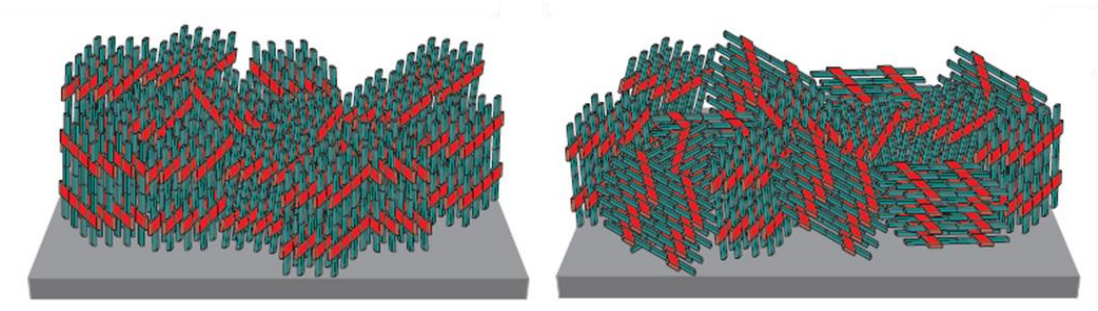

(a) **(b)**

Figure 1.3.2.3.1 Schemes of packing arrangements of crystals at the buried interface of films with: **(a)** OTS, and **(b)** HMDS treated surface.[68]

As was confirmed both preferential orientations change with the increase of the film thickness leading for a very thick films to the same organization characteristic for bulk. The correlated measurements of electrical properties of transistors (i.e. device for which in-plane charge transport is favored) indicated around 1000-fold higher charge carrier mobility in thin film deposited on OTS in comparison to the corresponding film on HDMS. These results evidently confirmed polymorphism of P3HT. They were also used to build a complete model of the complex relationship between chain packing in thin-films of this polymer and charge transport.

The molecular orientation at the interface is a complex matter for optimization especially in the case of semiconductors which exhibit polymorphism. In the light of studies presented above, it is especially interesting to focus on molecular arrangements at the interface. Nowakowski et al. investigated 2D organization of non-planar perylene derivative (DPP-PTCDI) on Ag(110).[69-70] Monolayers of two different structures have been distinguished for this adsorbate depending on the preparation procedure (**Figure 1.3.2.3.2**). A monolayer of flat lying (with reference to the perylene core) molecules was formed by direct deposition. However, a significantly different, more densely packed structure with molecules perpendicularly oriented with respect to the substrate surface, was formed when the monolayer was prepared by thermal evaporation of multilayer coverage. The important question arises whether switch from flat to edge-on orientation of this molecule in the monolayer (first layer) is generated by influence of molecules in upper layers or by heating process. The clear answer was provided by Knor et al.[71] In this studies

similar however not the same perylene derivative, 4-n-BuPh-PTCDI, was investigated on two substrates (HOPG and Au(111)) at liquid–solid interface and room temperature (**Figure 1.3.2.3.3**). In-situ conditions enabled to precise control of the adlayer coverage (enabling changes from monolayer to multilayer and again to monolayer) by concentration of molecules in the solution. Generally, the same effect was observed indicating that the change of molecular orientation in the monolayer is not caused by heating. This is a clear effect of the upper-lying layers on the first monolayer which presence changes the balance in the molecule-substrate and molecule-molecule interactions. This "2D polymorphism" is of importance from the point of view of organic electronics since it enables to generate two different organic – inorganic interfaces in which the charge carriers transport is favored in two perpendicular directions.

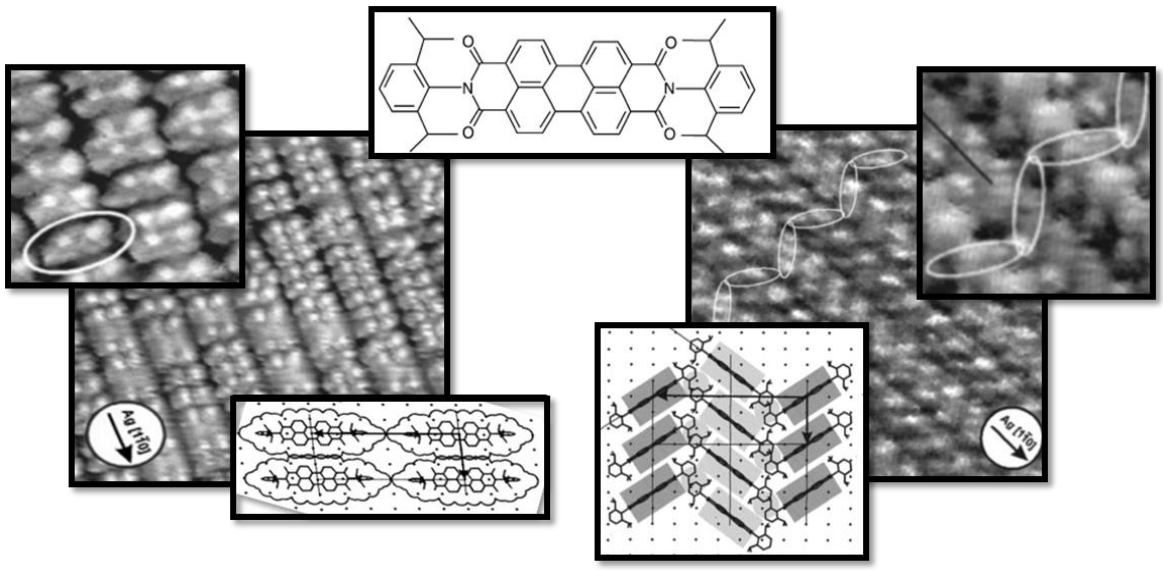

Figure 1.3.2.3.2 Structure, STM images and real-space models of adsorption geometry in monolayers of DPP-PTCDI molecules prepared via: **(a)** direct deposition, **(b)** thermal evaporation of multilayer coverage.[70]

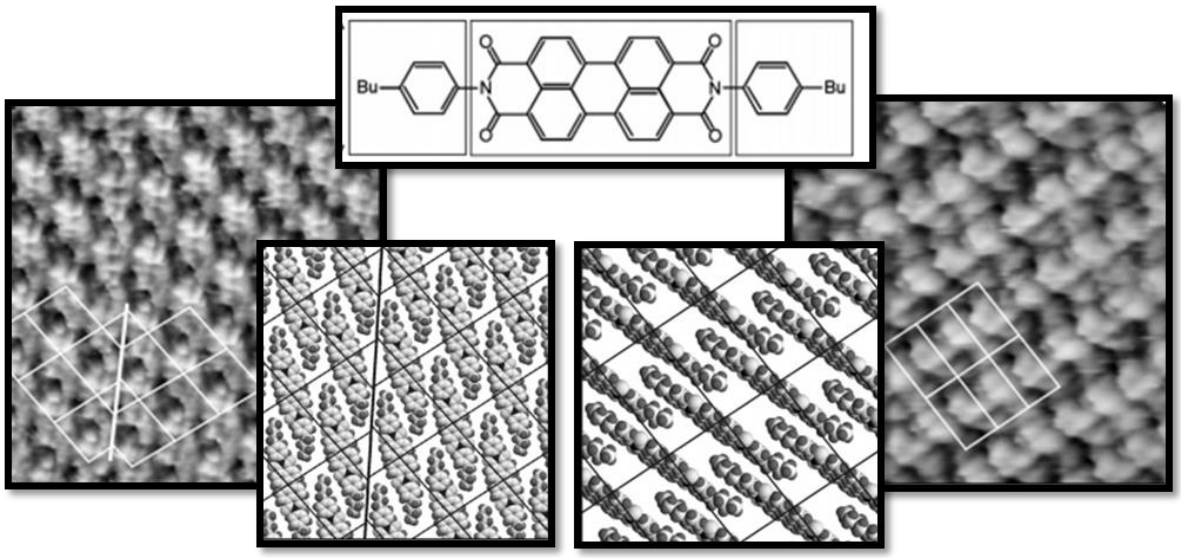

Figure 1.3.2.3.3 Structure, STM images and real-space models of adsorption geometry in monolayers of 4-n-BuPh-PTCDI on HOPG prepared via: **(a)** direct deposition, **(b)** controlled dissolution of a previously deposited multilayer.[71]

Another situation is presented by Rivnay et al.[72] Authors demonstrated that supramolecular organization in bulk of thin films can be modified by thermal annealing. In this example, the orientation of naphthalene-thiophene derivative (P(NDI2OD-T2){[N,N-9-bis(2-octyldodecyl)naphthalene-1,4,5,8-bis(dicarboximide)-2,6-diyl]-alt-5,59-(2,29-bithiophene)} in thin layers was changed from face-on (77.5%) to almost 100% edge-on orientation by the sample heating. The effect occured in bulk as was clearly confirmed by X-ray diffraction analyses. Additionally, the annealing process lead to two-fold increase of crystallinity. Stil, electrical measurements indicated that observed change of the film texture and degree of structural order did not influence the charge carrier mobility in OFETs.

This unexpected effect can be a consequence of the fact that structural modifications of the film occurred only in bulk and did not significantly influenced semiconductor/dielectric interface. In contrast, a six-fold decrease of current was observed in the case of diode confirming importance for this device of molecular organization in the bulk of the film.

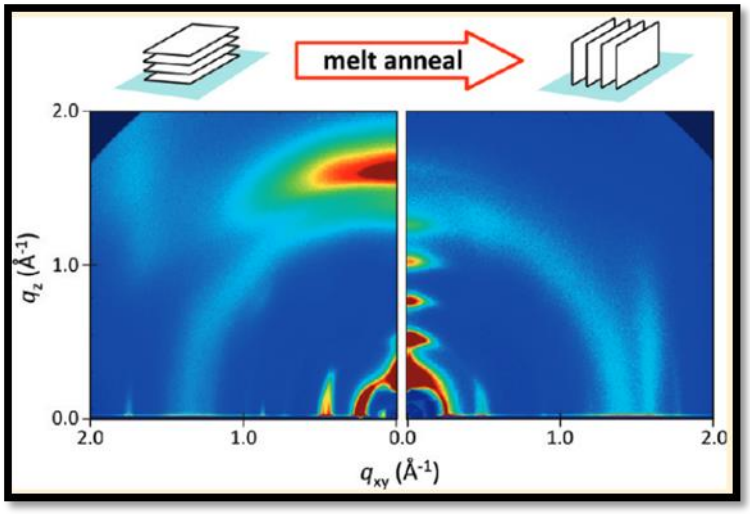

(a) **(b)**

Figure 1.3.2.3.4 X-ray scattering patterns of P(NDI2OD-T2) studied by Rinvay et al. **(a)** before and **(b)** after annealing procedure (to melt and slow cooling).[72]

1.3.2.4 Spatial distribution of electron density in the molecule

It has to be reminded that supramolecular organization is one of two important structural factors which determine charge carrier mobility in organic films. The second one is a spatial distribution of electron density inside the molecule. Several authors discussed the second factor from the point of view of good electrical conductivity of n-type or ambipolar semiconductors.[73] Adachi et al.[74] concluded that promising strategy for constructing high-performance TADF (thermally activated delayed fluorescence) for OLEDs is to design molecules in which HOMO and LUMO would be located at different parts of semiconductor and therefore would be separated in space. Similar concept for OLEDs, based on interruption of conjugation between the electron-donating and electron-withdrawing molecular segments was postulated for derivatives of triphenylamine and oxidiazole.[75-77] Also Proń and coworkers[41] suggested the same concept for ambipolar semiconductors based on arylene bisimides suitable for OFETs. Authors investigated bisimides with perylene backbone core and N-substituted with triphenylamines (showed as **P1** and **P2** in **Figure 1.3.2.4.1**). According to DFT calculations HOMO and LUMO were fully separated in the case of N-substituted derivative (**P1**). HOMO was located in triphenylamine moieties and LUMO in central perylene segment. This distribution was different in the core substituted molecule (**P2**). In this case both segments interacted

stronger leading to partial overlap of areas of corresponding orbitals. Authors suggested that this difference in molecular electronic structure could be a reason why ambipolar behaviour was observed only in **P2**, while **P1** was a typical p-type semiconductor.

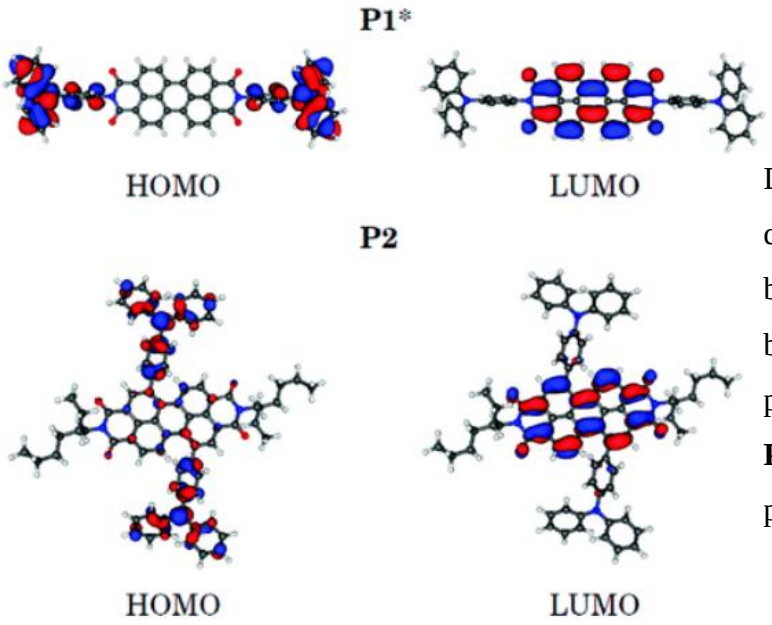

Figure 1.1
Different electron density distributions in perylene based bisimides differently substituted by triarylamine moieties. **P1** is a p- type semi-conductor while **P2** shows ambipolar properties.[41]

Another very interesting studies, showing evident effect of supramolecular organization on charge carrier mobility in ambipolar semiconductor was published by Kim et al.[78] Authors investigated two thienylenevinylene-phthtalimide alternating donor-acceptor copolymers substituted by linear (consisting 12 carbon atoms) and nonlinear (2-ethylhexyl) hydrocarbons (PTVPhI-C12 and PTVPhI-Eh, respectively). In these macromolecules thienylenevinylene groups characterized by extended π -conjugation were electron-donating segments, while phthtalimides was introduced as electron-acceptor ones. They were studied with a combination of several methods, inter alia: calculations of electron-state density, atomic force microscopy, Raman spectroscopy, and XRD. The pristine films of both polymers were characterized by low hole and electron mobilities. This was explained to be a consequence of inefficient pathway of charge transport caused by weak supramolecular organization. It was also confirmed that interchains electron transport is more limited compared to hole transport because the LUMO is less delocalized along the molecular backbone then the HOMO. Thermal annealing significantly improved molecular organization and electrical conductivity of the films however this improvement was not symmetrical for electrons and holes. The better molecular organization in the annealed layers (**Figure 1.3.2.4.2**) affected more electron mobility. It was a consequence of the

generation of new pathway in the layer enabling efficient movement of electrons between neighboring molecules.

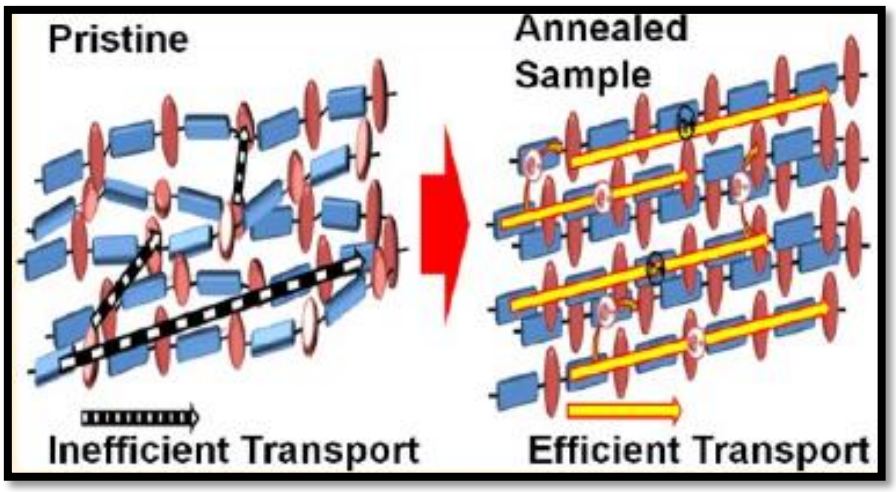

Figure 1.3.2.4.2 Schematic illustration of the change in polymer chain conformation caused by annealing process: (a) nonannealed polymer film and (b) annealed polymer film (Kim et al. experiment[78]).

Two last examples evidently confirm that optimization of electronic properties of ambipolar organic films is a complex matter which must take into account spatial distribution of electron density of both HOMO and LUMO inside the molecule.
Aforementioned examples also emphasize, that electrical transport properties of LMWSC, as well as HMWSC are closely related to their molecular packing. Impurities, defects, size and shape of crystallites, their degree of orientation and interfacial behavior, all have impact on charge carrier transport. The challenges that must be addressed in order to realize the full potential of organic electronics cuts across various fields of science. Synthesis must be supported by information on the surface phenomena and guided by the results from technicians. Chemists, physicists and material scientists have to combine their expertise and work together to gain better control of supramolecular behavior of used organic semiconductors. This work is a part of such a venture. Molecules, designed with building block approach, with the aim to achieve certain electronic properties, were comprehensively studied in 2D monolayers as well as in thin films of various thickness. Established correlations between chemical structure of the molecule and its supramolecular behavior are a fundamental knowledge that will enable further optimization of organic materials in optoelectronic applications.

2. Research goals

Information presented in theoretical part of this dissertation indicates some important facts. Firstly, it demonstrated that organic semiconductors are still a subject of high scientific interest in both basic research and practical applications, just to mention their role in various branches of nanotechnology (including existing and expected novel devices). This interest is evidenced by continuously growing number of scientific publications and books following that topic.

Secondly, in the group of electro-active molecules, small organic semiconductors synthesized by "building block approach" are of particular interest. Such materials have a number of advantages and are interesting alternative to polymers. Primarily because of actual abilities of organic synthesis which enable the precise tune of optical, electronic and redox properties of molecules by their chemical modification. Another advantage is easier, processibility of low weight molecules.

On top of that, the actual hot task in the field of plastic electronics is fabrication of low-weight and air-stable organic semiconductors exhibiting ambipolar conductivity. Basic approach to achieve this objective is chemical synthesis of molecules consisting appropriate combination of segments of different electron affinity. These arguments are the reason why small molecules of donor-acceptor-donor type are the objective of this dissertation.

In addition to chemical composition of molecule, other factors which significantly affect the properties of active layers in organic electronic devices (mobility of charge carriers, emission spectra, the efficiency of LEDs, and others) are supramolecular properties of semiconductors used (many examples have been presented in the literature part of this dissertation). Charge transport in organic semiconductors, unlike the band structure in inorganic semiconductors, is directional and therefore it depends on molecular arrangements in the conductive layer. It usually prefers characteristic directions defined by the supramolecular organization (crystalline arrangement). In the case of amorphous or worse ordered layers its bottleneck is the hopping process of charge carriers between neighboring molecules. Organization in turn (type of order or its lack) may vary

significantly (within the same molecule) with the layer preparation process, or because of influence of the substrate chemical and topological properties. Also, one has to keep in mind, that interfacial supramolecular structures formed between organic film and a substrate are often different from the bulk structure (polymorphism effect).
In the light of combination of presented arguments, it is obvious that knowledge of supramolecular organization in various environments (for example with or without presence of the substrate) and in differently prepared layers is necessary to optimize such complex electroactive organic systems for electronic applications.

The main aim of this work is therefore to establish correlations between chemical structure of the molecules and their supramolecular organization which will allow to develop better control over interactions ruling molecular aggregation. The strategy is to investigate for a few chosen semiconductors logically designed series of derivatives differing in details of molecular structure. In this way the comparative studies will provide a precise correlation between elements of molecular structure and supramolecular organization (and governing it interactions). Moreover, selected **s**emiconductors will be comprehensively studied in different systems: at the interface (as monolayers) as well as in single crystals, powders and films of various thickness. Comparison of differences in supramolecular organizations, if exist, will enable to discuss polymorphism of the investigated molecules.
In addition, to improve discussion, an attempt was made to correlate for selected semiconductors the obtained information about organization with the type of conductivity.
The objective of studies in this dissertation were new semiconductors of donor-acceptor-donor type, from two popular families, namely: arylene based bisimides and thiophene derivatives. Two modern investigation techniques were involved. The first one is scanning tunneling microscopy (STM). It is a powerful tool for the investigation of interfacial structures providing images at molecular resolution of organic monolayers with local information about molecular organization. The correlation of the observed structures of the layers with the van del Waals size and geometry of the molecules allowed to propose for each semiconductor model of the layer and discuss distribution of interactions between molecules. The second technique, X-ray diffraction method (XRD) is complementary to STM. It enabled to provide statistical information about molecular organization in various 3D systems: single crystals, powders and thin films. Thin layers were prepared for these measurements by different deposition methods (dropcasting, spincoating, zonecasting) and with various substrates used (graphite, SiO_2, gold, glass).

I expect that undertaken research will make it possible to answer the important questions regarding the impact of the size and strength of the central unit, number and position of substituents, or terminal alkyl chain length in the process of two- and three-dimensional self-organization of the selected semiconductors.

It is important to emphasize, that in order to achieve the main aims of the work, it was necessary to overcome a variety of additional issues, like: purification of the investigated materials (very time consuming and important step), optimization of preparation methods of continuous monolayers on HOPG, as well as of single crystals and thin films on various substrates.

3. Experimental

3.1. Investigated molecules

Two families of organic compounds having potential applications in electronic and photovoltaic devices were investigated in the frame of this thesis: arylene bisimides and thiophene based donor-acceptor derivatives.

Both types of investigated molecules are examples of low molecular weight semiconductors. They were synthesized according to "building block approach" strategy, by prof. Małgorzata Zagórska and prof. Adam Proń from Warsaw University of Technology, with the purpose to obtain novel electroactive organic molecules of very attractive ambipolar behavior. For this reason, conjugated segments of opposite electronic affinities were assembled together by appropriate chemical coupling. The investigated molecules consist of conjugated core of central acceptor unit (arylene bisimide or thiadiazole (tetrazine), respectively) which is surrounded by one or more types of intervening groups that were introduced to precisely modify the molecular electronic structure. Moreover, terminal substituents, alkyl or alkoxy chains, were attached to the conjugated core of the molecule to improve solubility and, what goes with it, processability of the synthesized molecules. It is worth to remind, that terminal substituents, due to their affinity to applied substrate (HOPG) and also their strong tendency for mutual intedigitation also facilitated the formation of an ordered structures in both 2D monolayers and 3D thin layers and crystals.

3.1.1 Arylene bisimides based DAD semiconductors

3.1.1.1. Names and chemical formulas

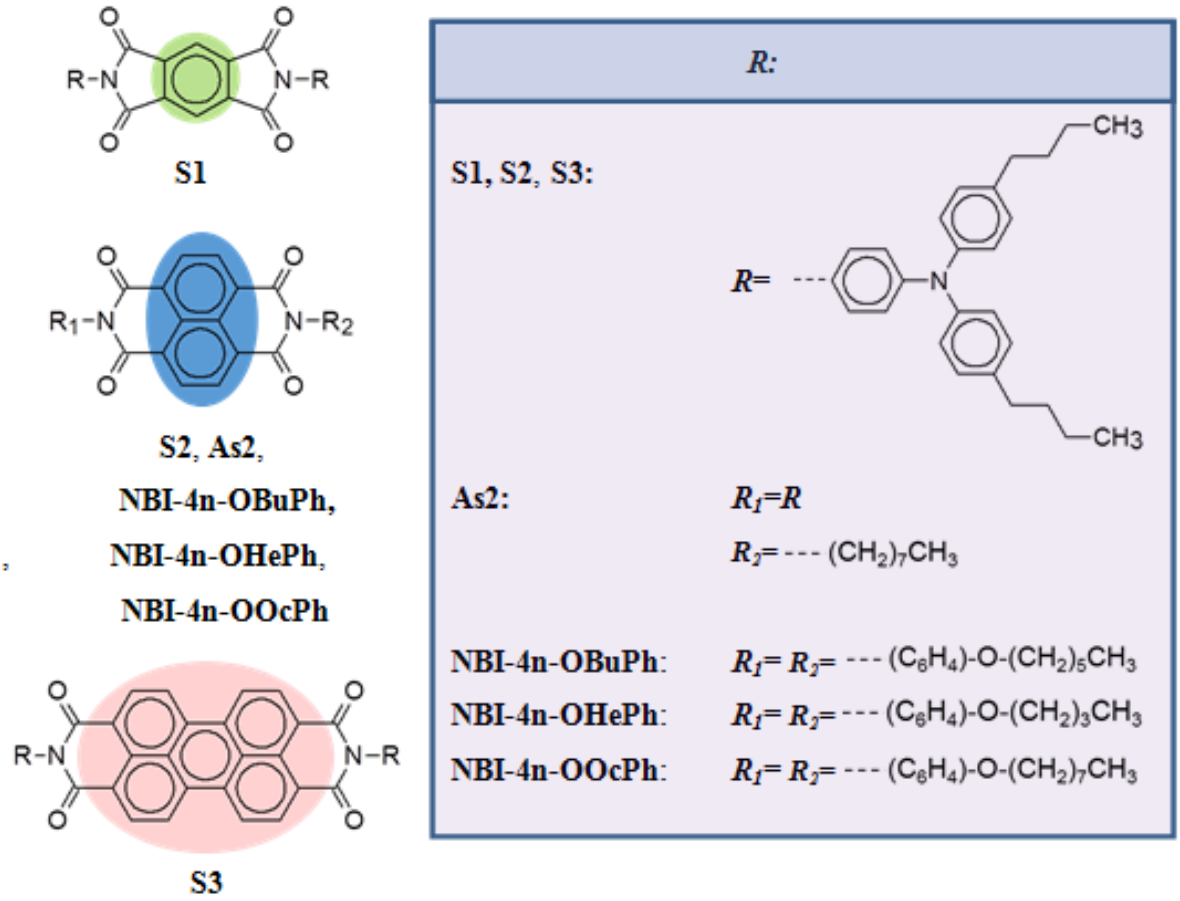

N,N0-bis{4-[bis(4-butylphenyl)amino]phenyl}-1,2,4,5-benzenetetracarboxylic-1,2:4,5-bisimide (**S1**)

N,N0-bis{4-[bis(4-butylphenyl)amino]phenyl}-1,4,5,8-naphthalenetetracarboxylic-1,4:5,8-bisimide (**S2**)

N,N0-bis{4-[bis(4-butylphenyl)amino]phenyl}-3,4,9,10-perylenetetracarboxylic-3,4:9,10-bisimide (**S3**)

N-{4-[bis(4-butylphenyl)-amino]-phenyl}-N0-octyl-1,4,5,8-naphthalenetetracarboxylic-1,4:5,8-bisimide (**As2**)

N,N′-bis(4- n-butoxyphenyl)-1,4,5,8-naphthalene tetracarboxylic-1,4:5,8-bisimide (**NBI-4n-OBuPh**)

N,N′-bis((4-n-hexyloxyphenyl)-1,4,5,8-naphthalene tetracarboxylic-1,4:5,8-bisimide (**NBI-4n-OHePh**)

N,N′-bis(4-n-octyloxyphenyl) -1,4,5,8-naphthalene tetracarboxylic-1,4:5,8-bisimide (**NBI-4n-OOcPh**)

3.1.1.2. General information

Arylene bisimides are well known components of active layers in organic electronic devices. There are several reasons of their popularity. First of all, arylene bisimides can be

synthesized from relatively cheap substrates like bisanhydrides and primary amines.[42] Moreover, these semiconductors usually exhibit n-type conductivity in transistors, because of their low lying LUMO level. Their important advantage is molecular stability in air enabling in most cases operation in ambient conditions. At this point it should be added, that stability can be improved by increase of electron affinity (EA) of the molecule. This can be obtain by chemical modification of aromatic core, for example by various types of amines.[79-83] Regrettably, drawback of this procedure is a complicated reaction pathway involving non-selective reactions.[23] Moreover, functionalization of imide nitrogen can be alternatively applied, which usually is a simpler procedure. For example, change of alkyl N-substituents to their highly fluorinated analogues was reported to lead to increase of EA.[36, 84-85]

Regarding the molecular backbone choice, the studies show, that naphthalene bisimides can be processed more easily in comparison to larger core ones and they are much more sensitive toward N-substitution.[86-87]

Above presented advantages are the reason why arylene bisimides have been intensively studied for decades.[43-44] Yet, in spite of this long interest, the synthesis and applications of new derivatives of this class of semiconductors are still very attractive research areas. These molecules show interesting reversible electrochemical behavior,[88-89] they can be applied as dyes[90] (bi- and tri-chromophoric perylene have been considered as "intense dyes" because of their exceptionally high extinction coefficients)[91]. They attract significant interest in spectroscopy[92], electrochemistry[93], or as active molecules in electron transfer systems, energy transfer cascades and photovoltaic devices.[94-97] However, the main reason of actual popularity of arylene bisimides in organic electronics is still related to fabrication of new solution processable and stable in air, LMWSC and polymetric semiconductors of n-type or ambipolar behavior.[41, 98-104]

In the frame of this work attractive new arylene bisimides functionalized by two substituents, namely: triarylamine (molecules: **S1**, **S2**, **S3**, **As2**) and alkoxyphenyl groups (**NBI-4n-ObUPh**, **NBI-4n-OhEPh**, **NBI-4n-OOcPh**) were investigated. Both substituents exhibit p-type conductivity. As a consequence, assembly in one molecule of n-type arylene bisimides with p-type substituents was anticipated to lead to organic semiconductors suitable for fabrication of ambipolar transistors.

Low and high molecular mass triarylamines despite being materials for semiconductors, are also interesting electrochromic[105] and electro-photochromic[106] materials.

3.1.2. Thiophene based DAD semiconductors

3.1.2.1. Names and chemical formulas

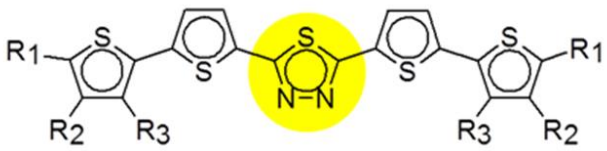

T1, T2, T3, T4, T5, T6, T8

	R:
T1:	$R_1 = R_2 = R_3 =$ ---H
T2:	$R_1 = R_3 =$ ---H
	$R_2 =$ --- $(CH_2)_7CH_3$
T4:	$R_1 =$ --- $(CH_2)_7CH_3$
	$R_2 = R_3 =$ ---H
T5:	$R_1 = R_2 =$ --- $(CH_2)_7CH_3$
	$R_3 =$ ---H
T3:	$R_1 = R_2 =$ ---H
	$R_3 =$ --- $(CH_2)_7CH_3$
T6:	$R_1 = R_2 =$ ---H
	$R_3 =$ --- $(CH_2)_3CH_3$
T8:	$R_1 = R_2 =$ ---H
	$R_3 =$ --- $(CH_2)_{11}CH_3$

2,5-bis(2,2'-bithiophene-5-yl)-1,3,4-thiadiazole (**T1**)

2,5-bis(4'-octyl-2,2'-bithiophene-5-yl)-1,3,4-thiadiazole (**T2**)

2,5-bis(5'-octyl-2,2'-bithiophene-5-yl)-1,3,4-thiadiazole (**T4**)

2,5-bis(4',5'-dioctyl-2,2'-bithiophene-5-yl)-1,3,4-thiadiazole (**T5**)

2,5-bis(3'-butyl-2,2'-bithiophene-5-yl)-1,3,4-thiadiazole (**T6**)

2,5-bis(3'-octyl-2,2'-bithiophene-5-yl)-1,3,4-thiadiazole (**T3**)

2,5-bis(3'-dodecyl-2,2'-bithiophene-5-yl)-1,3,4-thiadiazole (**T8**)

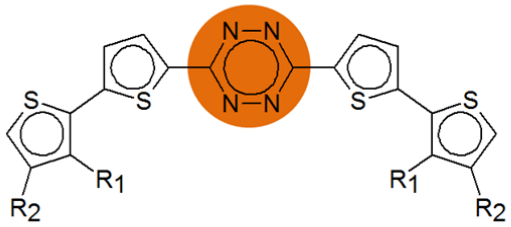

	R:
TT2:	$R_1 =$ ---H
	$R_2 =$ --- $(CH_2)_7CH_3$
TT3:	$R_1 =$ --- $(CH_2)_7CH_3$
	$R_2 =$ ---H

3,6-bis(4'-octyl-2,2'-bithiophene-5-yl)-1,2,4,5-tetrazine **(TT2)**

3,6-bis(5'-octyl-2,2'-bithiophene-5-yl)-1,2,4,5-tetrazine **(TT3)**

3.1.2.2. General information

Unsubstituted and alkyl-substituted oligothiophenes constitute a wide class of p-type semiconductors used in various devices: organic field effect transistors,[23,107-109] photovoltaic cells,[110-112] light-emitting diodes,[113-114] active materials for lasing,[115-117] components for electroluminescent switches or other photovoltaic devices[118]. Ditihienylthiadiazoles (three ring compounds) are tested as steel-corrosion inhibitors.[119-120] By analogy to bisimides, electrochemical behavior of thiophene based semiconductors might also be changed by appropriate chemical functionalization. For example, various groups investigated and applied donor-acceptor copolymers containing electron-donor segments of oligothiophene alternating with different electron-acceptor ones, like: pyrrolopyrrole dione,[121] or oxadiazole unit.[122] Taking that in mind, it seemed a tempting idea to combine familiar thiophene donor units with electron-withdrawing group in the search of yet another type of new ambipolar compounds. Two families of new derivatives centrally functionalized by thiadiazole (**T1**-**T6**, **T8**) or tetrazine (**TT2**-**TT3**) rings were investigated and comparably discussed in the frame of this work. Literature reveals that compounds having thiadiazole nucleus are attractive for application in pharmaceutical and biological fields.[123] Moreover, as have been reported ,introduction of arylene electron-donating group between electron-withdrawing thiadiazole rings already afforded novel ambipolar compounds.[124] The second used electron-withdrawing group, tetrazine is also extremely interesting compound attractive in biomedical applications.[125-127] In this work, it has been used as stronger acceptor unit than thiadiazole, which might stronger affect the change of electrochemical properties and supramolecular organization of obtained semiconductors in both 2D and 3D systems.

3.2. Layers preparation

3.2.1. Monolayers preparation

Monomolecular layers of benzene, naphthalene and perylene bisimides were formed on a freshly cleaved surface of HOPG (SPI Supplies, USA) being in contact with their saturated solutions in trichlorobenzene (**S1**, **S2**, **S3**, **As2**) or in 1-phenyloctane (**As2**). They were investigated "in situ" by immersing the STM tip directly in the droplet of the solutions.
In the case of thiophene based semiconductors the monomolecular layers were prepared by dropcasting of a solution (5 μm) of each investigated compound in hexane (~2 μg/ml) on a freshly cleaved surface of HOPG. Samples were imaged by STM after drying in air. Change of solvent to chloroform, or the use of chloroform/hexane mixture did not cause any observable difference in the monolayer structure. This procedure was conducted for three derivatives (**T3**, **T6** and **T8**). In addition, I had also managed to fabricate a **T3** monolayer by spincoating technique. In this case a droplet (5 μm) of solution of this derivative in hexane (~200 μg/ml) was deposited on a fast rotating plate. The monolayers obtained by this method and dropcasting technique were characterized by the same supramolecular organization.

3.2.2. Thin films preparation

Thin films of the studied materials were prepared by means of three techniques: dropcasting, spincoating and zonecasting.
Five substrates were used: Au (George Albert PVD, Germany), HOPG (SPI Supplies, USA), glass, and two types of crystalline Si wafers covered with native (few nm thick) or thicker (100 nm) thermally prepared SiO_2 layer. HOPG surface was always cleaved by adhesive scotch tape just before sample deposition. Gold substrates were prepared by thermal annealing and rinsing with Mili-Q water. All substrates except HOPG were cleaned by rinsing with distilled water and then drying in argon flux.

In the case of dropcasting technique, a fixed volume (3.5 μl) of solution of a given compound was deposited on the respective substrates. Typical thickness of the deposited

layers varied between 150−250 nm and was higher on the edges than in the center of the sample. In the case of spincoating technique, a constant amount of solution of each semiconductor (10 μg/ml, volumes: 3.5 μl, 10 μl, 5 μl) was dropped on the surface of already rotating substrates (3500 rpm). The speed of rotation was maintained for 60 seconds after deposition. The layers of thickness about 20 nm were obtained in these conditions. Spincoater model Spin150 were used for samples preparation.

Zonecasted samples were prepared in group of prof. Adam Tracz, the Centre of Molecular and Macromolecular Studies of the Polish Academy of Sciences in Łódź. In this method a chlorobenzene solution of selected semiconductors were continuously supplied onto a moving substrate (glass) from a stationary flat nozzle. Due to continuous evaporation of the solvent the gradients of temperature and solvent concentration were created in the meniscus which was formed between the nozzle and the substrate. These gradients were the driving forces of unidirectional crystallization. To obtain uniform, highly ordered layer, optimization of several parameters for each individual semiconductor was required, including: concentration and temperature of the solution, its supply rate, height of the meniscus, temperature of the substrate and its moving speed.

3.2.3. Single crystals preparation

Single crystals of **NBI-4n-ObUPh**, **NBI-4n-OhEPh** and **NBI-4n-OOcPh** were formed by evaporation of approximately 0.2 ml of their saturated solutions in chlorobenzene at atmospheric pressure and room temperature. Almost the same method was used to obtain single crystals of **T3**, except the solution concentration (10 mg/l).

3.2.5. Powders preparation

Powders for X-ray measurements were prepared from acetone suspensions of the investigated compounds by direct deposition on Si wafer of known orientation.

3.3. Layers characterization methods

3.3.1. X-ray diffraction

3.3.1.1. Method description

X-ray diffraction is a powerful measurement technique, that allows to gather averaged information about supramolecular structure in 3D systems (thin layers, powders and single crystals). The simplified scheme of X-ray diffraction measurements is illustrated in **Figure 3.3.1.1.1**.

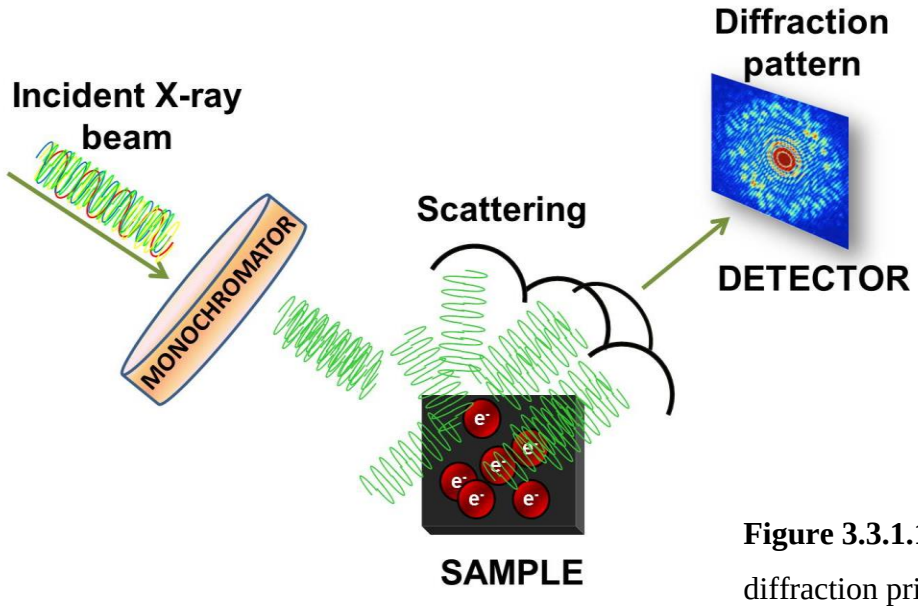

Figure 3.3.1.1.1 X-ray diffraction principles of operation.

In principle in this method X-rays are used to produce the diffraction pattern. When a beam of X-rays hits a sample, it interacts with electrons within the sample. The scattering occurs subsequently as electrons oscillate and became the secondary point sources of radiation of the same frequency (energy) as the incident X-ray beam. Secondary X-rays are propagated in all directions from each electron source and interfere with each other leading in majority to canceling each other out. However in the case where material is characterized by crystalline structure with interatomic (intermolecular) spacing of the same order of

magnitude as incident wavelength, the scattered X-rays are in-phase in certain directions and constructive interference (diffraction) occurs. X-ray photons are then captured by the detector in the form of diffraction pattern.

Angular relationship between reflections in the diffraction pattern gives information about interatomic (intermolecular) spacing and can be used to discern the crystal structure with dimensions of the unit cell. Recorded information is however expressed in reciprocal space, and therefore has to be transformed to data in direct space (real space).

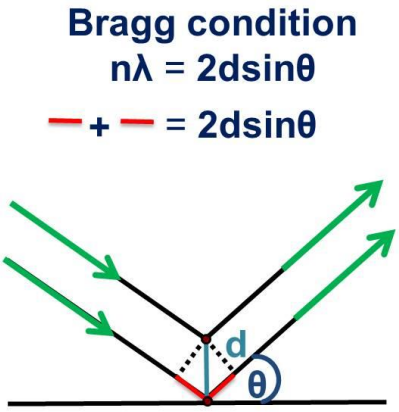

Figure 3.3.1.1.2 Bragg condition.

The necessary condition for constructive interferences is described by Bragg relation (presented in **Figure 3.3.1.1.2**). In this equation n is an integer describing order of the reflection from one reciprocal plane, λ is wavelength of incident wave, θ is the angle between direction of incident ray and scattered plane and d is interplanar spacing in the real space. If Bragg's equation is not satisfied, no reflection occurs. On the other hand, if Bragg's equation is satisfied, reflections are observed (with the exception of systematic absences).

In the frame of this dissertation, X-ray scattering measurements were used to characterize various types of 3D samples: single crystals, powders and thin films. Accordingly, a suitable implementation of the measurement method and mode had to be chosen for each sample. However, all measurements are based on angular relationships between the reflections described by Bragg relationship. Moreover, the differences in reflection intensities have been used to work out the arrangements of atoms in the unit cell. This can be done only in the case of single crystal measurements. For all remaining samples, the intensities were not taken into account. Experimental results were presented in the thesis as

a dependence of scattered intensity (given in arbitrary units scale) versus either 2θ or scattering vector q or d. The scattering vector q is defined as (**Figure 3.3.1.1.3**):

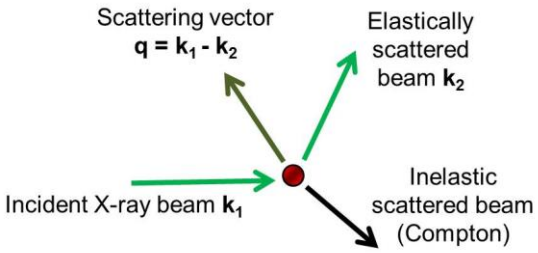

$$|\vec{q}| = \frac{4\Pi sin\theta}{\lambda} = \frac{2\Pi}{d}$$

Figure 3.3.1.1.3 Scattering vector q

Furthermore, in the case of samples other than single crystals, the width of reflections allowed to determine the average size of crystallites. This could be done by following the Sherrer formula:

$$\xi = \frac{0{,}9\lambda}{\Delta cos\theta}$$

where: ξ represents crystalline size in Å, λ is wavelength of the incident X-ray wave (also in Å), and Δ is full width at half maximum of the reflection (of the peak) in radians. In addition, studies of Kiessig fringes made it possible to determine the thickness of thin films. The periodicity in q of those fringes can be related to the film thickness d via the following relation: $q=2\pi/d$.

3.3.1.2. Apparatus used and modes of measurements

For single crystals investigations the X-ray Crystallography Diffraction data were collected at 150 K using an Oxford - Diffraction X Calibur S Kappa geometry diffractometer (MoKα radiation, graphite monochromator, λ = 0.71073 Å). The cell parameters were obtained with intensities detected on n_{batch} batches of 5 frames. For three settings of ϕ and ψ, N_{imag} narrow data were collected for 11 increments in ω with an exposure time t_{exp}. Unique intensities detected in all frames by means of the Oxford-diffraction Red program were used to refine the values of the unit cell parameters. All hydrogen atoms were fixed in

optimal positions. The parameters N_{imag} , n_{batch}, t_{exp}, the total number of reflections $N_{tot.refl}$, the number of independent reflections $N_{indrefl}$ and the final indices R_1 and wR_2 are collected in **Table 3.3.1.2.1**.

	T3	**NBI-But**	**NBI-Hex**	**NBI-Oct**
n_{batch}	3	6	3	6
N_{imag}	267	434	493	423
t_{exp} [s]	1	220	20	80
$N_{tot.refl}$	10379	13871	13926	9191
$N_{indrefl}$	5053	4095	6431	5214
R_1	0,0317	0,0784	0,0818	0,079
wR_2	0,0765	0,1054	0,1255	0,1207

Table 3.3.1.2.1 Experimental parameters used for determination of crystallographic unit cells of alkoxyphenyl-substituted naphthalene bisimides and **T3**.

Powder diffractograms were recorded in the reflection geometry (Bragg Brentano θ/2θ) using a Panalatycal powder diffractometer equipped with a CuKα radiation source (λ= 1.5418 Å) and a divergence slit of 1/4°. The powders were investigated on a crystalline Si substrate to minimize the background contribution of the sample holder. Continuous scans were recorded between 2 and 60° in 2θ during 3h using a X'Celerator detector. Each scan was collected for 2θ from 2° to 60° with a step of 0.01° or less and counting time 60 s per step.

X-ray diffraction studies of thin films of all semiconductors deposited on various substrates were carried out in the same diffraction geometry as powders, on a Panalatycal Empyrean diffractometer (CoKα_1 radiation, λ=1.789 Å). The system was equipped with a mirror and a divergence slit of 1/32° on the incoming beam side. Moreover in the case of 1D scanning mode a PixCel3D rapid detector and Soller slits of 0.04° were used on the diffracted beam side. Continuous scans were recorded for 2θ from 2° to 30-60° and the total time from 0.5 to 7 hours, depending on the scattering power of the studied layers.

Both, powders and thin films samples were investigated in reflection mode, which means that the periodicity of molecular organization was measured in a direction perpendicular to

the axis of the substrate. This information is especially important for discussion of XRD measurements of thin films.

3.3.2. Scanning tunneling microscopy

3.3.2.1. Method description

Scanning Tunneling Microscope (STM) is a unique experimental tool for surface investigations that is able to provide real space images at atomic resolution of surface topology as well as local measurements of its electronic properties. The simplified scheme of STM measurements is illustrated in **Figure 3.3.2.1.1**.

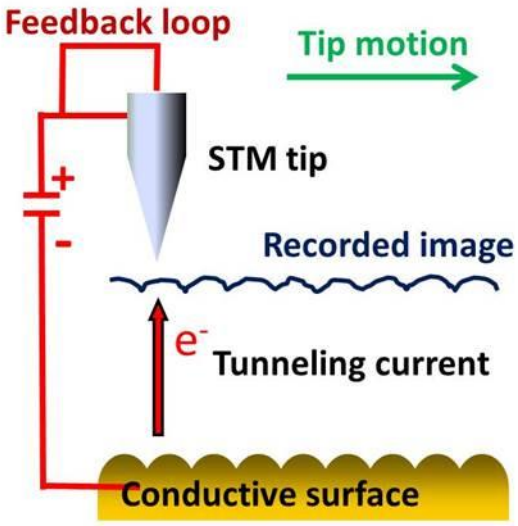

Figure 3.3.2.1 STM principles of operation

In this technique metallic STM probe is approached to the surface up to a few Å under which conditions wave functions of electrons at the end of STM probe (tip) and of the investigated surface overlap. Then, a bias voltage is applied between a probe and the sample leading to flow of tunneling current of pA, up to nA range. Due to the extreme sensitivity of current to the probe-surface separation this parameter is used to obtain indirectly information about the surface topology. Since STM is based on measurement of electrical current the main limitation of this technique is conductivity of the investigated sample.

The current is usually recorded over the scanning surface area at spatial resolution 256x256 points. Relative position of the STM probe and the sample surface is electronically controlled at subatomic resolution (usually about 0.2 Å) by applying a voltage to the piezoelectric scanner.

When probing tip across the surface, two basic modes of measurements are possible: constant-height mode, in which z-position of the tip is kept constant, and constant-current mode, in which the measured current is constantly compared to a preset value by a feedback circuit. In the second mode of operation, the feedback circuit corrects a voltage to the scanner at every scanning point in order to adjust z position of the probe and finally to keep the same current intensity. As a consequence the probe scans the surface with the constant distance to it (constant separation). The results of STM measurements are therefore coded into one-color, z-scale images of distribution of current (constant-height mode) or corrections of vertical position of the probe (constant-current mode) over the scanning area.

In general opinion, the constant-height mode yields better resolution since it is faster method and less susceptible to influences of any noises (electrical, mechanical, thermal etc.). On the other hand, disadvantage of this method of imaging is that the position of the tip does not respond to changes in surface topology. In the case of protrusions of a height greater than the separation, probe hits scanned surfaces. The alternative in the form of the constant-current operating mode as said before, in which the height of the probe in each step is adjusted according to the surface topology, is a slower method, more prone to noise influences. All STM measurements in the frame of this thesis were recorded in constant current mode.

The tunneling current during STM measurements is proportional to:

$$I \sim \left(B * \rho(E_F) * \frac{V}{d}\right) * e^{(-Ad\sqrt{\phi})}$$

where: I is tunneling current, V is a voltage between the sample and tip, d is the distance between these two electrodes, ϕ is averaged value of the work function for both electrodes, $\rho(E_F)$ is density of electronic states of the surface near the Fermi level, and A and B are theoretic constants. This formula confirms extreme sensitivity of current to the probe-surface separation. This is a fundamental relation which enables to get information about surface topology by the tunneling current measurement. However this formula also

indicates that current simultaneously depends on two parameters which characterize electronic properties of the surface, that are: density of electronic states near the Fermi level (that means states which take place in the tunneling process), and work function. This turn to conclusion that STM method provides real surface topology only in cases when both parameters are constant over the scanned surface area. If it is not a case, the influence of the variation of electron properties on the surface must be taken into account in the image formation. In general, the STM image is therefore influenced by two basic factors: real surface topology and electronic factor which can locally change conditions of tunneling process. This point is especially important in the case of investigations at atomic or molecular resolution of monomolecular layers of complex in electronic structure molecules, as in this work. It has been frequently demonstrated in various publications (for example [172] and [173]) that STM image contrast in these conditions can be dominated by electronic factor and usually is correlated to electron densities of appropriate molecular orbitals of the investigated molecule in the adsorbate state. In such studies, the negative tip polarization reveals the shape of LUMO orbitals, while the positive one, the shape of HOMO ones. This is a consequence of different tunneling direction and orbitals of the surface electrons which take place in this process. When tip is negatively charged with respect to the sample, it effectively raises the Fermi level of the tip electrons with respect to the sample electrons. Therefore, electrons will tend to flow from filled states of the tip to empty states of the sample (**Figure 3.2.1.2 (a)**). In contrast, when tip bias is positive, tunneling current flows in opposite direction (**Figure 4.3.2.1.2 (b)**).

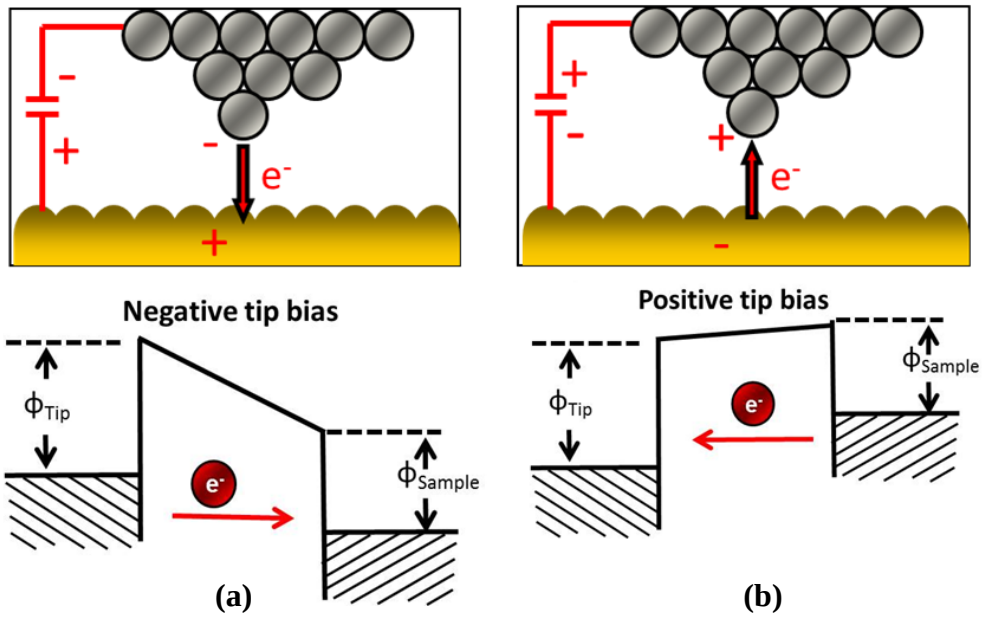

Figure 3.3.2.1.2 Directions of tunneling current for **(a)** negative, and **(b)** positive tip polarization.

3.3.2.2. Apparatus used and modes of measurements

For STM studies a home-made microscope (fabricated at the University of Bonn, Germany) was used. All images were recorded in standard constant-current mode using mechanically cut Pt/Ir (80/ 20%) tips.

All investigations of bisimides were carried out "in situ", at liquid–solid interface and room temperature by immersing the STM tip directly in the solution droplet.

The studied thiophene derivatives were dissolved in hexane to yield a concentration of 2 μg/ml. Then, a droplet of this solution was deposited onto a freshly cleaved surface of highly oriented pyrolytic graphite (HOPG, SPI Supplies, USA). After they were dried in ambient conditions, the organic films were then imaged in air at room temperature.

Microscopic investigations were repeated several times for each adsorbate on different samples and at different surface areas to avoid artifacts and get statistical information. The tunneling conditions were optimized for each studied molecule.

The models of adsorption geometry of the investigated semiconductors in monomolecular layers on HOPG were postulated by the correlation of the layer structure observed by STM and the van der Waals size and geometry of the molecules (obtained using the HyperChem software package).

4. Results

4.1. Arylene bisimides

The first part of own investigations concerns selected derivatives of arylene bisimides. Totally, seven bisimide derivatives have been studied in the frame of this dissertation, they were listed and named in **section 3.1.1**. The chosen experimental results have been compared in subsequent chapters to determine the influence of different structural elements of this family of organic semiconductors on their supramolecular organization: the type of conjugated molecular backbone (**section 4.1.1**), as well as, molecular symmetry induced by the type of substituents (**section 4.1.2**) and the substituent length (**section 4.1.3**).

4.1.1. Influence of the type of conjugated unit

In this section, the influence of the type of centrally located conjugated molecular unit on supramolecular organization of arylene bisimides is analyzed on the example of bisimides containing triarylamine groups as N-substituents. Hence, the results concerning three derivatives (**S1**, **S2** and **S3 in Fig. 4.1.1.1**), differing from each other by the type of the central unit (benzene, naphthalene and perylene, respectively), have been compared.

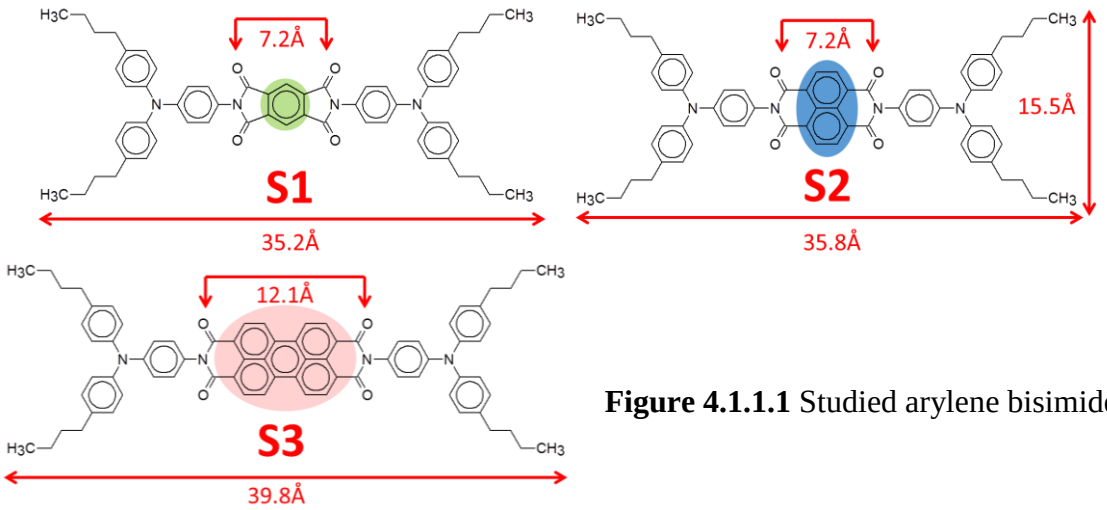

Figure 4.1.1.1 Studied arylene bisimides.

Before discussion of own results it is worth to emphasize characteristic feature of the investigated family of semiconductors. Theoretical modeling (DFT calculations)[88] indicates, that for all three derivatives, the central arylene unit is planar in optimal molecular geometry, whereas the triphenylamine substituents are expected to be nonplanar. This is due to a twist of each phenyl ring around C-N bonds yielding C-N-C-C dihedral angle of ca. 43°. Moreover, both units also keep opposite character in electronic structure of the molecule. The same theoretical calculations indicate that for all three investigated semiconductors, HOMO and LUMO are located at different parts of the molecules, and therefore well separated. HOMO density is calculated to have its largest values in areas of triphenylamine moiety, whereas the LUMO orbitals are localized mainly in arylene core. It is suggested that very weak conjugation between both parts is a consequence of nearly perpendicular orientation (79º) to the conjugated core of phenyl rings directly attacked to the imide nitrogen atoms. **Figure 4.1.1.2** presents plots of HOMO and LUMO orbitals calculated for **S2** molecule.

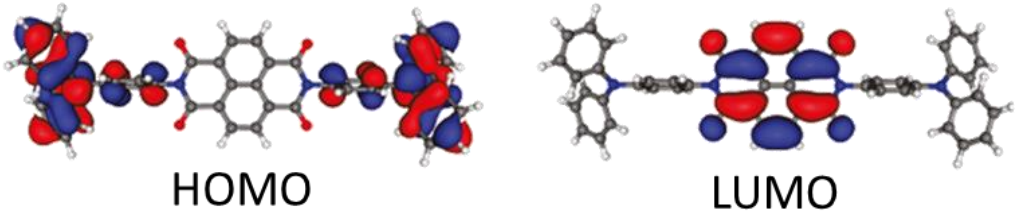

(a) **(b)**

Figure 4.1.1.2 Plots of calculated **S2** molecular orbitals[88]

In the first part, the discussion is focused on differences between 2D organizations of investigated semiconductors in monolayers on HOPG. Despite effort made, preparation of well-organized monolayer of derivative **S1** with smallest conjugated part (benzene), was not successful. This situation is changed for derivatives with larger molecular backbone: naphthalene (**S2**) and perylene (**S3**).

Figure 4.1.1.3 shows representative STM image of **S2** monolayer. The molecules are evidently ordered. Two adjacent, large domains of different orientations are highlighted with blue and yellow colors in the large-area image. The image of the monolayer in a single domain is characterized by parallel bright stripes. These areas correspond to parts of the layer of higher electrical conductivity, namely, linear arrangements of conjugated backbones of well-ordered molecules into parallel molecular rows.

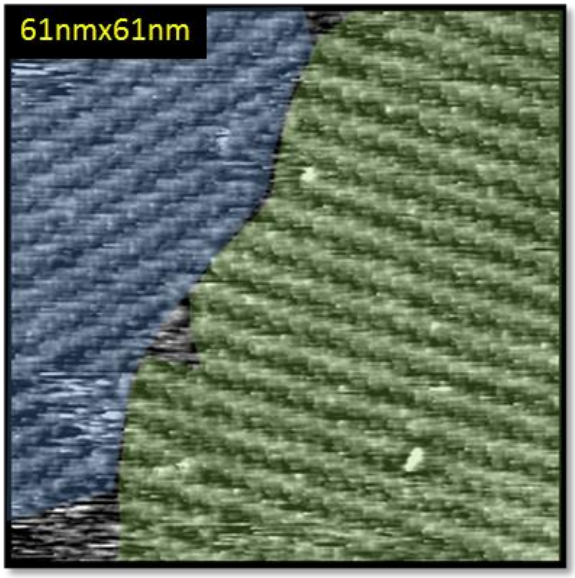

Figure 4.1.1.3 STM images of **S2** monolayer at liquid-solid interface (HOPG-trichlorobenzene solution) (V_{bias}=1V, I_t = 0.3nA). Two coexisting domains are marked by blue and green highlights.

Careful inspection provides more detailed information. Single molecule in the monolayer is observed at submolecular resolution as a set of several (5-6) mutually linked bright spots, (**Figure 4.1.1.4)**. The resulted complex submolecular image, of spider-like shape, is most probably a consequence of non-planar arrangement of the adsorbed molecules (due to expected tilt versus the substrate plane of each phenyl ring from triphenylamine substituents). This repetitive motif in the image enabled to determine the unit cell of **S2** monolayer (**3.4 ± 0.1nm, 2.8 ± 0.1nm, 59° ± 2°**), however due to the complex submolecular image, the precise molecular arrangement in the monolayer is not evident.

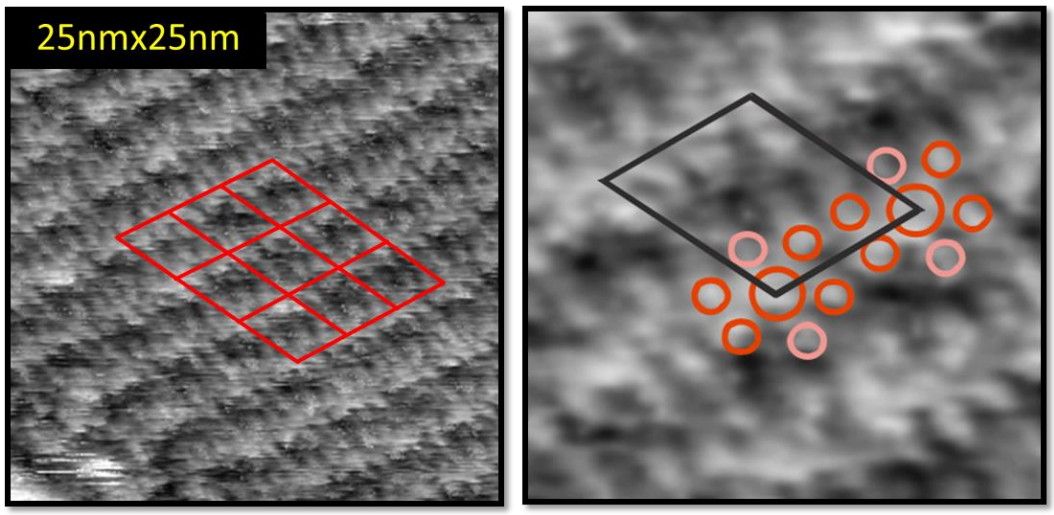

Figure 4.1.1.4 STM image of **S2** monolayer at liquid-solid interface (HOPG-trichlorobenzene solution) and postulated unit cell (V_{bias}= -1.3V, I_t = 0.8nA).

To answer this question it has been decided to take an opportunity given by specific electronic structure of the investigated bisimides, namely, separation of HOMO and LUMO orbitals within the molecule. At this point it is worth to remind that STM tip working with positive polarization reveals the shape of electron abundant areas of the molecular layer and therefore the image can reflect the shape of HOMO orbitals, whereas the tip working with negative polarization – the electron deficient centers and in a consequence the shape of LUMO orbitals.

Comparison of images acquired with different tip polarizations (**Figure 4.1.1.5**) unequivocally demonstrate that the parameters of the unit cell determined from both images are the same (and correspond with parameters listed above), however the contrast pattern depends on the polarization. The bright spots observed in both images seem to be not the same ones, differing in shape, being either round or elongated depending on the scanning conditions. Hence, important question arises whether they are localized in the same or different areas?

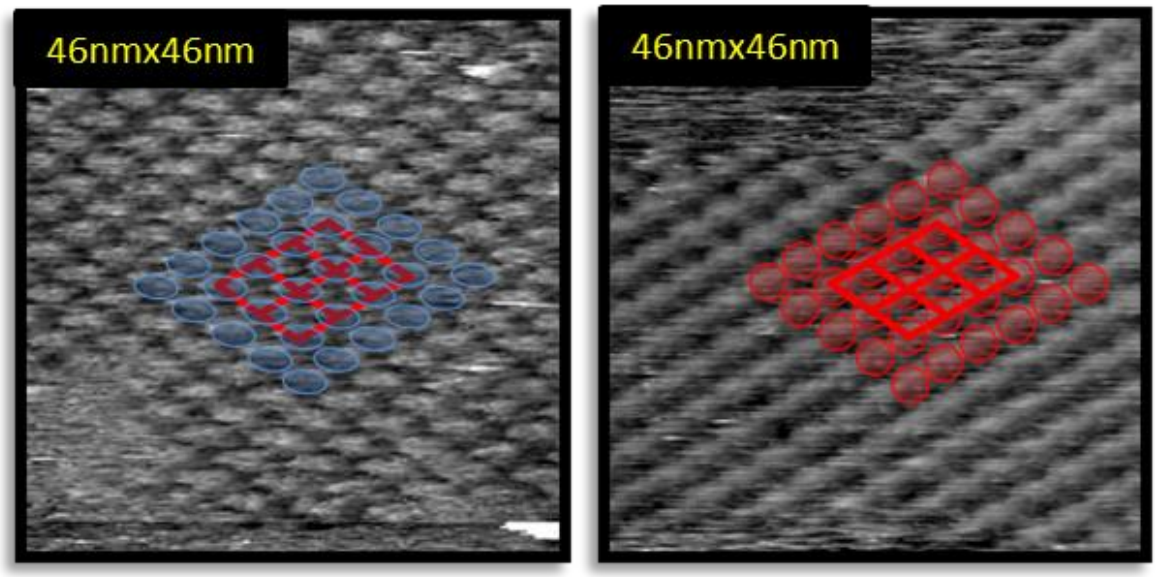

(a) **(b)**

Figure 4.1.1.5 STM images of **S2** monolayer at liquid-solid interface (HOPG-trichlorobenzene solution) observed for **(a)** positive, and **(b)** negative tip polarization (a) V_{bias}=1V, I_t = 0.8nA (b) V_{bias}= -1.1V, I_t = 2.5nA

The clear answer was obtained by carrying out an experiment which involved one-step switching of the tip polarization during scanning a single image. The representative result of this experiment is presented in **Figure 4.1.1.6 (a).** At first, image was recorded at 1V

(corresponding area of the image is indicated by A-B), and then the bias voltage was changed to -1.4V (C-D). This double bias experiment enabled to precisely determine the relative position of the bright spots observed in both cases. Based on theoretical calculations indicating separation of HOMO and LUMO orbitals in the investigated molecule it can be assumed that the bright spots observed for negative tip polarization correspond to the areas of naphthalene cores. They are marked in the image (**Figure 4.1.1.5 (b)** and **Figure 4.1.1.6 (a**)) by red circles. A crucial point is that these spots are located exactly in between two elongated spots observed with positive tip polarization (marked by blue ellipsoids in **Figure 4.1.1.5 (a)** and **Figure 4.1.1.6 (a**)). The different positions of both parts of the investigated molecule in monolayer allowed to propose geometry of the **S2** adlayer, that is consistent with STM images and in perfect arrangement with DFT calculations. The model is presented on **Figure 4.1.1.6 (b).**

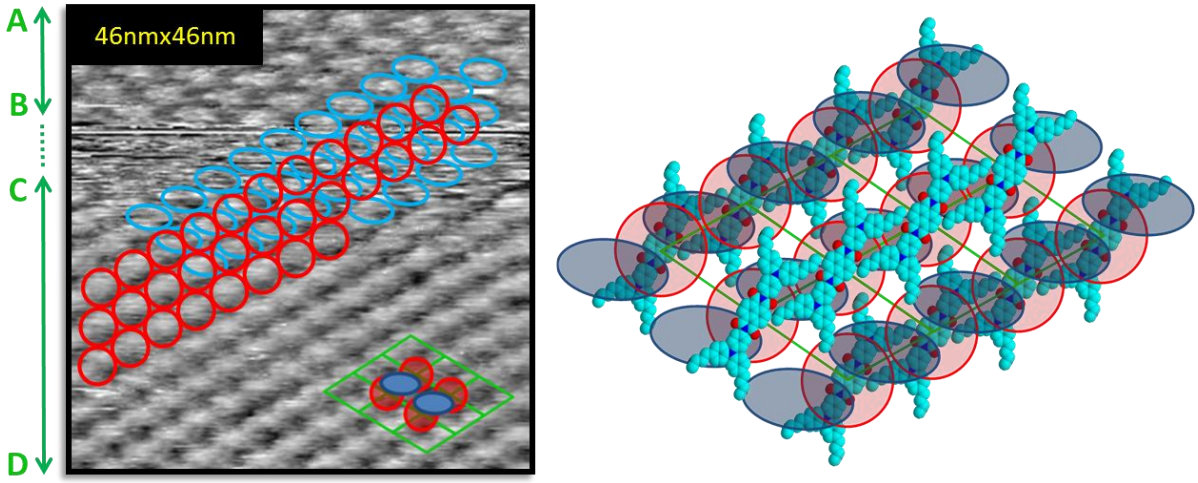

(a) **(b)**

Figure 4.1.1.6 (a) STM image and **(b)** postulated real space model of adsorption geometry of **S2** monolayer at liquid-solid interface (HOPG-trichlorobenzene solution) **(a)** image obtained with one step polarization switching from V_{bias}=1V (areas indicated as A-B) to -1.4V (C-D), I_t =0.8nA.

The third bisimide, **S3**, is characterized by the largest arylene core: perylene. Its 2D organization on HOPG is quite different to that one observed for **S2**. The monolayer of **S3** consists of randomly oriented molecular clusters instead of individual flat lying molecules (**Figure 4.1.1.7**).

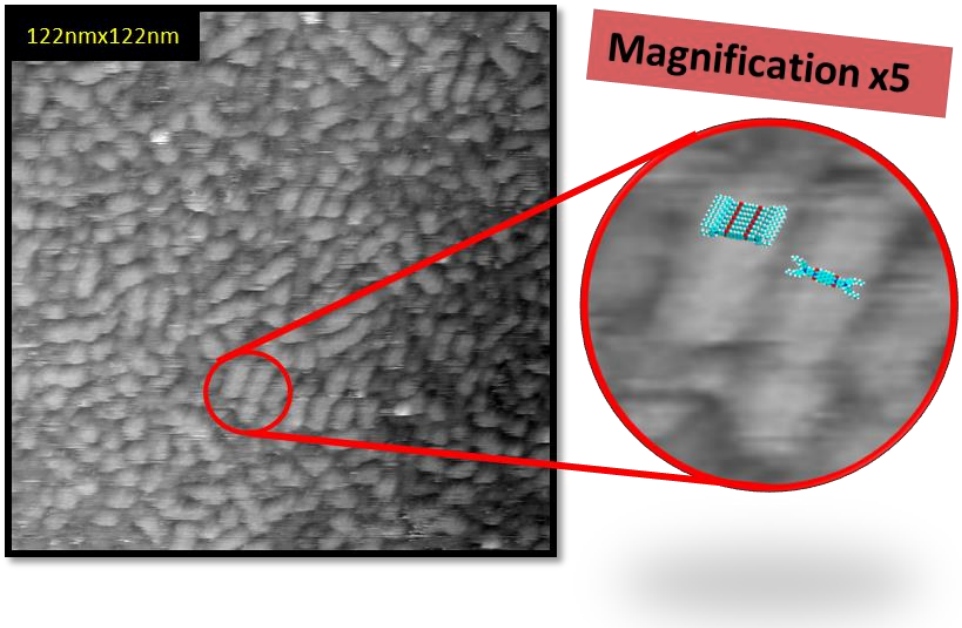

Figure 4.1.1.7 STM image of **S3** monolayer at liquid-solid interface (HOPG-trichlorobenzene solution) V_{bias}=1.2V, I_t =1nA.

Statistical inspection over large area of the film indicates identical width of all aggregates. Their width, about 4 nm, corresponds to the length of **S3** molecule in its fully extended conformation. This correlation suggests that molecules in clusters are π-stacked and oriented perpendicularly to longitudinal axis of the aggregates. It is interesting to emphasize, that this organization indicates different molecular orientation in space versus the substrate plane in comparison to **S2**. **S3** molecules in the layer do not lie flat, or nearly flat, on the substrate, as can be suggested for **S2** monolayer. Instead, **S3** molecules adopt edge-on position, i.e. they stand more or less perpendicularly to the substrate surface. Although the width of clusters remains constant, their length varies from less than four to dozen nanometers. Dissimilarities in size in this direction reflect differences in number of stacked molecules in clusters. At this point an interesting question arises whether stacking of molecules occurs on the substrate, or is it established in advance, in the solution? To assert this point the same investigations were performed with layer prepared from the solution diluted twenty times more in comparison to the already discussed monolayer. It was believed, that despite the smaller concentration, the way in which **S3** molecules interact with the substrate should not change. Therefore, if stacking occurred on the substrate surface, a similar or comparable clusters length should be observed regardless of the solution concentration.

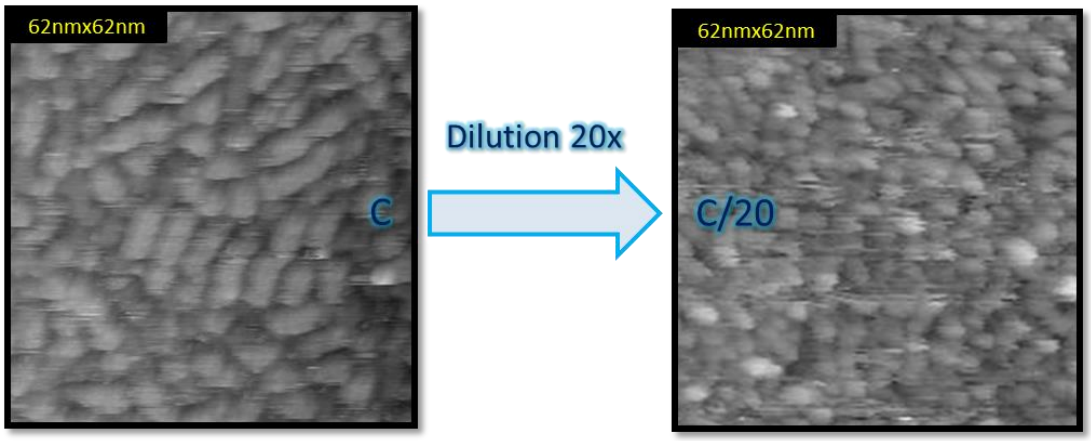

(a) **(b)**

Figure 4.1.1.8 STM images of **S3** monolayer at liquid-solid interface (HOPG-trichlorobenzene solution) obtained for different concentration of the solution **(a)** C=0.7μg/ml, V_{bias}=1.2V, I_t =1nA **(b)** C=0.035μg/ml, V_{bias}=0.8V, I_t =1nA.

Figure 4.1.1.8 compares STM images of both monolayers prepared. The clusters of the monolayer obtained from more diluted solution are evidently shorter, although their diameter remains the same. Shorter average length of molecular stacks rather suggests that self-organization of **S3** molecules is a complex, two-step process. Firstly it is performed in the solution where molecules are pre-organized in the form of π-stacked clusters. It is logical that the probability of stacking process in the solution increases with the size of conjugated cores of molecules due to the magnification of intermolecular interactions. Then, after deposition of the solution on the substrate surface, the process of adsorption and organization mainly concern whole stacks instead of individual molecules. The shorter length of the molecular stacks observed in the case of less concentrated solution is a result of smaller probability of stacking caused by higher dispersion of investigated molecules by the solvent.

To conclude this part of the discussion, it can be stated, that 2D organization of investigated bisimides is a result of coexistence and competition between two kinds of intermolecular interactions generated respectively by planar core and non-planar substituent units. The observed and presented above evolution of 2D organization with increase of the size of the molecular conjugated unit (series **S1-S3**) is a solid confirmation of this conclusion.

The first kind of two competing interactions is direct interaction between conjugated cores of the molecules which leads molecules to stack. Accordingly, an increase of the size of

the aromatic core of the molecules promotes the growth of this interaction influence. π-stacking tendency of molecular organization is however limited in the investigated adsorbates by triphenylamine substituents. These non-planar units located symmetrically in both sides of the molecules generate steric hindrance for direct interaction of aromatic cores. Moreover these groups due to their conformation significantly increase the number of possible structural configurations of the molecules adsorbed on the substrate surface what may impede well defined molecular organization. These are most possible reasons why derivative with smallest aromatic core (**S1**) does not order in the monolayer. It is a result of expected domination of substituents influence. On the other hand, interactions of both molecular parts are comparable, and therefore can effectively compete, in the case of **S2** derivative with larger naphthalene core. As a consequence, this larger derivative forms well-ordered monolayer of flat lying molecular cores versus the substrate surface. This situation is changed again with further increase of the aromatic part. In the case of derivative with largest perylene core the molecular tendency to stack is stronger and dominates over the influence of triphenylamines. Consequently **S3** molecules are stacked in the solution and are adsorbed in the form of pre-organized clusters instead of individual molecules.

Due to relatively weak abilities of the investigated semiconductors to form well-defined 3D structures, the evident evolution of 2D supramolecular organization with increase of the molecular conjugated core is much harder to observe in the case of 3D systems (powders, thin films and monocrystals). This is already valid for supramolecular organization in powders. This part of studies have been carried out and already published by Djurado at al.[2] before own investigations and is presented here for integrity of the discussion and comparison purpose. The corresponding diffraction profiles of a series of investigated molecules are compared in **Figure 4.1.1.9.** In general, the powder XRD measurements of all investigated molecules exhibit weak supramolecular organization. In the case of larger molecules (**S2** and **S3)** the diffractograms are similar to those typically obtained for smectic liquid-crystal like phases, with only a long interlayer period (or periods for **S3**) and a large halo distributed in a wide q range. A broad diffuse scattering of **S2** and **S3** centered around 1.4$Å^{-1}$ in q (4.7Å in d) reveals the presence of disorder in the powders. Narrow low angle Bragg peaks can be distinguished corresponding to periodicity 21.40Å for **S2**, and two periodicities: 23.47, 28.37Å for **S3,** respectively. The smallest derivative **S1** can be noted here as the sole representative of typical crystal among the

investigated compounds. Its powder diffractogram exhibits resemblance to a typical profile of a 3D crystalline substance, with the presence of peaks originating from various crystallographic planes (18.8 and 26Å).

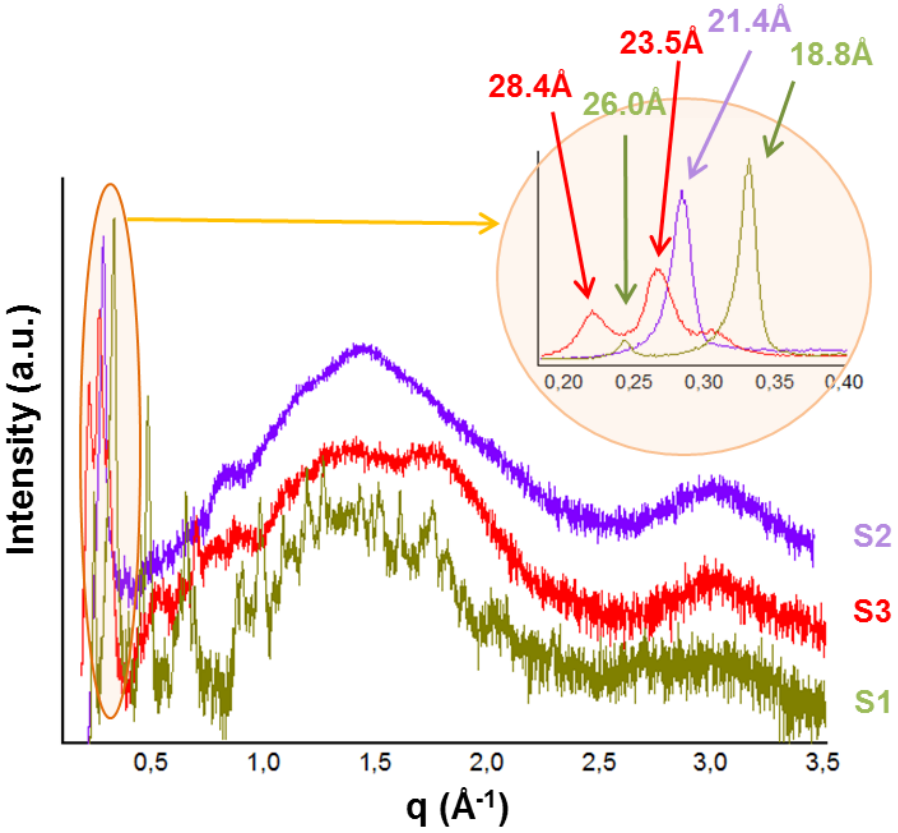

Figure 4.1.1.9 X-ray powder profiles of **S1**, **S2** and **S3.**

At this point it is interesting to remind supramolecular properties of pure triphenylamine, the molecule which corresponds to substituents of the investigated derivatives (**S1-S3**). Wu et al.[128] reported that this pure molecule self-organizes into well-defined structures in both single crystal and powders. As it is expected due to non-planar shape of the molecule these organizations are based on relatively weak intermolecular interactions. The experimental results reported in this paper clearly confirm this conclusion. The highly ordered structures of triphenylamine are as a consequence very sensitive to changes of environmental conditions including temperature and pressure. Coming back to investigations of arylene bisimide derivatives with two such substituents, one can state, that attendance of arylene core in the molecule impedes tendency of these derivatives to self-organize in powders in comparison to pure triphenylamine. Obviously this influence on supramolecular organization should increase with the size of this aromatic unit. This effect is exactly observed by comparison of structural properties of powders of the investigated three molecules. The trace of 3D crystal structure is only noted in powders of derivative **S1** with smallest arylene unit (benzene) for which influence of arylene unit is the weakest one. For

derivatives with slightly larger aromatic core (**S2** and **S3**) molecular orders show lower symmetry resembling to the organization typical of smectic liquid-crystal like phases. This behavior is not an exception since smectic-like powders of other PTCDI derivatives were already reported (exclusively for molecules with N-substituents consisting phenyl ring).[129-130] Another point which is worth to note is the negative correlation of molecular capabilities to form ordered structures in 2D and 3D systems. As it is observed from present comparison the derivatives which exhibit ordering in monolayers (**S2** and **S3**) hardly organize in powders and vice-versa (**S1**).

In Table 4.1.1.1 applied conditions for the layer preparation of the investigated molecules are collected. The studies include different: deposition methods (spincoating, dropcasting, zonecasting), substrates (SiO_2, glass, HOPG, gold), and solvents (1-phenyloctane, chlorobenzene). In general, in spite of various preparation conditions the layers of three investigated molecules were rather amorphous with in some cases very weak signal indicating molecular ordering. The summary of XRD measurements is presented in **Table 4.1.1.2**.

	dropcasting	**spincoating**	**zonecasting**
SiO2	1phenyloctane (various concentrations) Chlorobenzene (various concentrations)	1phenyloctane 10mg/ml Chlorobenzene 10mg/ml	No measurements
HOPG	1phenyloctane (various concentrations) Chlorobenzene (various concentrations	Chlorobenzene 10mg/ml	No measurements
glass	Chlorobenzene 10mg/ml	Chlorobenzene 10mg/ml	Chlorobenzene 10mg/ml (with exception of **S1**)
Au	No measurements	Chlorobenzene 10mg/ml	No measurements

Table 4.1.1.1 Deposition conditions for prepared layers of **S1**, **S2** and **S3**

	dropcasting	**spincoating**	**zonecasting**
S1 films	amorphous	amorphous	no measurements
S2 films	amorphous on HOPG, Au, SiO2 on glass – possible peak around 24Å	amorphous	peak at 20.4 Å
S3 films	bump (23Å - 28Å)	amorphous	bump (23Å - 28Å)

Table 4.1.1.2 3D organization of **S1**, **S2** and **S3**

The lack of molecular ordering is especially characteristic for thin films prepared by spincoating method (the film thickness determined by the presence of Kiessig fringes varied in this case between 17 and 23 nm). No corresponding signals were detected in these samples of all three molecules in spite of the fact that peaks from the substrates were perfectly distinguishable in the predicted positions. Moreover in the case of smallest **S1** derivative no molecular ordering was detected also in thicker films formed by dropcasting technique. It can be therefore concluded, that similarly to the case of monolayers, the layers of this smallest derivative are completely amorphous. It is interesting to add here, that own results fit with literature findings. Indeed, thin films of molecules in which the dominant structural part is driven by triphenylamine moieties are known to be glass-like, amorphous. [131-133]

The weak signals corresponding to molecular ordering were detectable in selected films of larger derivatives (**S2** and **S3**). Hence, results indicate that organization of these molecules depend on the preparation conditions.

S2 exhibits elements of molecular ordering in the layer when they are deposited on a glass substrate by both dropcasting and zonecasting techniques. In the former case, it is possible to distinguish not well defined peak around 21.2Å, and in the latter case, more distinct signal at 20.4Å. Both diffractograms together with **S2** powder profile are presented on the **Figure 4.1.1.10.** It is worth to note that observed **S2** tendency to crystallize is characteristic only for layers deposited on amorphous glass substrate (the corresponding films prepared on any different substrates were totally amorphous). Let's remind that chemical nature of glass surface corresponds to the surface of silicon covered with SiO_2, for which substrate no molecular ordering was detected. The important difference between both substrates concerns the surface topology. Hence the results show how supramolecular organization of

S2 molecule in the layer depends on surface defects of the substrate, which may act as active sites in the crystallization process.

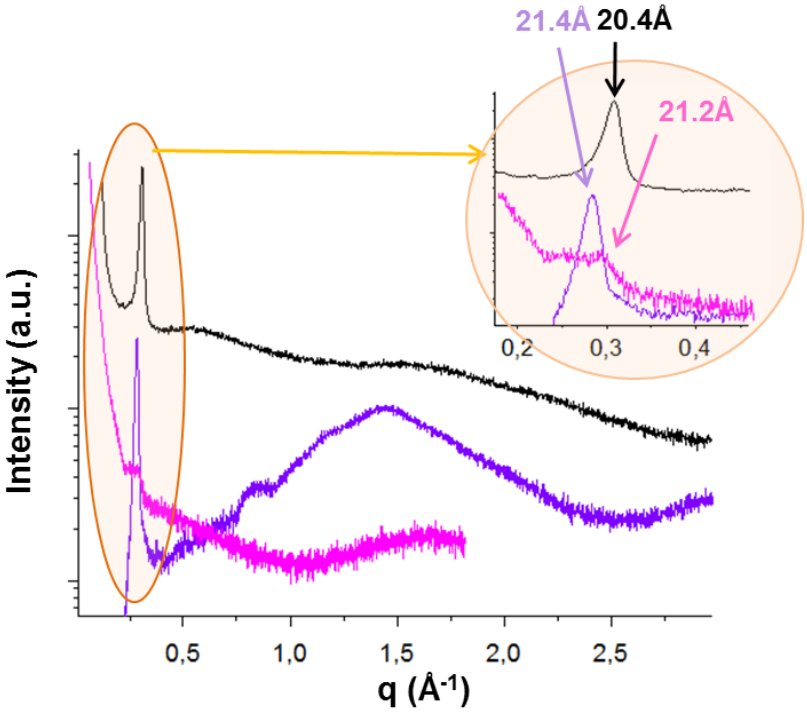

Figure 4.1.1.10 Comparison of XRD results obtained for **S2** layers: dropcasted (magenta), zonecasted (black). **S2** powder profile (violet) for comparison.

It can be noted here, that many authors report well-organized films of NTCDI analogues deposited on various substrates. [85,134-137] This tendency for molecular ordering is typical for naphtalene derivatives bearing pure alkyl substituents. On the other hand, NTCDI-analogues with phenyl ring as the direct N-substituent as a rule tend to be entirely less ordered in films (for the less branched substituents) or completely amorphous,[85] at least deposited on SiO_2.

Two comparisons are worth to discuss in the case of **S2**. The first one concerns small difference in the periodicities detectable for films obtained by different deposition methods (20 Å and 21 Å in the cases of zonecasting and dropcasting, respectively). One can wonder whether zonecasting, as the "directional" method of the film deposition could induce a greater tilt of molecules in the layers and smaller periodicity in the direction perpendicular to the substrate surface.

The second comparison concerns periodicities detectable in **S2** films and powder. It is interesting, that distances recognized in films are even smaller than observed in powder crystal grains. Typically, this relation is opposite, as the packing is usually denser in crystals. The observation may suggest different way of the chains organization in both 3D systems.

Finally the largest derivative **S3** exhibits again very weak effect of molecular organization in the layers. No substrate effect was observed for this molecule as was described for smaller analogue (**Figure 4.1.1.11**). Only for thicker layers (dropcasted or zonecasted) an amorphous bump between 0.22Å^{-1} and 0.28Å^{-1} in q (28.5Å - 22.7Å in d, 3.59° - 4.23° in 2θ) could be distinguished at low angles. This can be interpret as some very weak trace of molecular ordering in a direction perpendicular to the substrate plane, although it is never well defined.

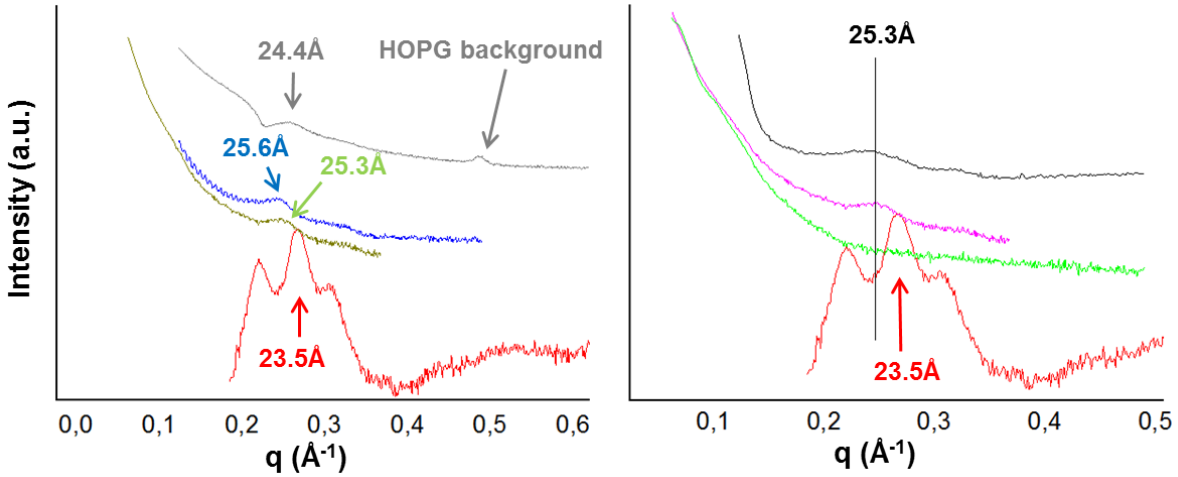

Figure 4.1.1.11 Comparison of XRD measurements between: **(a) S3** dropcasted on various substrates: HOPG (grey), SiO_2 (blue), glass (green), **S3** powder profile (red), and **(b) S3** deposited on glass: spincoated (green), zonecasted (black), dropcasted (magenta), **S3** powder profile (red).

Hence, it is time to summarize the investigations on the influence of central unit on organization of the investigated family of arylene bisimides. It is important to state in view of both STM and XRD results, that the size of the molecule core influences the final structure both, in 2D and in 3D. For **S1** we can note excessive disproportion between the structural influence of triphenylamine substituents to benzene core with favor of the first one. That leads to formation of amorphous 2D monolayers as well as 3D films and typical crystalline powder (features also characteristic to pure triphenylamine,[128] and other reported DAD derivatives with small benzene core, similar to **S1**[138]). In the case of **S2** molecule, the influence of both structural factors (core and substituents) seems to be balanced. Particularly, **S2** as the sole representative of the S-series was found to create organized monolayer in 2D. Also, its 3D films (although limited to glass substrate) tend to

exhibit the highest level of arrangement among three molecules under study. By contrast, **S3** with perylene core manifested strong core influence on the final structure. The clearest display of this influence was observed in 2D, as **S3** organized itself into π-stacked clusters randomly dispersed on HOPG substrate. Although own results do not directly confirm π-stacking in 3D systems, the careful literature investigations proved, that columnar π-stacking exist for similar PTCDI analogues, for whose direct N-substituent consists phenyl ring (the powder diffractogram of such analogues is also smectic-like).[129-130] Additionally, **S3** thin films, despite not being well organized, display an interlayer period which may indicate that the multilayers are simply an multiplication of monolayers.

To conclude, it would be instructive to correlate at the end of this chapter the ordering of the molecules with macroscopic electronic properties of formed structures.

All three molecules were tested in the field effect transistors (fabricated on a poly(ethylenenaphtalene) substrate, using gold (source and drain) and silver (gate) electrodes, and a CYTOP (Asahi glass, Japan) dielectric layer. Organic films (of **S1**, **S2** and **S3**) were spincoated from a chloroforme solution (concentration 7mg/ml, spin speed of 600rpm during 20s) reaching thickness of about 100nm. Despite investigated molecules design, which is based on direct assembly of parts of opposing electronic character, no ambipolar behavior have been found in the fabricated transistors. However, they showed field effect in p-channel configuration, what implied, that carriers transport occurs in majority via triarylamine parts.

How does it can be related to self-organization of these semiconductors?

Own studies clearly indicate that thin layers of investigated bisimides obtained by spincoating method, i.e. the same technique which is usually used for preparation of organic layers for OFETs and conductivity measurements, are completely amorphous. The strong difficulties of these molecules to form ordered layers are related to the presence of triphenylarenes substituents which, as independent molecules, usually does not crystalize in films. It is well known that in the case of arene bisimides molecular ordering plays a crucial role in charge carrier mobility in the layers in macroscopic scale.[139] Usually high mobilities of electrons (n-type conductivity) are obtained for these semiconductors when the layers consist of highly oriented crystallites.[140] On the other hand, this dependence is much less important for aryl amines, including cyclic triarylamines, for which correct mobilities of holes (p-type conductivity) are noted for thin amorphous layers.[141] It can be

therefore concluded, that the lack of ambipolar behavior of the investigated derivatives is directly related to the layer structure. Presence of three-dimensional triphenylamine N-substituents prevents organization of molecules in the layers which selectively hinders electron mobility. As a consequence the formed layers exhibit holes conductivity (p-type) via triarylamine substituents which is less dependent on molecular organization. This example clearly confirms importance of supramolecular organization on the type of conductivity of organic electroactive layers.

4.1.2. Influence of molecular symmetry

In this section, I focus on 2D organization of new derivative of napthalene bisimide, denoted by **As2**, asymmetrically substituted at N position with only one triphenylamine substituent on the one side and with linear octyl chain on the other side.

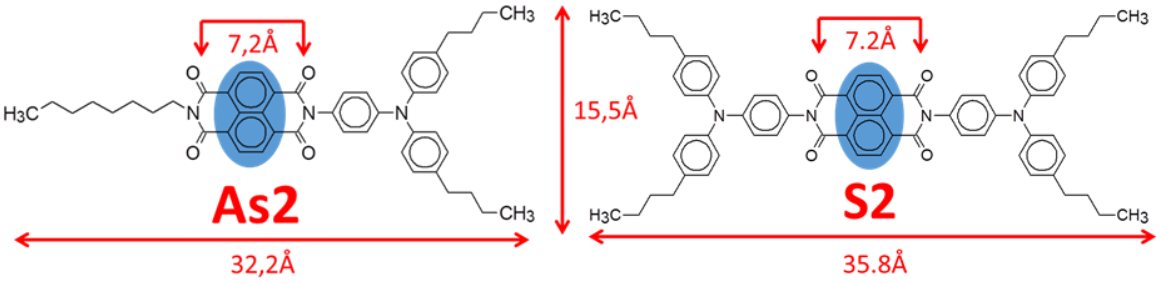

Figure 4.1.2.1 Studied arylene bisimides

Generally, asymmetry of the molecule can be treated as a factor which decreases molecular ability to form homogenous layers of well-ordered supramolecular structure. One argument in favor of this statement, coming from simply geometrical point of view, is that asymmetrical molecule can adopt many more possible arrangements in supramolecular systems. The obtained information about self-organization of **As2** asymmetric derivative will be discussed in the light of organization of symmetrical analogue discussed in the previous section (derivative **S2**). The sizes of both derivatives are comparable. The main difference concern molecular symmetry induced by the types of molecular substituents. Hence, the comparison provides information about the significance of molecular symmetry in self-organization of this family of organic semiconductors.

It is important to remind that, similarly to its symmetrical analogue, **As2** is also characterized by separation in space of frontier orbitals: HOMO is located on the triphenylamine substituent, while LUMO on the napthalene core.[89] Both molecules can be therefore considered as hybrids of electron donating and electron accepting moieties linked together by a covalent bond. As a consequence, different symmetry of both derivatives induces analogous differences in the molecular electronic structure (which is symmetrical and asymmetrical for **S2** and **As2**, respectively).

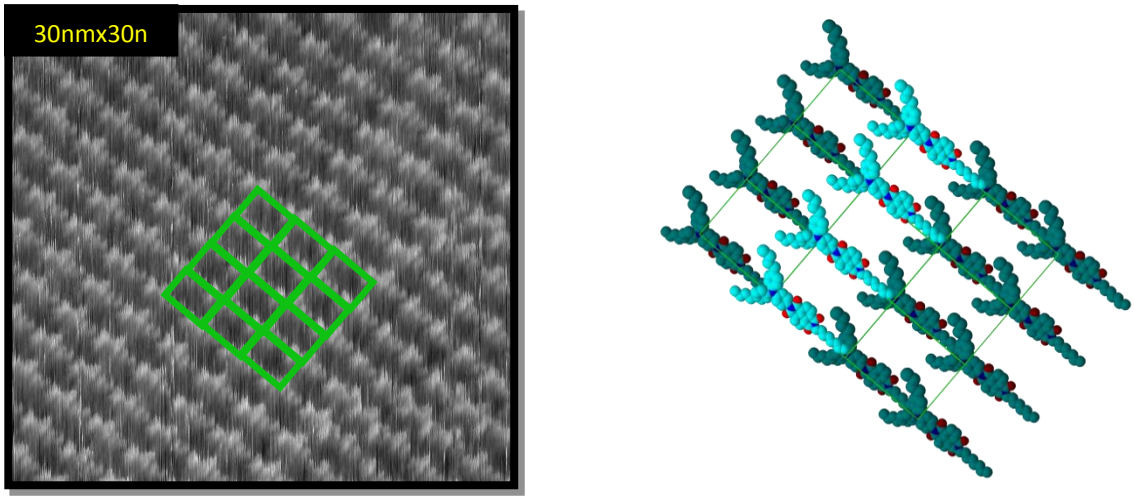

(a) **(b)**

Figure 4.1.2.2 (a) STM image and **(b)** postulated real space model of adsorption geometry in **As2** monolayer at liquid-solid interface (HOPG-1-phenyloctane solution) (V_{bias}=0.8V, I_t =0.8nA).

Figure 4.1.2.2 presents **(a)** STM image of **As2** monolayer and **(b)** corresponding model of adsorption geometry. The layer surface is visible as a set of parallel bright stripes. Therefore, in spite of asymmetrical shape of this adsorbate, its monolayer exhibits high order and well-packed supramolecular organization. The unit cell parameters determined from STM measurements are: **3.2 ± 0.1nm, 2.3 ± 0.1nm, 90° ±2°**. Some distinct differences between organizations of this derivative and symmetrical analogue are therefore distinguished. The monolayer of asymmetric **As2** derivative is denser which is manifested by slightly smaller dimensions of the unit cell. However the main and evidently observed difference concerns symmetry of both organizations. Contrary to hexagonal unit cell determined for monolayer of **S2** (symmetrical) derivative, the organization of asymmetrical analogue **As2** exhibits two-fold symmetry. This can indicate stronger adsorbate-adsorbate interactions in comparison to the adsorbate-substrate ones. Based on these observations one can conclude about relatively weak influence of the substrate surface on the organization of this asymmetric molecule. However, it is worth to point that a slide effect of the substrate topology can be observed in this monolayer. Inspection of large areas indicates that **As2** monolayer is a set of coexisting large domains of different orientations (**Figure 4.1.2.3**).

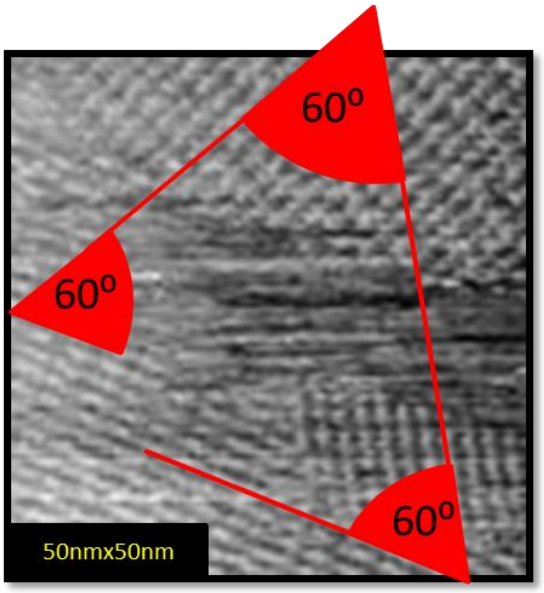

Figure 4.1.2.3 STM image of **As2** monolayer at liquid-solid interface (HOPG-1-phenyloctane solution) (V_{bias}=0.8V, I_t =0.8nA)

They are rotated with respect to each other by 60 degrees, which correlates with three-fold symmetry of HOPG plane. This coincidence can be explained by affinity of linear alkyl substituent (octyl chain) located on one side of the asymmetric **As2** molecule to the substrate surface. It is expected that this chain should be adsorbed along one of the graphite axes imposing orientation of adsorbed molecules and whole molecular domains. Such preferential orientation is frequently observed in the case of saturated linear hydrocarbons on HOPG,[142] as well as, alkyl substituents of larger adsorbates.[19] Obviously this kind of the substrate influence does not occur for symmetrical derivative (**S2**) since it consists in two non-planar substituents (triphenylamine).

Careful inspections of images at higher resolution (**Figure 4.1.2.2 (a)**) show internal structure of each stripe which consists a set of two bright spots occurred periodically. It is worth to remain at this point, that STM contrast is determined by two coexisting factors: pure geometry, and electronic factor resulted from differences on the surface in local conditions of tunneling process (density of electrons and work function). The presented images were obtained for positively polarized tip (+0.8 V), i.e. when electrons tunnel from the molecule to the tip. This means that observed contrast should be related to localization of HOMO orbital. Based on DFT calculations indicating discussed above separation of HOMO and LUMO orbitals in **As2** molecule it can therefore be postulated that bright spots are related to triarylamine substituents. The proposed model of **As2** self-assembly, consistent with this interpretation, is presented in **Figure 4.1.2.2 (b).** Moreover, the size of unit cell indicates, that the molecule cannot adopt most extended configuration. As a

consequence this linear alkyl substituent must partially overlap triarylamine segment of the adjacent molecule in the molecular row. Such effect was previously reported also for organization of another related compounds.[143-144]

Finally it is worth to note that discussed submolecular contrast is locally perturbed. In these places only one bright spot instead of two is seen (areas marked by green arrows in **Figure 4.1.2.4**). This seems to indicate an effect of geometrical factor on the image contrast as the twisting of the phenyl rings in the triphenylamine substituent can locally vary.

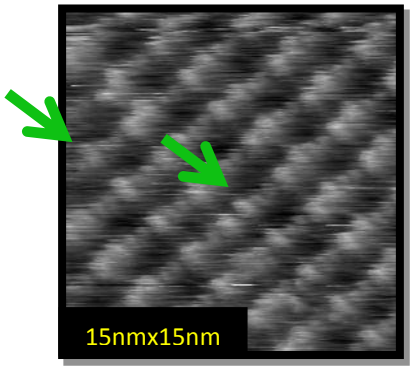

Figure 4.1.2.4 STM image of **As2** monolayer at liquid-solid interface (HOPG-1-phenyloctane solution) (V_{bias}=0.8V, I_t =0.8nA).

3D crystalline structure of **As2** is also different in comparison to the organization of symmetric analogue. Let's remind that powder diffractogram of symmetrical **S2** gives a profile somehow characteristic of a liquid-crystal smectic-like phase. In contrast, **As2** powder is crystalline, yielding diffractograms with well-defined Bragg reflections (see **Figure 4.1.2.5**).

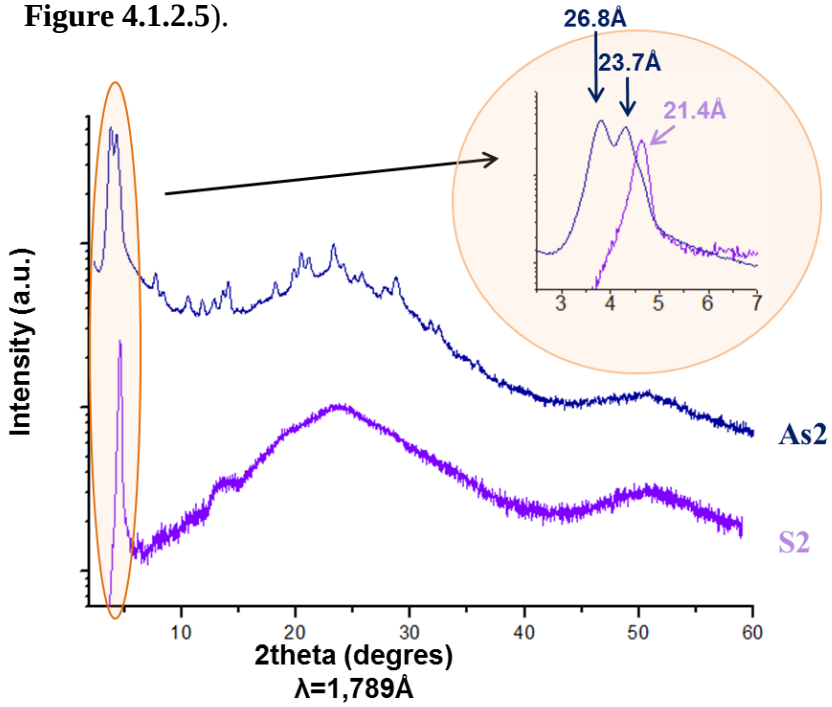

Figure 4.1.2.5 X-ray powder profiles of **S2** and **As2**

Notably, and also in contrast to the totally amorphous layers of symmetrical derivative, thin films of **As2** deposited on the used substrates exhibit periodic structures. **Table 4.1.2.1** presents deposition conditions for the preparation **As2** layers.

As2	**dropcasting**	**spincoating**	**zonecasting**
SiO2	Chlorobenzene 10mg/ml 1phenyloctane (various concentrations) DMF 50 mg/ml	Chlorobenzene (various concentrations)	No measurements
HOPG	Chlorobenzene 50mg/ml	Chlorobenzene (various concentrations)	No measurements
glass	Chlorobenzene 10mg/ml	Chlorobenzene 50mg/ml	Chlorobenzene 50mg/ml

Table 4.1.2.1 Deposition conditions for prepared layers of **As2**

In each case, a periodicity in the direction perpendicular to the substrate plane was observed. In **Table 4.1.2.2** positions of 001 peak (without any additional peaks, characterized as members of the same family) obtained for different deposition conditions are compared, while **Figure 4.1.2.6** shows representative five selected diffraction patterns, in which the presence of extreme peaks can be observed.

As2	**dropcasting**	**spincoating**	**zonecasting**
SiO2	32.8 Å 29.5 Å 28.9 Å 24.8 Å 23.1 Å	27.8 Å 24.8 Å 23.1 Å	No measurements
HOPG	32.8 Å 29.4 Å	24.6 Å	No measurements
glass	27.7 Å	27.8 Å	27.8 Å

Table 4.1.2.2 001 peaks obtained for different deposition conditions for prepared layers of **As2**

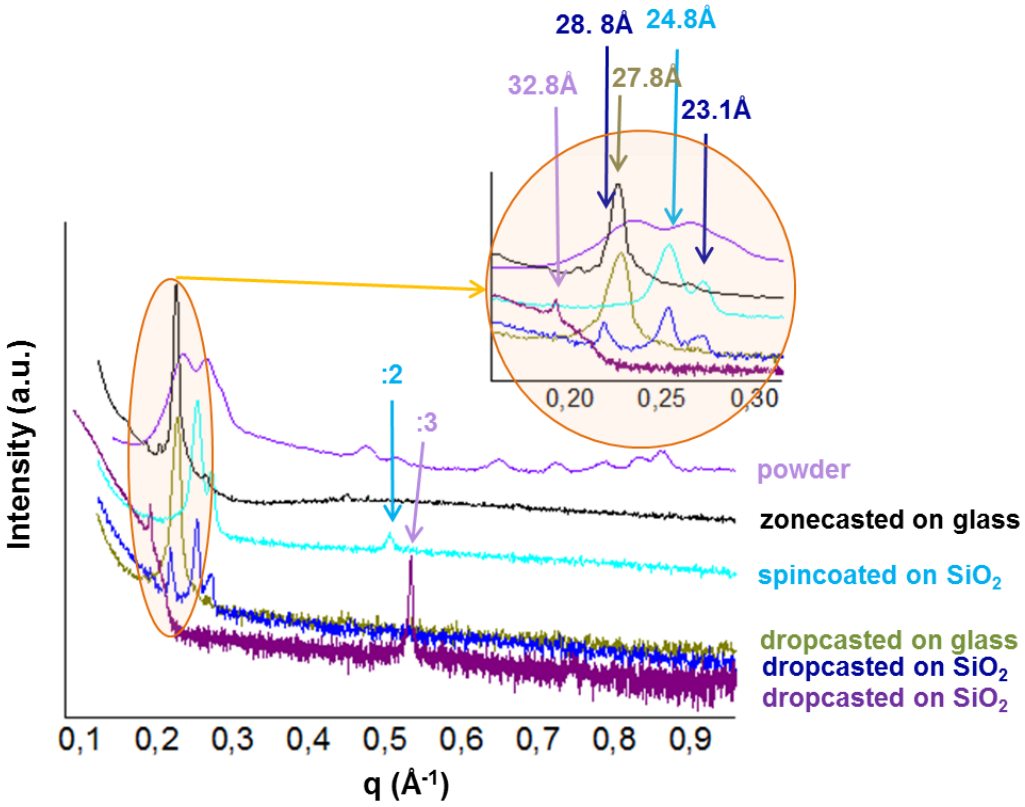

Figure 4.1.2.6 Selected thin-layer diffractograms of **As2** deposited on various substrates from chlorobenzene solution obtained using different deposition methods.

Statistical inspection shows especially large number (5) of different positions of 001 peak for films deposited on SiO_2. Usually, in these preparation conditions each sample was characterized by up to three unrelated periods. This observation can suggest a presence in the film of several domains of various molecular arrangements versus the substrate plane. It is interesting to point out, that all periods obtained by XRD for thin films and powder are in the range of two extreme molecule-molecule distances determined by STM for monomolecular layer (these distances 3.2 nm and 2.3 nm correspond to dimensions of 2D unit cell). Unfortunately, it was not possible to clearly correlate periodicities determined for thin films with the preparation conditions.

To summarize, own results evidently indicate that asymmetrical derivative **As2** exhibits stronger tendency to self-organize in powder and thin films in comparison to symmetrical **S2**. It is worth to note, that **As2** applied in thin layers as active material in the field effect transistors shows attractive ambipolar properties (whereas its symmetrically disubtituted **S2** analogue behaves like a p-type semiconductor).[89] It is known that lack of molecular

ordering in thin films leads to significant decrease of electron mobility at microscopic scale.[140] This is a further confirmation that a large extent of supramolecular ordering of donor-acceptor molecules is essential for obtaining ambipolar conductivity in OFETs.

4.1.3. Influence of alkoxy chain length.

In this section, 3D organization of new naphthalene bisimides containing alkoxyphenyl substituents will be discussed. Comparison of results obtained for series of three derivatives with alkoxy chains of different length enabled to analyze influence of the length of this substituent on supramolecular organization. The molecules under studies are presented in **Figure 4.1.3.1.**

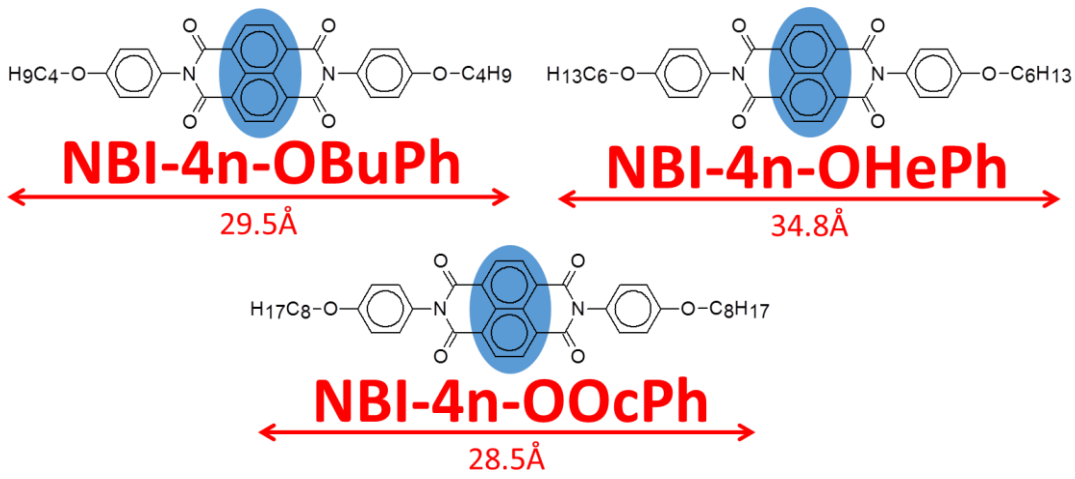

Figure 4.1.3.1 Studied naphthalene bisimides with aloxyphenyl N-substituents of different length.

The discussion is started from molecular organization in single crystals. In **Figure 4.1.3.2** the crystals packings projected in the (*b*-*c*) plane of three molecules are compared. The corresponding unit cell parameters are presented in **Table 4.1.3.1**.

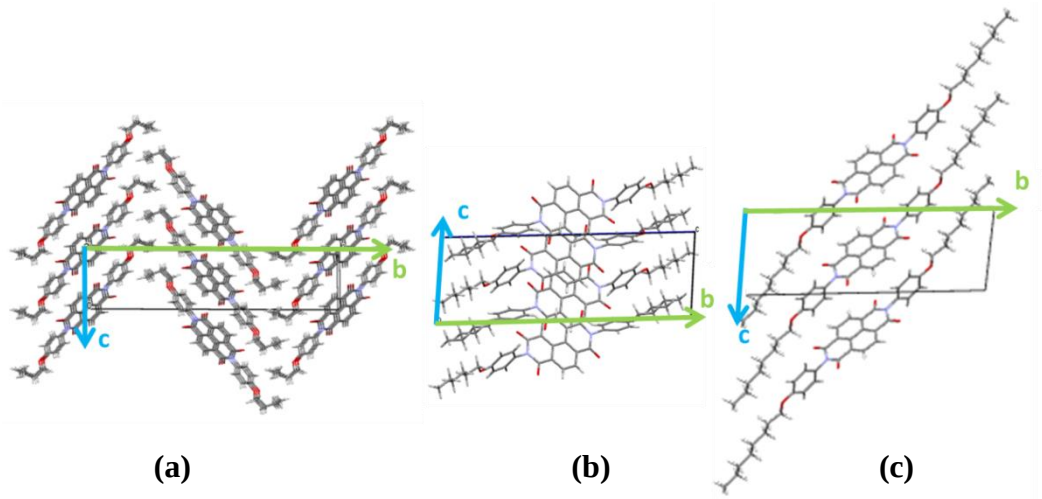

(a) **(b)** **(c)**

Figure 4.1.3.2 Projections in the (*b*-*c*) plane of crystallographic structures of **(a) NBI-4n-OBuPh, (b) NBI-4n-OHePh, (c) NBI-4n-OOcPh**.

	Crystal system	**Unit cell dimensions**					
		a	**b**	**c**	**α**	**β**	**γ**
NBI-4n-OBuPh	Monoclinic	5.04 Å	33.74 Å	7.99 Å	90°	100°	90°
NBI-4n-OHePh	Triclinic	8.44 Å	24.01 Å	8.89 Å	89.1°	62.8°	80.5°
NBI-4n-OOcPh	Triclinic	5.23 Å	22.37 Å	7.62 Å	96.4°	100.3°	95.1°

Table 4.1.3.1 Unit cell parameters of **NBI-4n-OBuPh**, **NBI-4n-OHePh**, and **NBI-4n-OOcPh** single crystals.

The derivative with the shortest alkyl substituent (**NBI-4n-OBuPh)** crystallizes into P21/c monoclinic space group. **Figure 4.1.3.3 (a)** presents the projection of the crystal structure in *b*-*c* plane. The molecules are organized into herringbone motif. This organization, typical for non-substituted oligoacenes, is characterized by two different molecular orientations. Hence, the molecules in adjacent rows are alternatively oriented versus *c*-axis by ±41° (it corresponds to angle ±49° in respect to *b*-direction). The projection of the crystal structure in *a*-*b* plane is presented in **Figure 4.1.3.3 (b)**. For clarity, only molecules contained in one (*a*-*c)* plane are drawn. As it can be clearly observed the planes of conjugated cores of all molecules (naphthalene bisimides part) are oriented in the same way, perpendicularly to this projection. It indicates π-stacking in *a*-*b* plane. The distance between two following molecules in the same row is smallest along the *a*-axis and equal to 5 Å. This separation is larger in c-direction (8 Å). The phenyl rings of N-substituents of the molecule are rotated in the crystal versus naphtalene plane by 79°. Moreover, the structure

indicates, that butyl chains are not totally planar. Only two carbons of each butyl chain which are closer to molecular backbone are in the same plane as phenyl rings.

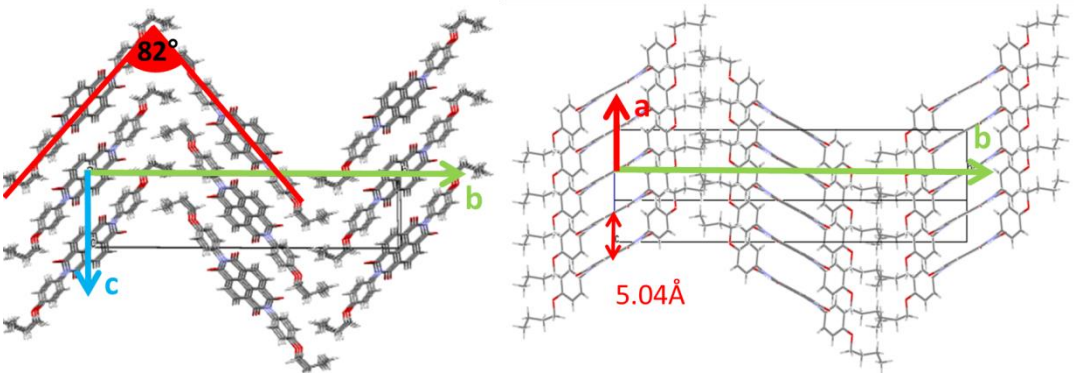

(a) **(b)**

Figure 4.1.3.3 Projections of crystallographic structures of **NBI-4n-OBuPh** in the **(a)** *b*-*c* plane, **(b)** *a*-*c* plane.

The derivative **NBI-4n-OHePh** with longer hexyl substituents crystallizes into a triclinic structure with P1 space group (**Figure 4.1.3.4**). In this case, all molecules are oriented in the same direction. The molecular backbones lie perpendicularly to *a* axis, their longitudinal axes are tilted versus c-direction by 69° and 48° in *b*-*c* and *a*-*c* planes, respectively. Additionally, these conjugated parts of adjacent molecules in stacks (along *a*-axis) are slightly shifted relatively to each other in *b*-direction which results in a shorter stacking distance of 4.2 Å (parameter *a* divided by 2). The molecules are not fully planar in the crystal structure, as N-substituted phenyl rings are twisted out of the naphthalene plane. However, this angle of internal torsion is not the same in opposite sides of the molecule. It is alternatively equal to 58° (the units marked in orange in the presented projections) or 72° (units marked in blue). As a consequence, two consecutive molecules in one molecular row (along *a*-direction) are differently arranged in space. Hence, although **NBI-4n-OHePh** favors regular organization instead of herringbone, its crystal structure is also characterized by two different molecular rows and, as a consequence, the unit cell contains two independent molecules.

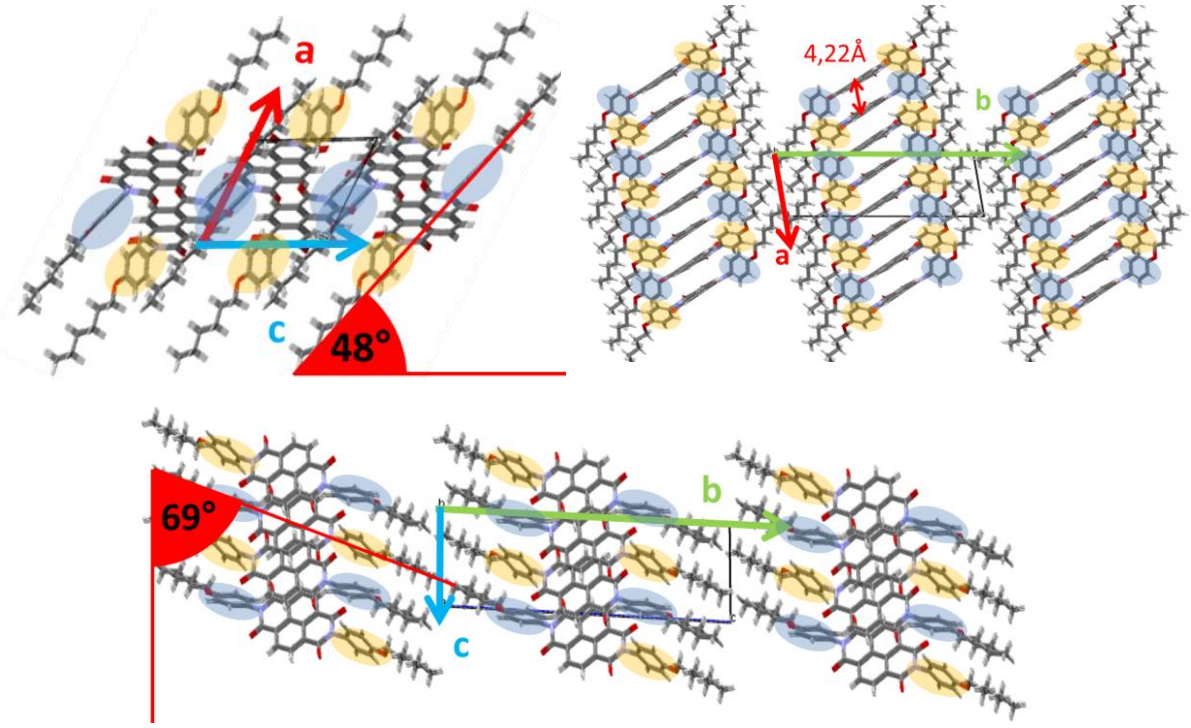

Figure 4.1.3.4 Projections of crystallographic structures of **NBI-4n-OHePh**

The biggest derivative, with octyl substituents, **NBI-4n-OOcPh** also forms crystals of triclinic structure (P1 space group). The interactions between longer alkyl chains impose the same, relatively extended conformation of the molecules as was observed in the case of the crystal of smaller analogue (**NBI-4n-OHePh**). The projections of corresponding crystallographic structure are presented in **Figure 4.1.3.5**. **NBI-4n-OOcPh** crystal is characterized by one molecular orientation with a tilting angle of 45° versus the *c* axis in *b*-*c* plane. The stacking of molecules is realized in such a way, that conjugated core and phenyl substituents alternatively face each other. The closest distance between conjugated cores of molecules in one row is 5.2Å. It is slightly larger in comparison to the stacking separation observed for smaller **NBI-4n-OHePh** molecule. The distance which characterizes the organization of this biggest derivative is a result of the phenyl ring orientations versus naphthalene core. Contrary to alternative tilts of these rings observed for organization of smaller analogue, these groups from both sides of this biggest derivative are rotated by the same angle (106°) with respect to the plane of molecular backbone. Moreover, the terminal alkyl substituents are in the same plane as phenyl rings. As a consequence of the same space arrangement of all molecules, the unit cell of this structure contains only one independent molecule.

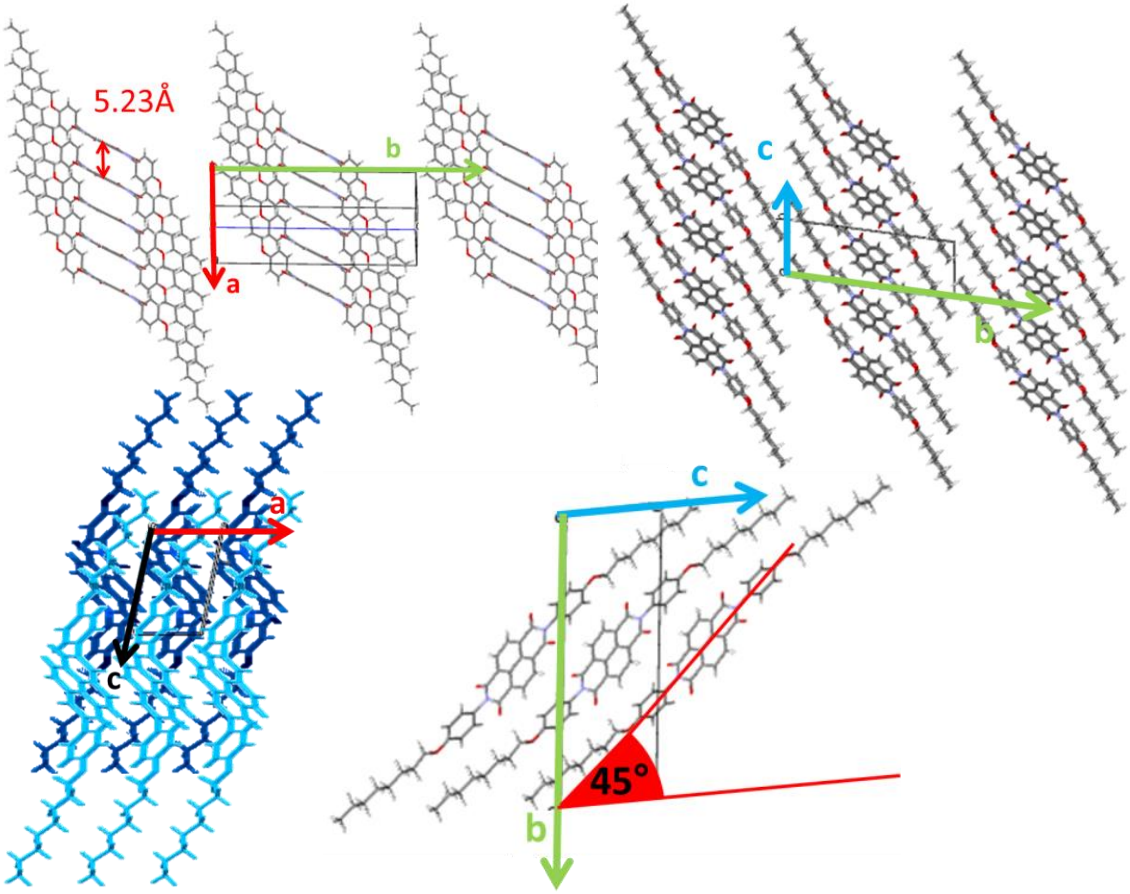

Figure 4.1.3.5 Projections of crystallographic structures of **NBI-4n-OOcPh.**

To summarize this part, it is well recognized, that the nature of side chains greatly affects the solid state packing. If these substituents are absent, e.g., in cases of non-substituted oligo-acenes, -thiophenes, or -phenylenes, the typical packing structure in crystals consists of the "herringbone" motif in which the molecules are mutually oriented more or less edge-to-face in two-dimensional layers and π-stacked in the third dimension. Lateral alkyl groups are expected to disrupt the herringbone packing pattern since a strictly edge-to-face packing is not possible if long alkyl side chains are present. Therefore, crystallization promotes the "lamellar" structure, in which chains maximize their mutual van der Waals interactions.

The structures of powders of the investigated series of molecules are well correlated with organization in single crystals, described above. The representative powder diffractogram profiles are presented in **Figure 4.1.3.6** for **NBI-4n-OHePh**, **NBI-4n-OOcPh** and in **Figure 4.1.3.7** for **NBI-4n-OBuPh**.

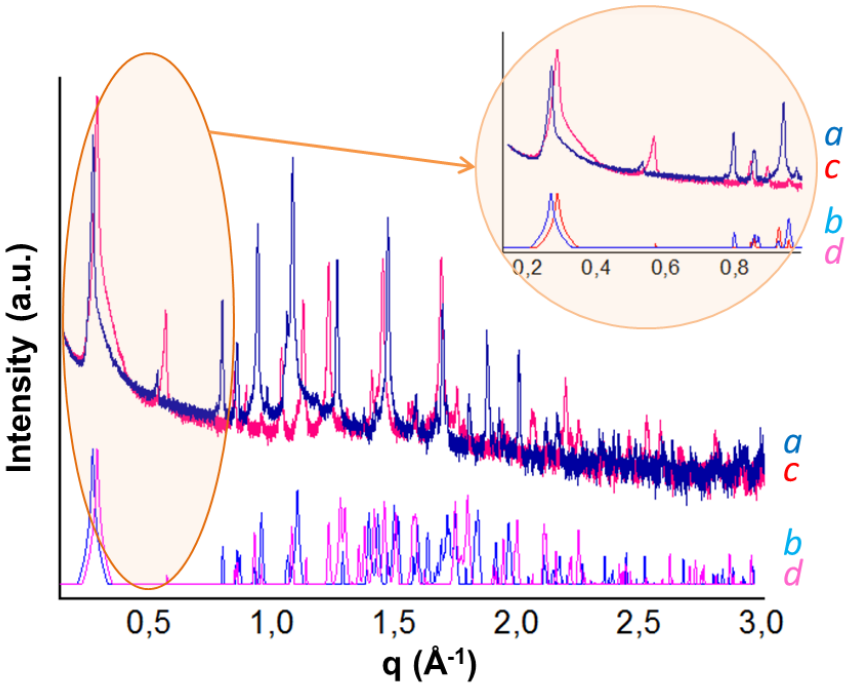

Figure 4.1.3.6 Comparison of: (**a**-dark blue) measured **NBI-4n-OHePh** powder profile, (**b** - light blue) **NBI-4n-OHePh** powder profile calculated from single crystal data, (**c** - red) measured **NBI-4n-OOcPh** powder profile, (**d** - pink) **NBI-4n-OOcPh** powder profile calculated from single crystal data.

In the case of the first two derivatives, powder diffractogram profiles fit well the corresponding ones calculated from the single crystal data. Hence, the identification of peaks in all powder profiles have not encountered any difficulties. The small shifts in the peaks positions are due to the fact that the measurements of single crystals have been performed at lower temperature (150K) in comparison to room temperature of powder measurements. In the case of smallest derivative **NBI-4n-OBuPh** powder diffractogram profile (**Figure 4.1.3.7**) contains one additional low angle Bragg peak which is not calculated from the single crystal structure (marked by star). It has been possible to separate two components in the powder when trying to grow single crystals. The additional peak which occurs only in powders, comes from a second phase which disappears during the formation of single crystals.

Table below the graph (**Table. 4.1.3.2)** gathers various conditions for the preparation of thin layers of the investigated semiconductors. The changing parameters are: deposition method (spincoating, drop casting), substrates (SiO_2, glass, gold, HOPG) and, in some cases, solvent (chloroforme, DMF, dichlorobenzene).

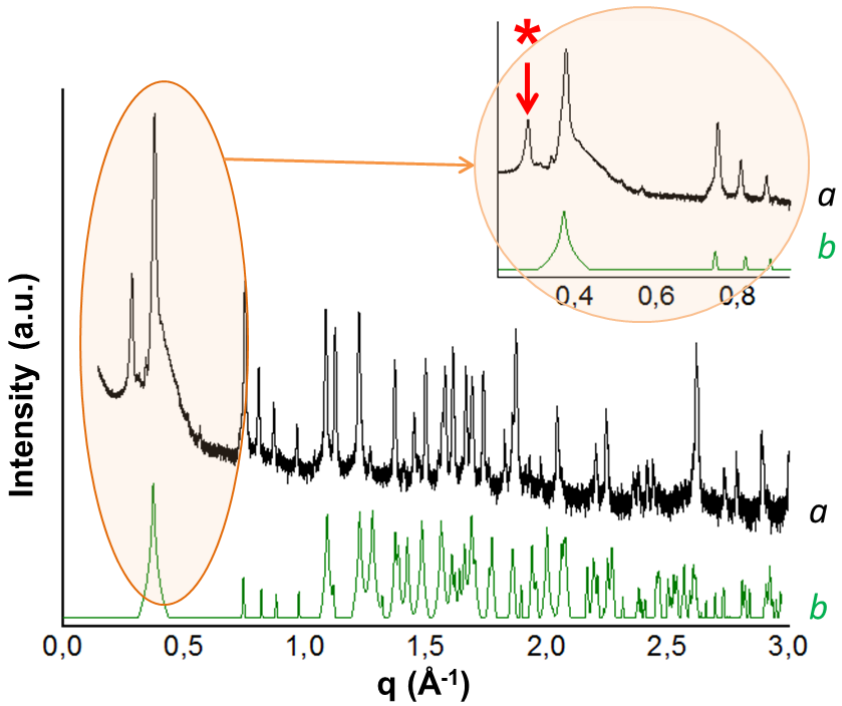

Figure 4.1.3.7 Comparison of **NBI-4n-OBuPh** powder profiles: (a - black) measured, (b - green) calculated from single crystal data.

	Dropcasting	**spincoating**
SiO2	Chloroforme 10mg/ml DMF saturated Dichlorobenzene saturated	Chloroforme 10mg/ml Chloroforme 5mg/ml Chlorobenzene saturated
HOPG	No measurements	Chloroforme 10mg/ml
glass	Chloroforme 10mg/ml	Chloroforme 10mg/ml
Au	No measurements	Chloroforme 10mg/ml

Table. 4.1.3.2 Deposition conditions for layers preparation of NBI-molecules.

An interesting effect of the layer thickness on supramolecular organization have been observed for **NBI-4n-OBuPh**. It can be illustrated, by comparing thin, spincoated layers of this molecule (under 20 nm thick, whose diffractogram is presented in **Figure 4.1.3.8 (a)**) with thicker layers (**Figure 4.1.3.8 (b)**). For the layers under 20 nm thick (as confirmed from FWHM value of the peaks and by applying the Sherrer formula), irrespectively of the substrate or the solvent used, one broad peak centered at 25Å is noted. It is worth to mention here, that the length of **NBI-4n-OBuPh** molecule measured as a distance between

two hydrogen's in terminal methyl groups in a single crystal structure is also 25Å. This correlation suggests, that thin layer consists of crystallites in which the molecules stand almost perpendicular to the substrate plane (**Figure 4.1.3.9 (b)**). For thicker layers (see **Figure 4.1.3.8 (b)**) made by either dropcasting technique, or by spincoating technique (but with slower spinning rate 500 rpm instead of 2000 rpm) additional peak at 19.4 Å is also noted (this periodicity does not correspond to any of identified peaks in powder profile). The period of 19.4 Å can be interpreted as originating from crystallites in which the **NBI-4n-OBuPh** molecules are tilted by ~50° to the substrate plane (projection of this molecule on a direction perpendicular to the *b* axis yields 24Å *sin 50° = 19.1Å. It is worth to notice here, that this is very similar tilting angle to the one noted for one of two independent molecules with respect to b-axis in a single crystal structure (49°, **Figure 4.1.3.3)**. Thus, it can be concluded that thick layers of **NBI-4n-OBuPh** is a mesh of crystallites of two different orientations versus the substrate plane (**Figure 4.1.3.9)**. The height if crystallites presented in **Figure 4.1.3.8 (b)** amounts to 22nm for spincoated sample and over 200nm for dropcasted ones (confirmed from the FWHM value of the peaks and by applying the Sherrer formula).

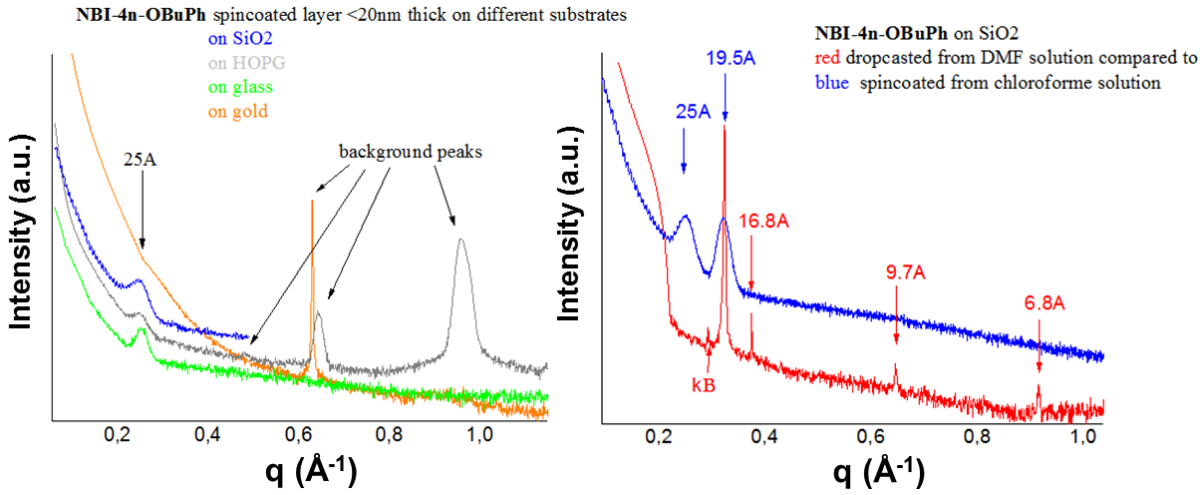

(a) **(b)**

Figure 4.1.3.8 X-ray diffractogram of a **NBI-4n-OBuPh** layers **(a)** under 20nm thick deposited on various substrates **(b)** over 20nm thick made by either dropcasting, or spincoating technique (with the slower spinning rate).

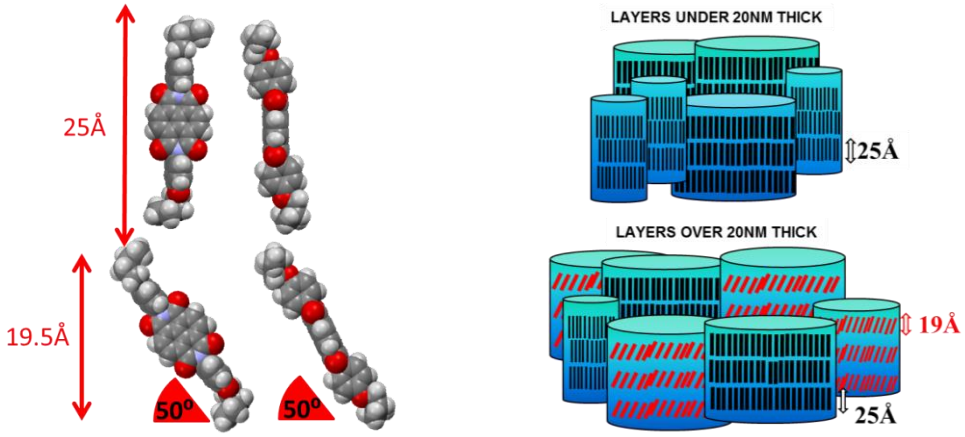

(a) **(b)**

Figure 4.1.3.9 (a) NBI-4n-OBuPh molecule in different orientations **(b)** corresponding models of **NBI-4n-OBuPh** layers of different thickness, consisting crystallites/domains of differently oriented molecules.

The larger derivatives **NBI-4n-OHePh** and **NBI-4n-OOcPh** adopt a regular stacking sequence in single crystals with alkyl substituents in their most extended conformation. These structural features should therefore facilitate the formation of highly ordered and oriented films.

NBI-4n-OHePh films deposited by dropcasting technique, irrespectively of the solvent or the substrate used, always consists of relatively large 3D crystals. They are recognizable even under an optical microscope. The corresponding film diffractograms lead to conclusion about the same supramolecular organization of dropcasted films as in powder. On the other hand, the same molecules spincoated on various substrates form uniform layers. Their representative diffractograms are shown **in Figure 4.1.3.10**. In all cases, uniform thin layers of the thickness of ca. 30nm were obtained (evaluated from the FWHM of the peaks and by applying Sherrer formula). The diffraction profiles, irrespectively of the substrate used, are similar to each other with one dominated broad refection centered at 24.1Å. Applying the same procedure for **NBI-4n-OBuPh** as in the case of smaller analogue this period indicates molecular tilt in the layer versus the substrate plane about 48° (**NBI-4n-OHePh** molecular length is 32.29 Å, 32.29*sin 48^0 = 24.0 Å). This orientation is exactly the same as determined for the same molecule in a single crystal versus *c*-axis in *a*-*c* plane (**Figure 4.1.3.4**).

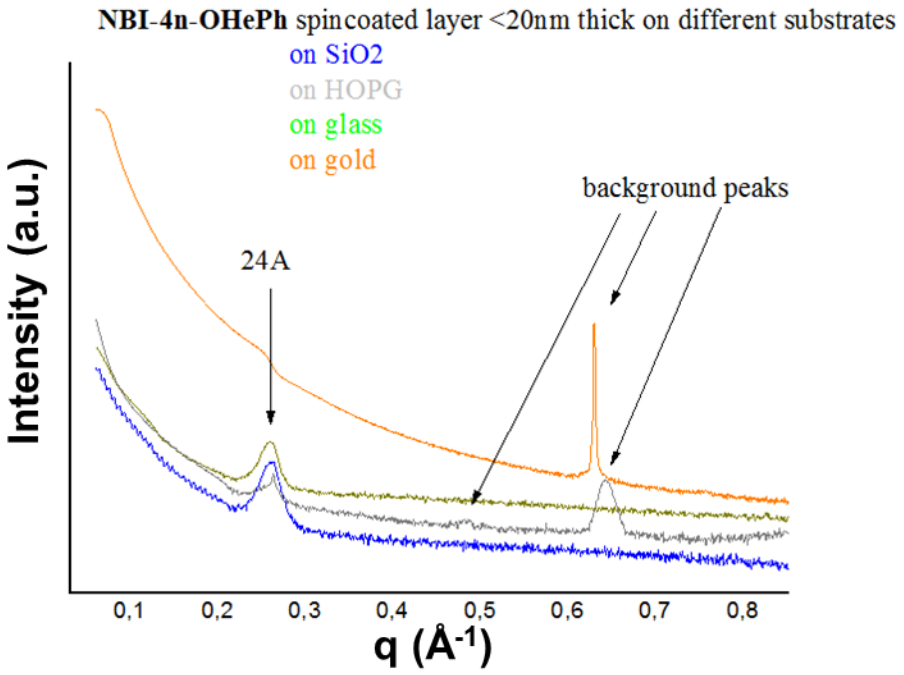

Figure 4.1.3.10 X-ray diffractogram of a **NBI-4n-OHePh** layers spincoated on various substrates.

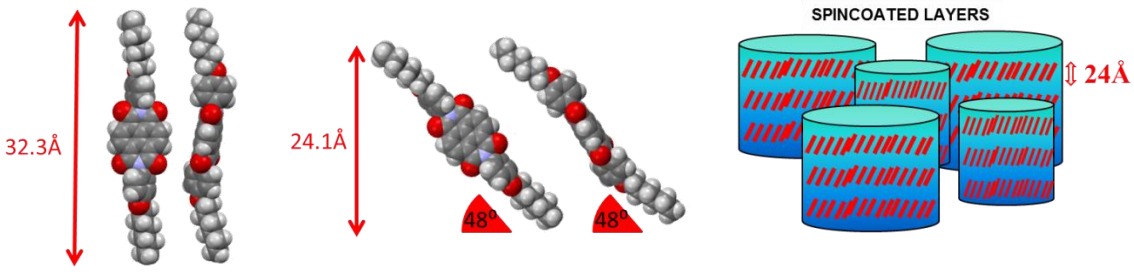

(a) **(b)**

Figure 4.1.3.11 (a) NBI-4n-OHePh molecule in different orientations **(b)** model of **NBI-4n-OHePh** spincoated layers.

The largest derivative **NBI-4n-OOctPh** is most consistent in its tendency to supramolecular organization. The well-defined period of 26.1Å can be distinguished for the layers regardless of the conditions of deposition. Representative diffractograms of **NBI-4n-OOctPh** spincoated layers are presented in **Figure 4.1.3.12**. The thickness of those layers was 26nm (evaluated from the FWHM of the peaks and by applying Sherrer formula). The results are very similar for dropcasted samples. However in this case not only first peak but also higher reflections of this family are well distinguished. The period of 26.1 Å can be attributed as originating from crystallites in which **NBI-4n-OOcPh**

molecules are tilted by 45^0 in respect to the substrate plane (molecular length 36.8 Å, 36.8 Å *sin 45° = 26 Å). Again, this orientation is correlated with tilt angle which is formed by arylene cores of this molecule in a single crystal with respect to *c* axis in *b*-*c* plane (45^0). Model of **NBI-4n-OOcPh** layer is presented on **Figure 4.1.3.13.**

Still, this molecule is extremely easy to crystallize. When glass is used as a substrate, instead of one, two periods have been always distinguished in the layers. The second peak position, at q = 0.28$Å^{-1}$ (4.57^0 in 2θ or 22.4Å in d) is well correlated with 001 reflection in a single crystal. The layers deposited on glass can be therefore considered as a mixture of domains of two different molecular orientations with tilts of 45° and 38° versus the substrate plane. It is worth to emphasize that in the second case the molecules are oriented in the same way as in a single crystal being in contact with the substrate surface by (*a*, *b*) plane.

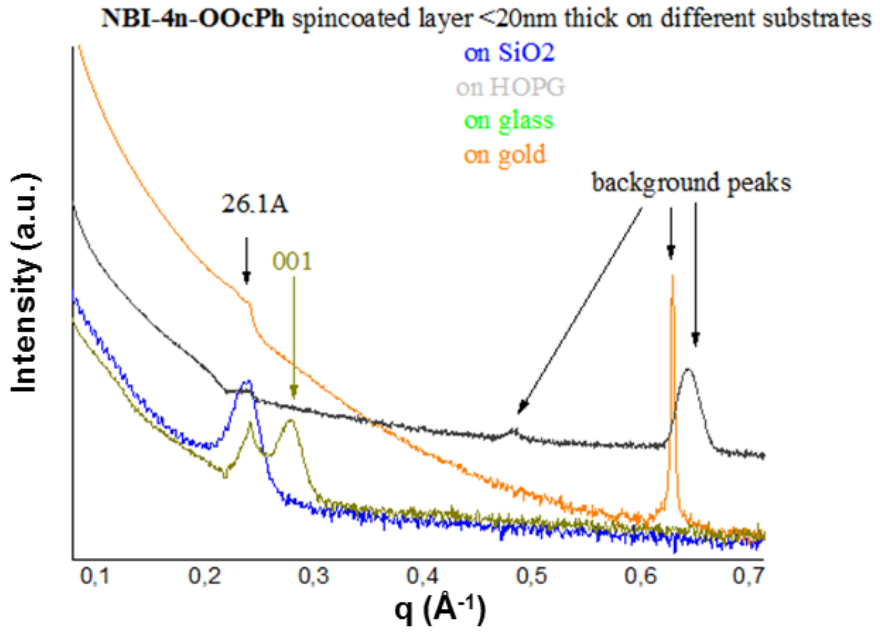

Figure 4.1.3.12 X-ray diffractogram of a **NBI-4n-OOcPh** layers spincoated on various substrates.

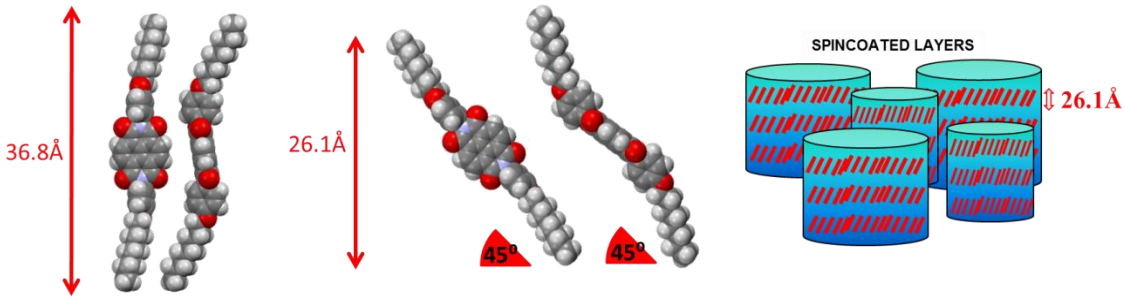

Figure 4.1.3.13 (a) NBI-4n-OOcPh molecule in different orientations **(b)** model of **NBI-4n-OOcPh** layers.

To conclude this section, it can be clearly stated that all three derivatives have a strong tendency to create organized layers. In all cases molecules are oriented more or less perpendicular to the substrate plane. This molecular preference was probably the reason why it was not possible to obtain monolayers of flat lying semiconductors in gas atmosphere (air). 3D supramolecular organization of the molecules becomes more extended with increasing chain length, favoring a regular stacking of the molecules in the unit cell. This is clearly observed in molecular organization in a single crystal, which evolves from herringbone-type organization (characterized by two orientations of molecules) to regular organization (with one molecular arrangement in the structure). The molecular packing in thin layers exhibits some similarities to the organization in single crystals. Hence, the naphthalene bisimide cores of the investigated molecules are well oriented in all 3D systems suggesting good n-type conductivity of the formed layers. This prediction was proved to be correct. OFETs fabricated by solution processing show good electrical transport parameters even when they operate unprotected in air.[145] The best charge carriers mobility and the highest ON/OFF ratio was obtained for transistor with active layer of **NBI-4n-OOcPh** i.e. the largest molecule which exhibits highest abilities for regular organization.

4.2. Thiadiazole derivatives

4.2.1. The influence of the position of the substituent – XRD studies

In this chapter, the effect of solubilizing substituent (alkyl group) position on 3D-self-assembly of thiadiazole-thiophene DAD type semiconductors is discussed. The investigated molecules (**Figure 4.2.1.1**) consist of thiadiazole central acceptor part, to which two dithiophene donor groups were symmetrically attached on each side followed by octyl chains in different positions of the terminal thiophene rings. The discussion is based on comparison of molecular self-assembly as a function of molecular topology. Hence, supramolecular organizations of: linear derivatives with and without substituents (**T1** and **T4**) will be confronted; **T2** and **T3**, both isomers having terminal alkyl substituents in *β*-position (outer or inner, respectively), will be compared with each other; and tetrasubstituted **T5** will be analyzed with appropriate references to its disubstituted analogues i.e. **T2** and **T4**.

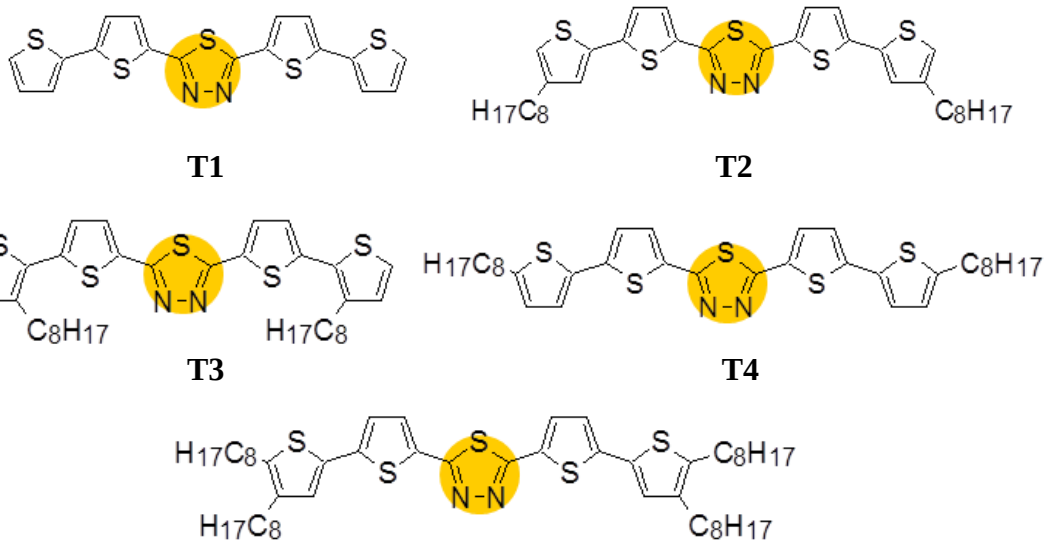

Figure 4.2.1.1 Investigated semiconductors.

For easier comparison, especially of non-linear molecules of complex geometry, the sizes of central part and terminal chains of investigated isomers are presented in **Figure 4.2.1.2** The dimensions were determined using ChemSketch 3D optimization algorithm.

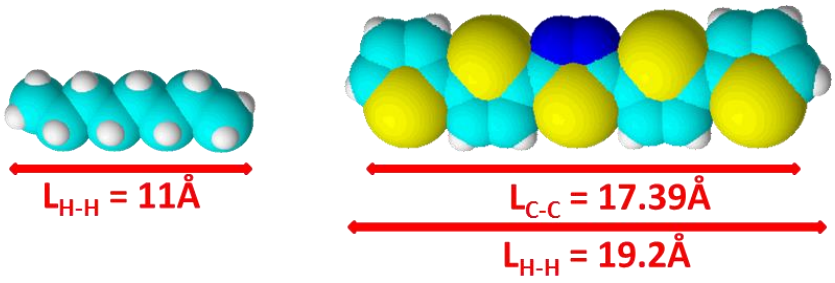

Figure 4.2.1.2 Sizes of parts of investigated semiconductors (Optimized by ChemSketch).

4.2.1.1. Linear T1 molecule

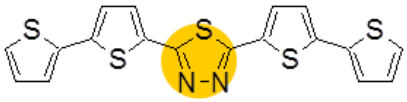

Representative powder and thin-layer diffractograms of **T1** are compared in **Figure 4.2.1.1.1**.

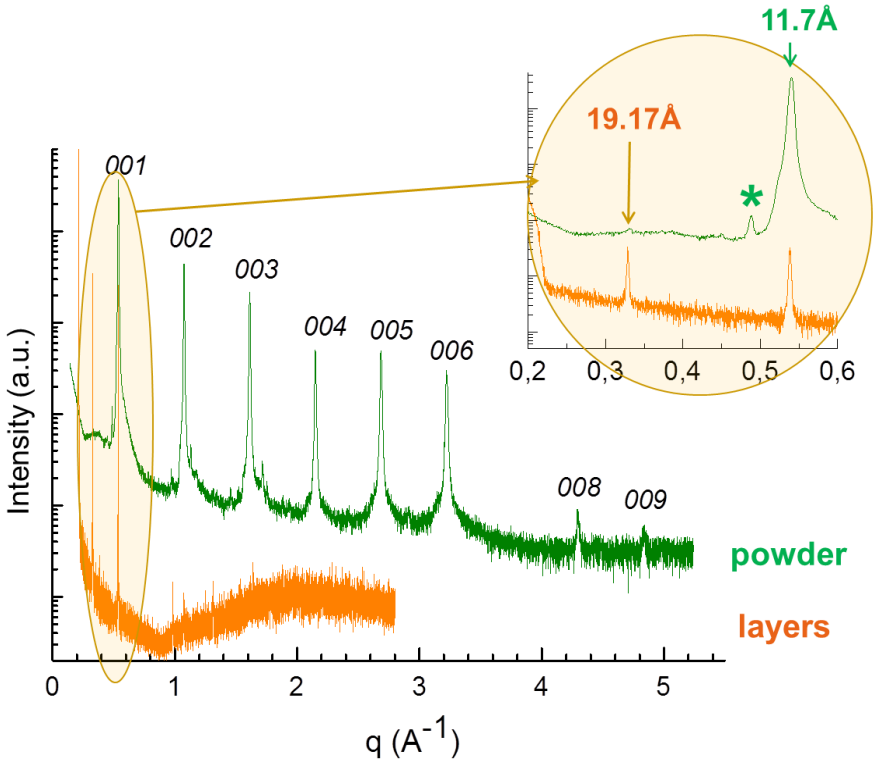

Figure 4.2.1.1.1 Powder and thin-layer diffractograms of **T1**. Low q range is shown in detail as an inset. The small peak indicated by a star originates from the K_β component of the copper radiation.

The powder diffractogram is characterized by a series of Bragg peaks which can be indexed as members of the same family of reflections (with increasing order). Typically, a powder sample contains numerous of randomly oriented grains. As a consequence, the peaks originating from various crystallographic planes should be distinguishable. However, it is not the case of the **T1** powder. Well-defined, single family of peaks observed in the presented diffractogram indicates that crystal grains of this molecule in powder: (i) are characterized by well-defined layer-like internal structure and (ii) agglomerate following a preferential orientation. The periodicity in the direction perpendicular to the substrate surface equal 11.7 Å is noted. According to these findings, the stacking mode for the molecular arrangement is proposed, in which every second row is shifted leading to the period consistent with that determined experimentally. The powder consists of aggregates of the size around 90 nm, as determined on the basis of FWHM of peaks and by applying Sherrer formula. The proposed model of **T1** powder structural organization is presented in **Figure 4.2.1.1.2.**

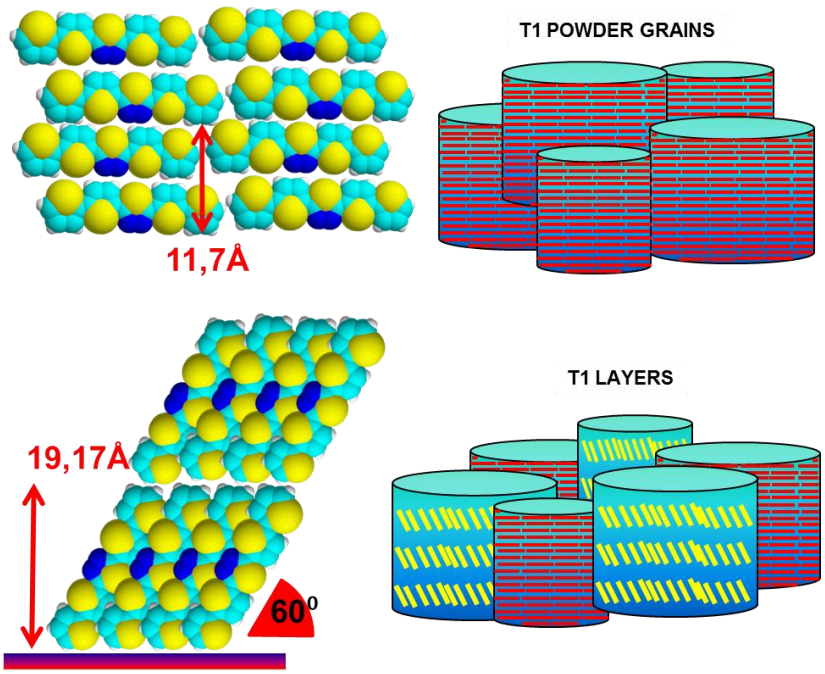

(a) **(b)**

Figure 4.2.1.1.2 (a) T1 molecule in different orientations **(b)** models of **T1** powder and layers consisting differently oriented crystallites.

The organization of **T1** in thin films is slightly different. Besides the same peak at 11.7 Å an additional reflection corresponding to a period of 19.17 Å is also detected in the diffractogram. It suggests that second, differently packed/oriented phase also coexists in the layer. The 19.17 Å distance is comparable to the longest dimension of the molecule. That implies, that in most probable case, the molecules stand up on the substrate surface with a tilt angle of approximately 60°. Consequently, it can be postulated that thin films of **T1** consist of a mixture of coexisting assemblies with two different orientations of molecules versus the substrate plane (the coherence length/crystallite size is in the range of 100-200 nm depending on the morphological homogeneity of the studied sample). Supposedly, both crystallites represent the same structural organization, with different crystallographic faces in contact with the substrate. As a consequence the studies of **T1** thin films enable to determine two parameters of the unit cell. Omega scans performed on (001) peak corresponding to d = 11.67 Å, give a FWHM of 0,9°, proving high degree of orientation of the molecules on the substrate. The proposed model of **T1** films organization is illustrated in **Figure 4.2.1.1.2 (b)**.

It is worth to emphasize, that discussed molecular organizations of **T1** in powder and thin films are essentially qualitatively and quantitatively independent of the investigated substrates (the measurements were also performed for SiO_2, glass and HOPG) and solvent used (chloroforme, chlorobenzene, 1-phenyloctane, DMF and ethylene glycol). Moreover, the results were consistent for thin films prepared by two different methods (spincoating or dropcasting), indicating that the organization of films is independent of the film thickness (150 nm in the case of films prepared by spincoating, and essentially much thicker films (more than 1μm) with less uniform thickness obtained by dropcasting). For the films thicker than 200nm, the higher orders of reflections could be distinguished.

4.2.1.2. Linear T4 molecule

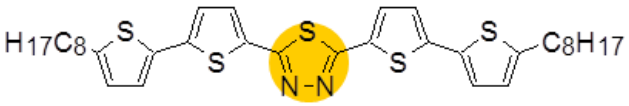

T4 compound might be considered as a simplest modification of **T1** with additional two octyl chains attached symmetrically in α-position to both terminal thiophene groups. The existence of alkyl substituents and their localization lead to significant increase of the length of the molecule, which reaches in the most extended configuration more than 40 Å **(Figure 4.2.1.2.1)**.

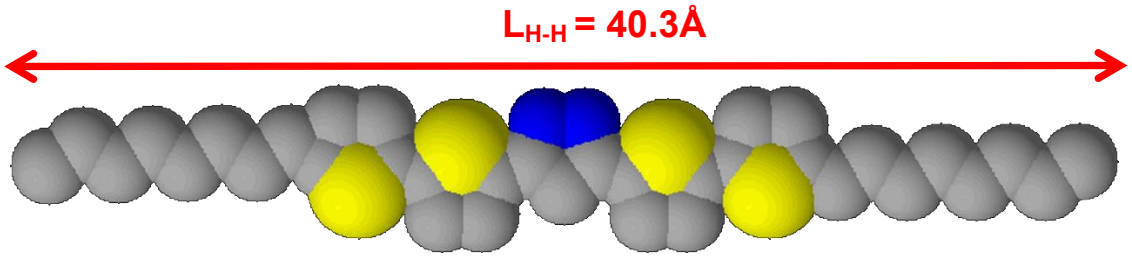

Figure 4.2.1.2.1 T4 molecule model.

Representative powder and thin-film diffractograms of **T4** are compared in **Figure 4.2.1.2.2**. Like in the previous case of **T1**, the **T4** powder diffraction pattern also reveals one family of well-defined Bragg peaks, suggesting macroscopic molecular organization. Position of 001 reflection indicates periodicity of 20.6 Å. The powder crystallites of **T4** most probably consists of assemblies of parallel molecules ordered into layers and oriented in the direction perpendicular to the substrate surface. Moreover, contrary to the case of **T1**, the powder diffractogram of **T4** exhibits in addition a second peak which cannot be indexed as originating from 001 family. Second reflection, corresponding to the larger periodicity of 26.8 Å, possibly represents another crystallographic plane of powder crystallites. Coexistence of two periodicities indicates less perfect orientation of powder grains as compared to **T1**.

It is worth to emphasize that both distances are significantly, almost two times, shorter than the length of the molecule in its fully extended conformation. In general, it can be clarified as a consequence of two different reasons: (i) a tilt of molecules versus the substrate plane which decreases effective thickness of the monomolecular layer as compared to the length of the molecule and/or (ii) significant interdigitation of molecules between two consecutive layers. A natural tendency of alkyl chains towards mutual interaction is a strong argument that interdigitation of these substituents plays important-role in the self-organization of **T4**.

However, considering the lengths of octyl chain (c.a. 10 Å) and molecular backbone (18 Å) one cannot simply expect regular stacking with fully interdigitated alkyl chains to obtain such small periodicity as 20.6 Å. At this point it is worth to emphasize that another interpretation of this series of Bragg peaks is also possible. According to it, a true first order reflection of 001 family might be located at even higher angles, centered at q corresponding to the length of the molecule (about 40 Å) and simply could not be recorded in the used diffraction geometry. In this case, internal structure of crystallites could be quite simple. However, another technique like small-angle analysis, would be necessary to assert this point.

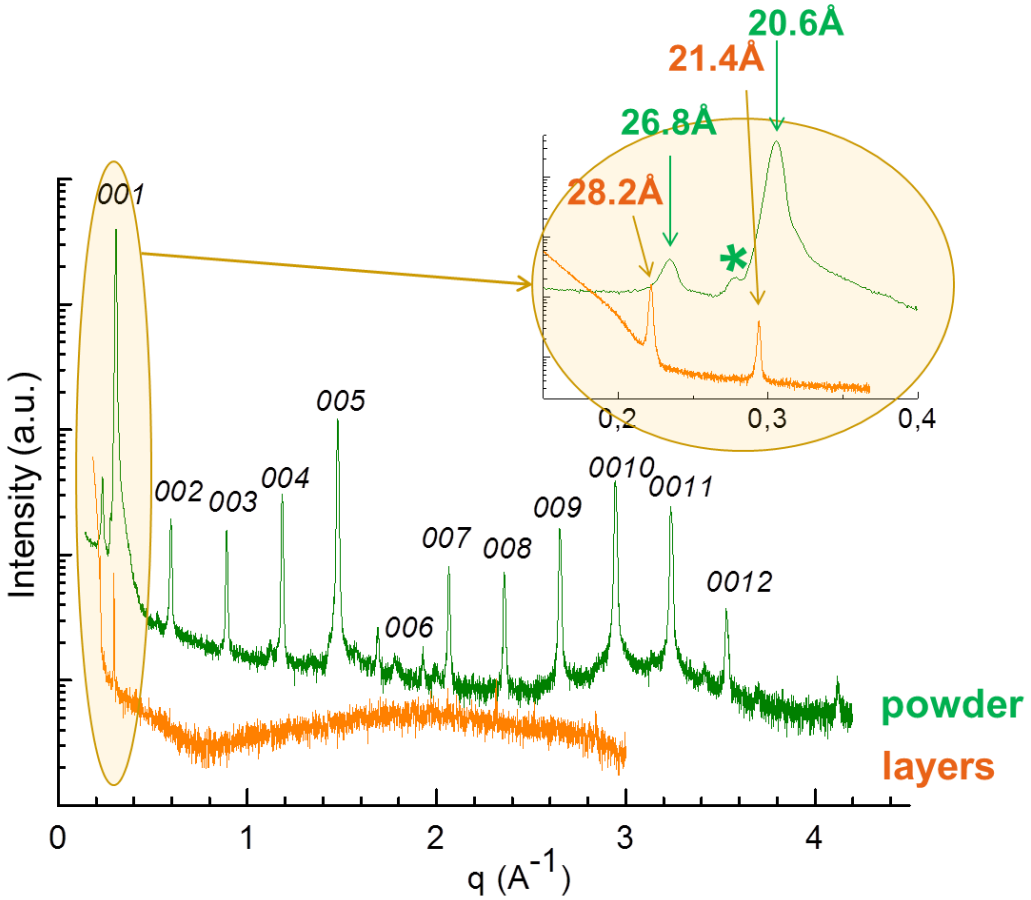

Figure 4.2.1.2.2 Powder and thin-layer diffractograms of **T4**. Low q range is shown in detail in the inset. The small peak indicated by a star originates from the K_β component of the copper radiation.

Thin films of **T4** always display, irrespectively of the preparation conditions (different substrate, deposition method and solvent), two distinct reflections at: 28.2 Å and 21.3 Å. These values are slightly bigger than corresponding periodicities determined for powder (20.6 Å, 26.8 Å). This dissimilarity suggests similar but less dense organization of this

molecule in films in comparison to powder. At the same time, the orientation of molecules on the substrate was significantly improved in comparison to **T1**. Ω scans performed for the peak corresponding to d equal 28.23 Å yielded FWHM of 0.1°. The coherence length in powder is 68 nm and 180 nm for deposited layer. This values are comparable to those obtained for **T1**.

It can be stated as a conclusion that internal structure of **T4** layers appears as very regular but the data is not sufficient to decide among all the evoked possibilities about the exact stacking mode of molecules.

4.2.1.3. Non-linear T2 molecule (chains in outer β position (C4))

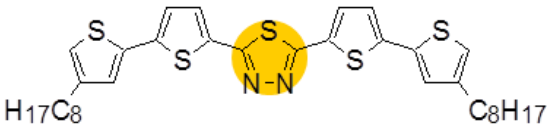

The only difference between **T2** and previously discussed **T4** isomer is a location of terminal alkyl substituents (outer β position (C4) and α position (C2), respectively). The representative powder and thin-film diffractograms of **T2** are compared in **Figure 4.2.1.3.1**.

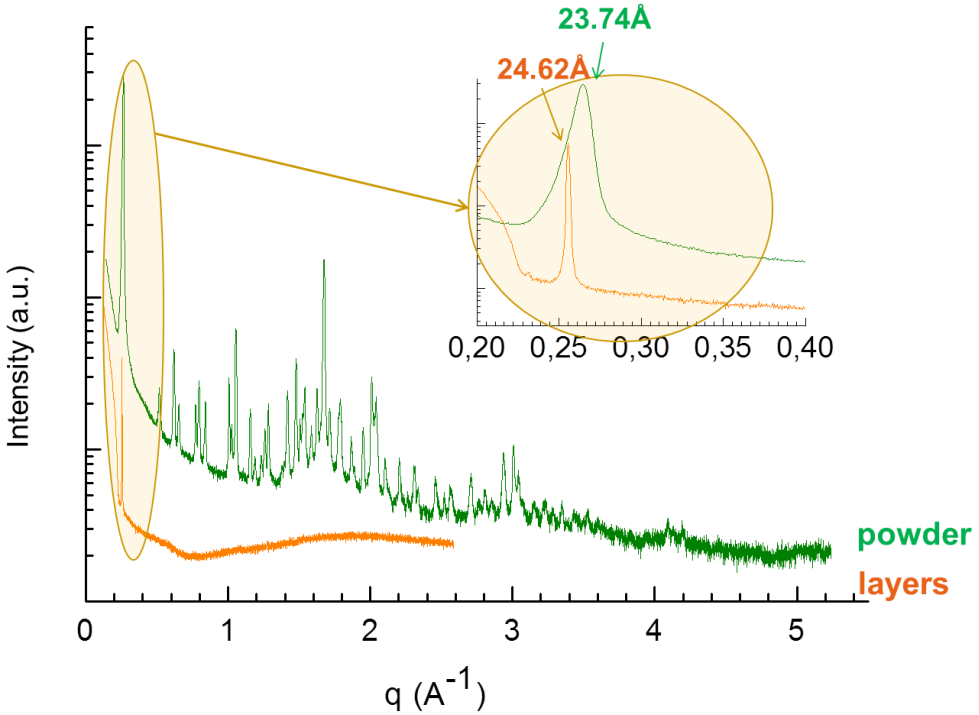

Figure 4.2.1.3.1 Powder and thin-layer diffractograms of **T2**. Low q range is shown in detail as an inset.

Powder diffractogram of this non-linear compound significantly differs from those obtained for linear **T1** and **T4**. Diffraction profile is much more complex and resembles a typical 3D low-symmetry profile of randomly oriented powder grains. However, a low angle dominant peak of high intensity can be noticed at 23.7 Å. It may have its origin from the stacking period of **T2** molecules.

In the case of thin films, irrespectively of preparation conditions, only two reflections can be distinguished: a weak one at 27.1 Å and a much stronger one at 24.6 Å. These periodicities are slightly larger than recorded in powder diffractogram which may indicate a less dense packing in the layer. The calculated crystallites size for powder is 60 nm, which is comparable to the substituted analogue discussed previously (**T4**). However, the coherence length obtained for dropcasted thin films was 290 nm which is much larger value than determined for corresponding layers of **T1** and **T4** molecules. Nevertheless, the orientation degree was smaller than in both previous cases, yielding FWHM value of peak Ω scan equal to 1.5°.

4.2.1.4. Non-linear T5 molecule

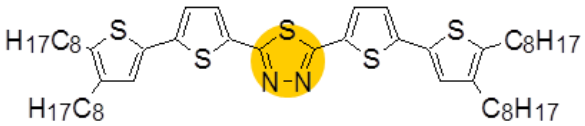

T5 molecule is the only tetrasubstituted compound of the investigated series. It contains four alkyl substituents located in α and outer β positions of both terminal thiophene units. From simple geometrical point of view it is therefore an exact combination of **T4** and **T2** derivatives. However, taking into account its larger number of flexible chains[146] and their possible different orientation in ordered structure the supramolecular organization of this derivative is very difficult, or even not possible, to predict from organizations of both **T2** and **T4** isomers. **T5** powder and thin-layer diffractogram profiles are presented in **Figure 4.2.1.4.1**.

Powder profile is similar to corresponding diffractogram of **T2** rather than **T4**. The peaks originating from various crystallographic planes can be distinguished. First reflection of powder profile appears at q corresponding to periodicity 27.3Å. It should be notice that the reflection corresponding to the same periodicity is also present in the profiles of thin films (marked in the figure as 001). Irrespectively of the substrate, solvent or deposition method used, the same organization pattern is noted for all investigated films, with only characteristic effect the layer thickness. For thick films made by dropcasting a series of

reflections from 001 family up to 11th order can be observed in the diffractogram, as demonstrated in **Figure 4.2.1.4.1 (**marked by orange line). For thinner films, of thickness under 200nm, only the first reflection can be distinguished. It is interesting to emphasize that 001 reflection corresponding to periodicity 27.3 Å is the only common one in both relatively different powder and thin film diffractograms. Therefore it can be postulated, that **T5** is polymorphic, exhibiting different crystallographic structure in powders and in thin films.

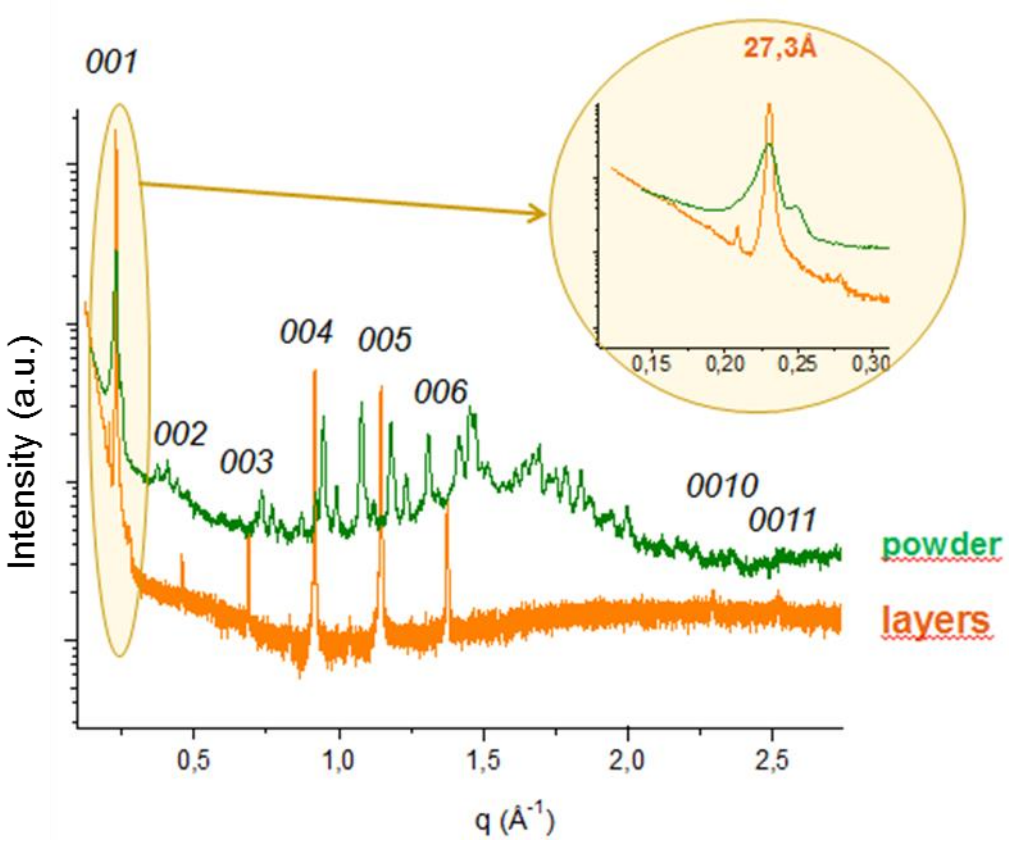

Figure 4.2.1.4.1 Powder and thin-layer diffractograms of **T5**. Low q range is shown in detail as an inset.

The comparison of period 27.3 Å and the size of **T5** implies, that the molecules within thin films should stand up on the substrate surface with some tilt angle of their backbones. Interdigitation of terminal octyl groups must also be assumed. Yet, it is important to notice, that despite significantly larger intensity of this family of reflection (001), the additional peaks of much lower intensities are also present on the thin films diffraction patterns. Those peaks cannot be indexed with the relation to the previous family. Hence, the more

detailed structural model would be required to explain their origin and to interpret the diffractogram of deposited layers in a more profound matter.

The crystallites size derived from the FWHM value of the diffraction peaks yields around 60 nm for the powder grains (which is in accordance to other substituted molecules of this series) and on average 250 nm for the 001 peak of the dropcasted layers. Omega scans performed for 001 peak of dropcasted sample give FWHM value of 0.5°, proving high orientation of the deposited film.

4.2.1.5. Non-linear T3 molecule (chains in inner β position (C3))

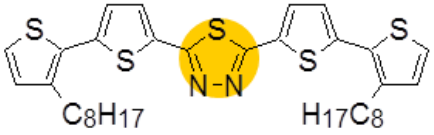

T3 is an isomer of the investigated series in with octyl separators are symmetrically attached to carbons in outer *β* position of two terminal thiophene rings. Small change in the position of alkyl substituents by one carbon atom (outer *β* position (C4) instead of inner *β* position (C3)) decreases linearity of the molecule and induces internal torsion and non-planar molecular conformation.

In optimal molecular conformation deduced from modeling of free molecule, the only central triad of conjugated backbone of **T3** isomer (i.e. thiophene-thiadiazole-thiophene) is planar. However, the reminding terminal thiophene rings are rotated versus the plane of the central part by 35°.[146] This is a much larger distorsion from planarity in comparison to that one observed for the rest of derivatives from the investigated series (for example it is equal to 15° for **T2** isomer). Electrochemical and spectroscopic measurements of this isomer confirm[146] theoretically calculated shifts of HOMO and LUMO levels caused by reduced planarity of the molecule. The purpose of investigations presented in this chapter is to answer the question how this change of molecular topology influence 2D and 3D structural organizations of this type of semiconductors?

In the case of **T3** isomer I succeeded in growing its single crystal which enabled to gain more precise information of its 3D supramolecular organization. This molecule forms a monoclinic cell (space group P2/n) with crystallographic parameters listed in **Table 4.2.1.5.1.** The graphic presentations of crystal packing projected in the (*a*-*c*) and (*b*-*c*) planes are presented in **Figure 4.2.1.5.1**.

	Crystal system	Unit cell dimensions					
		a	b	c	α	β	γ
T3	Monoclinic	12.88Å	8.41Å	15.95Å	90°	104°	90°

Table. 4.2.1.5.1. Parameters of **T3** crystallographic structure.

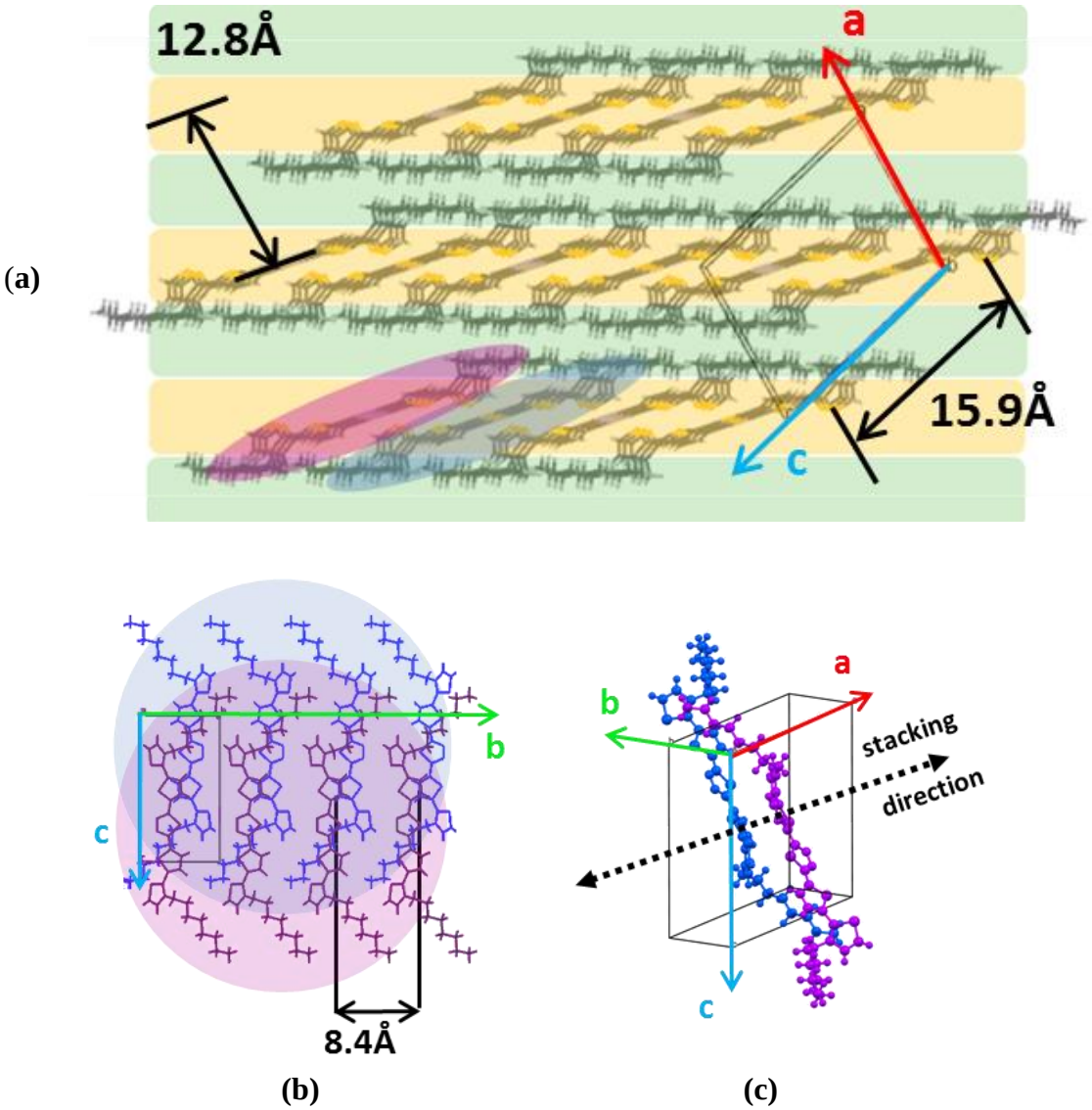

Figure 4.2.1.5.1 Projections in the **(a)** (*a*-*c*), **(b)** (*b*-*c*) planes and **(c)** 3D representation of crystallographic structure of **T3.**

The nonplanar shape of **T3** is particularly striking when looking at molecular arrangement in 3D ordered structure. A single crystal consists of layers of stacked molecular backbones separated by layers of terminal chains (highlighted in yellow and green respectively in **Figure 4.2.1.5.1 (a)**). All molecules are oriented in one direction in the layer. However, the molecular torsion leads in the crystal to the coexistence of two different rotations of molecules and their alternative arrangement versus the layer plane. This is a consequence of the fact that the stacking of two molecules is centered on thiophene rings mutually shifted with respect to the central thiadiazole ring (Figure **4.2.1.5.1(b,c)**). Then the two molecules are mutually rotated around their longitudinal axes. This results in a face to face arrangement of centrally located thiophene rings leading to energetically justified dense stacking (with intermolecular separation equal to 8.4 Å). As a consequence of these molecular arrangement the alkyl substituents of two following molecules are also alternatively oriented. Hence, having these alternative positions they are not able to interdigitate.

Experimentally obtained powder diffractogram was found to be in perfect accordance with the powder diffraction profile calculated from a single crystal structure. Both profiles are compared in **Figure 4.2.1.5.2.** Distances corresponding to *c* and *a* unit cell axes (i.e. 001 and 100 reflections) are marked by grey arrows and are systematic absences. The small peak indicated by star originates from K_β component of the copper radiation. First distinguishable reflection is 10-1 peak. It conforms with periodicity 11.3 Å. This separation corresponds to the distance between two closest molecules in the adjacent layers (compare with **Figure 4.2.1.5.3)**. It is worth to remind here, that closest molecules are differently rotated in the *a*-*c* plane (molecules marked in schemes by blue and purple). This fact differentiates 10-1 and 100 reflections. The latter one corresponds to the separation between molecules in adjacent layers of exactly the same 3D arrangement (i.e purple to purple). **T3** powder diffractogram is characteristic for 3D structure of low symmetry, similarly like was observed for **T2**. The crystallites size, determined from FWHM of the 10-1 reflection, is 60 nm. It is comparable value to the crystallites dimensions determined for the previously discussed molecules.

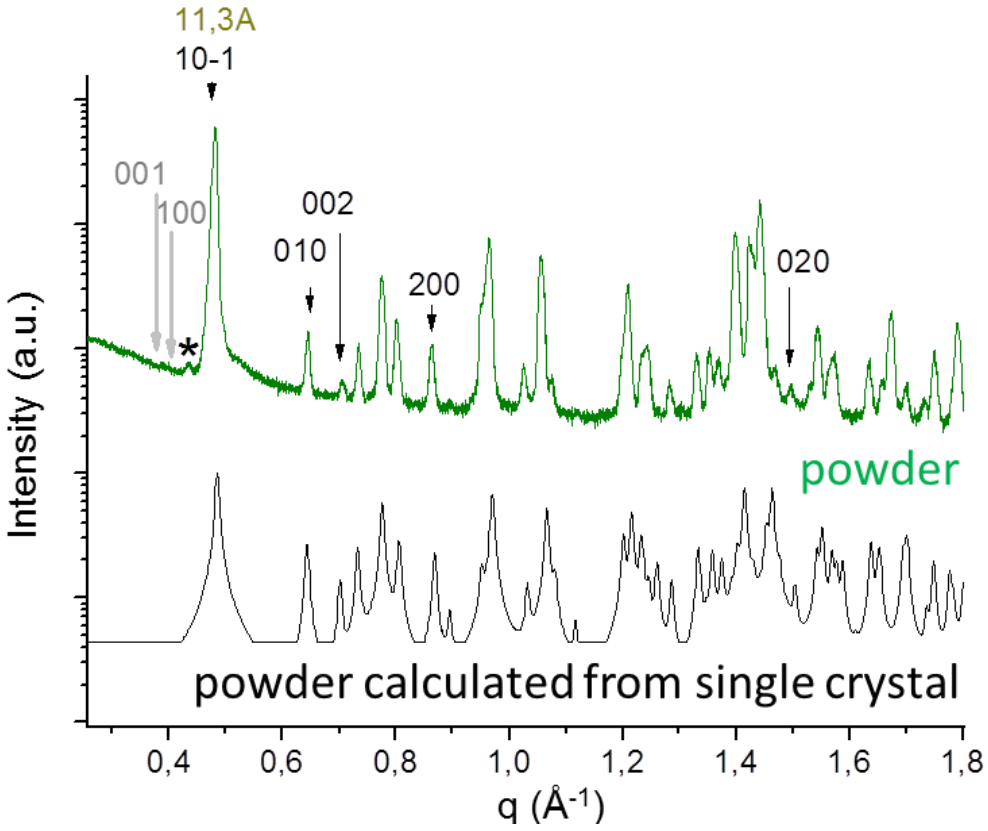

Figure 4.2.1.5.2 Diffractogram of **T3** powder and powder pattern calculated from single crystal.

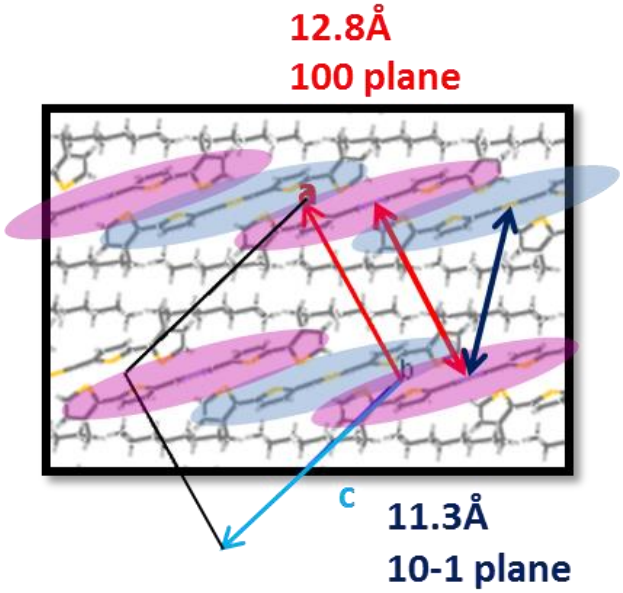

Figure 4.2.1.5.3 Projection in the (*a*-*c*) plane of crystallographic structure of **T3** with marked distances corresponding to 001 and 10-1 planes.

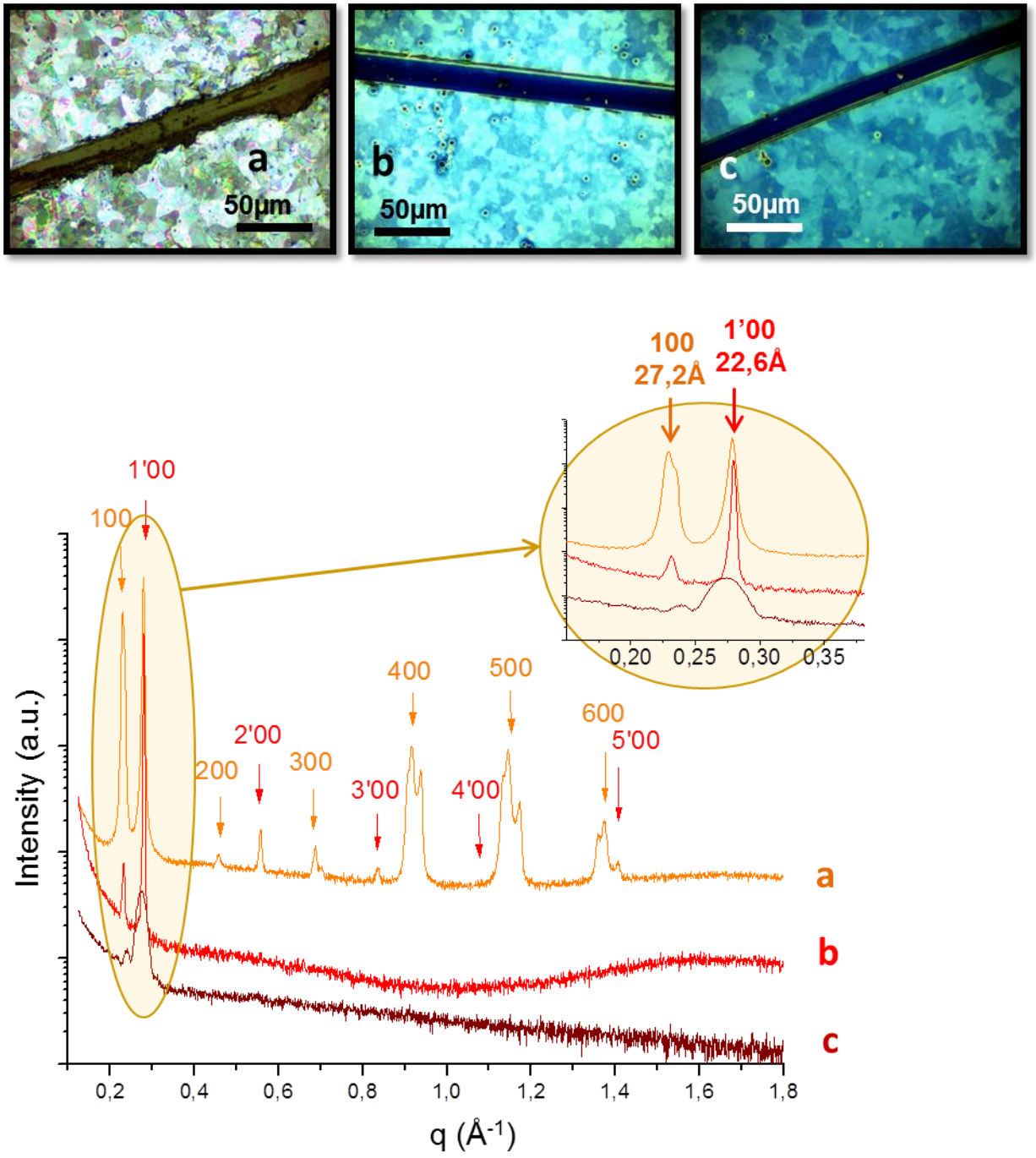

Figure 4.2.1.5.4 Selected diffractograms of **T3** thin films. Low q range is shown in detail in the inset. On the top, microscopic images labeled as the corresponding diffractograms are provided. The thick lines visible on these images correspond to scalpel cuts enabling layer thickness measurements by means of profilometer.

a) T3 layer dropcasted from 10g/L chlorobenzene solution on glass substrate,

b) T3 layer spincoated from 10g/L chlorobenzene solution on glass substrate,

c) T3 layer spincoated from 10g/L chlorobenzene solution on SiO_2 substrate.

3D organization of **T3** in thin films is different than in powder. The films preparation parameters were varied in the same manner as for other investigated molecules of the investigated series and included: deposition method (spincoating and dropcasting), substrate (glass, gold, graphite and silica), solvent (chloroforme, chlorobenzene, hexane and 1phenyloctane) and the solution concentration (5mg/ml and 10mg/ml).

The undertaken studies indicated that in the case of **T3** the thin film structure is relatively sensitive to the preparation conditions. The factors which are influential are film thickness and solvent. Studies included XRD measurements and optical observation by means of polarized optical microscopy. Representative results of three typical **T3** films as a function of the film thickness are presented in **Figure 4.2.1.5.4**.

The first type of organization (**a**) characterizes thick films (estimated thickness above 1μm). It usually occurs when **T3** film is prepared by dropcasting, irrespectively of the substrate and the solvent used. Two families of peaks can be distinguished in this type of diffractogram, indexed as 100 and 1'00. Peaks at least up to sixth order might be indexed indicating nicely ordered layer-type organization. Hence, the first order reflections correspond to two periodicities of 27.2 Å and 22.6 Å, respectively. The crystallite sizes calculated from FWHM are 106 nm (100) and 160 nm (1'00) clearly suggesting coexistence in thick films of two types of domains of different crystallographic structures, i.e. the same type of layer-like internal organization but different periodicities. It is interesting to emphasize that these periods are characteristic only for films, and both of them are much larger than observed in powder (15.95 Å). This dissimilarity clearly indicates polymorphism of **T3** isomer. Due to particular shape of this molecule, the internal structure of grains is not evident from the presented diffractogram. Generally, it resembles diffractogram of **T4** corresponding to model assuming molecular intedigitation (showing coexistence of two distinct reflections with periodicity of the first one around 28 Å) rather than **T2** (with much smaller largest intercellular separation around 24.6 Å).

At this point it is worth to emphasize that 1'00 reflection in this diffractogram of **T3** film (22.6 Å) relates exactly to doubled position of 10-1 reflection observed in the organization of this molecule in a single crystal (11.3 Å). This correlation may suggest similar organization in thin film and single crystal with characteristic coexistence of alternative layers of stacked molecular backbones and of terminal substituents. However taking this interpretation one important detail must differentiate both organizations – the space orientation of molecules in the layers. Contrary to two different molecular rotations alternatively coexisted in one layer in a single crystal (illustrated in schemes by purple and

blue colors of molecules), the organization in thin films may be characterized by exactly the same rotation of all molecules (only blue or only purple) within the same layer. In the latter organization the difference in molecular orientation occurs between molecules from two following layers. In such a model, the 100 peak located at 22.6 Å would correspond to the closest distance between identical molecules located every second row instead of every next row. This would explain the 22.6 Å period without the terminal octyl chains interdigitation.

Second type of diffraction profiles **(b)** characterizes films of medium thickness (about 200nm). 100 and 1'00 first order reflections corresponding to periods equal 27.2 Å and 22.6 Å are still present in the diffractogram, but alone without higher order peaks. As presented before, this type of change of diffraction profile is typical and is observed frequently for other molecules when film thickness decreases.

Finally, the last type of diffraction profile **(c)** characterizes very thin layers (30nm thick as determined from the present Kiessig fringes). Only one reflection, at 22.6 Å can be distinguished in this case. This result can suggest homogeneous molecular organization in the film with one periodicity. However, considering typical ratio 1:10 of peak intensities between 100 to 1'00 reflections, it is also possible, that two types of crystallographic domains still coexist in very thin films and 100 reflection is not detectable due to its insufficient intensity.

Careful investigation of compared diffractograms revealed interesting feature concerning mutual relation between peak intensities. As clearly observed in **Figure 4.2.1.5.5** the intensity ratio of peaks 100, 1'00 is changed depending on the solvent used. For films prepared from hexane solution, the 100 peak at 27.2 Å dominates the profile, while in the cases of other solvents (chloroforme, chlorobenzene) the ratio is favorable for 1'00 reflection at 22.6Å. The difference is even more noticeable, when looking at polarized microscope images. Films prepared from chlorobenzene (**Figure 4.2.1.5.4(a-c))** or chloroform (**Figure 4.2.1.5.5 (b),(d))** solution, irrespective of the film thickness, looks very similar. They are–continuous layer of well-defined domains of various polarization. On the other hand, samples prepared from hexane solution are different. In this case, a thick, dropcasted films (over 1μm thick) are discontinuous consisting of large relatively well-separated crystals whereas thinner layers under 100nm thick seems to be continuous and characterizes by a set of crystallographic domains mutually interwovened. This dissimilarity in **T3** supramolecular organization in the films must be a consequence of the solvent influence (to be true it is one and only well-noticeable solvent influence on the thin

films organization of all studied molecules meaning, that only **T3** organization is solvent dependent).

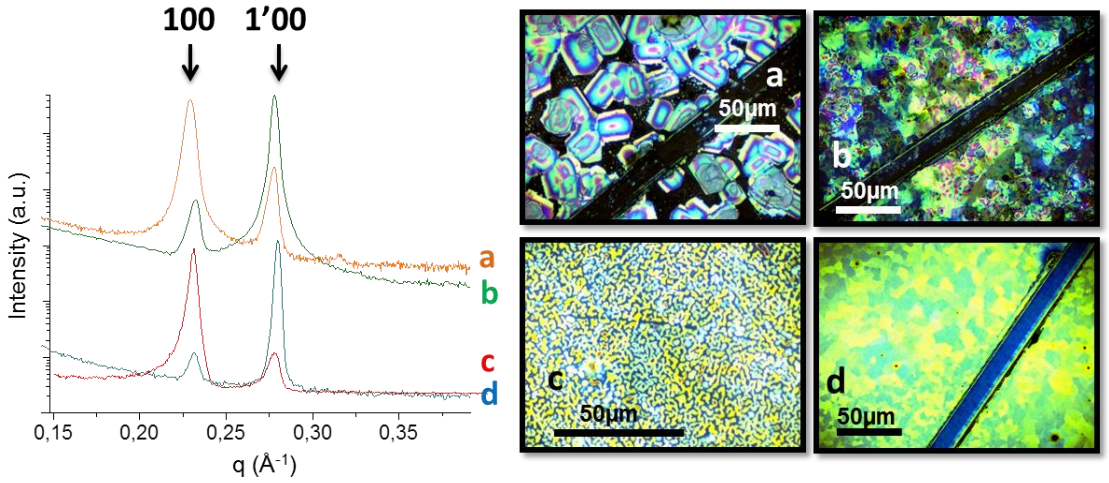

Figure 4.2.1.5.5 Selected diffractograms of **T3** thin films. Low q range is shown in detail as an inset. On the side, microscopic image of the layer corresponding to a given diffractogram is provided. The thick line drawn through the center of samples is scalpel cut enabling layer thickness measurements by profilometer.

a) T3 layer dropcasted from hexane solution,

b) T3 layer dropcasted from chloroforme solution,

c) T3 layer spincoated from hexane solution,

d) T3 layer spincoated from chloroforme solution.

4.2.2. The influence of the position of the substituent – STM studies

As evidenced by the above presented results, unsubstituted **T1** and linearly substituted (in α position) **T4** and **T5** derivatives exhibit strong tendency to form 3D ordered aggregates. In powders and thin films alike, they agglomerate in layer-like structures in which molecules are oriented almost perpendicularly to the substrate plane. The similar molecular behavior was confirmed for many already reported thiophene oligomers with α-alkylated substituents.[147-154]

It is therefore justifiable to conclude that strong tendency of these molecules to organize into 3D aggregates impedes their ability to form monomolecular layers. I did not succeed in preparation of monolayers of α-substituted derivatives of the investigated thiophene-based semiconductors. The similar difficulties in preparation of stable ordered monolayers on HOPG were also reported for α-alkylated oligothiophenes[155-157] although for some of them the monolayers at liquid-solid interface were obtained on different substrate as, for example MoS_2.[155, 158] Hence, the authors postulated that reported difficulties in 2D organization of such molecules on HOPG are a consequence of mismatch between the graphite substrate and alkyl chains, which is generated when these substituents are located to terminal thiophenes in α position.[159] This situation changes for β-substituted alkyl derivatives. Consequently, coherence lengths in films as well complex powder profiles of two investigated β-substituted derivatives (**T2** (outer β-position, C4) and **T3** (inner β-position, C3)) demonstrate, that these isomers have smaller tendency for 3D aggregation in comparison to their linear analogues. Hence, in both cases monomolecular layers on HOPG were obtained and characterized by STM. This enabled comparison of 2D and 3D molecular organizations of these derivatives.

4.2.2.1 Non-linear T2 molecule (chains in outer β position (C4))

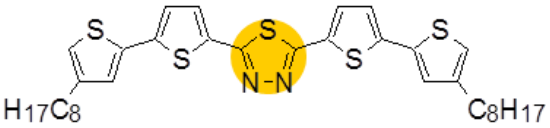

The representative STM images of **T2** monolayer on HOPG are presented in **Figure 4.2.2.1.1(a, b)** together with proposed model of absorption geometry and determined unit cell (**c** and **d** respectively). Monolayer is characterized by large, well-ordered domains of the size of few hundred of nanometers. Adjacent domains are rotated against each other in increments of 60 degrees (see the bottom left corner of **Figure 4.2.2.1.1(a)**). The angle is correlated with three fold symmetry of the HOPG substrate and indicates substrate influence on the adsorbate organization.

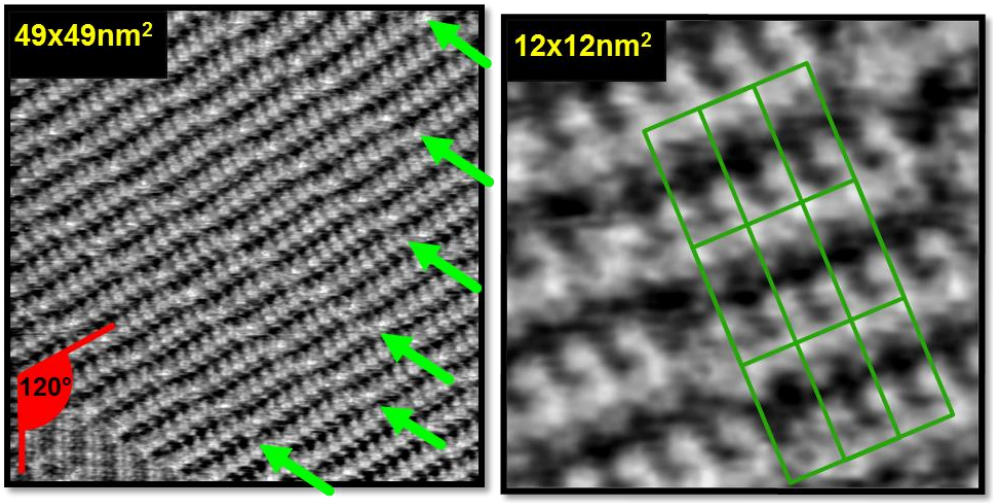

(a) **(b)**

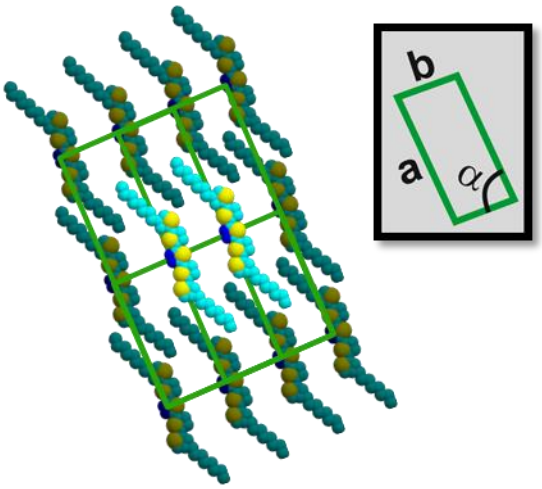

(c) **(d)**

Figure 4.2.2.1.1 (a-b) STM images**, (d)** unit cell and **(c)** postulated real space model of adsorption geometry of **T2** monolayer on HOPG (V_{bias}= -370mV, I_t =0.3nA)

Each domain comprises rows of stacked molecules oriented in one direction. Image obtained at higher magnification (**Figure 4.2.2.1.1 (b)**) enables to determine the unit cell parameters (***a* = 3.1 ± 0.2 nm, *b* = 1.5 ± 0.2 nm, *α* = 85° ± 2°**), and to propose model of **T2** adsorption geometry. Longer dimension of the unit cell (parameter ***a***) corresponds to the distance between molecular rows. It is significantly smaller than the length of the molecule (c.a 25%). This confirms that the alkyl substituents of the molecules from adjacent rows must be mutually interdigitated. The observed structure of **T2** is therefore a set of alternatively located parallel rows of ordered molecular backbones and of interdigitated alkyl substituents. The second unit cell parameter (***b***) is related to the distance between cores of adjacent molecules within the same row. It is equal 1.5 nm which is significantly larger than expected separation from the van der Waals size of the molecular backbone. It is worth to remind that this distance is also larger than the corresponding molecular separation observed in monolayers of pure alkylthiophene oligomers (0.9 nm).[19,160] It is therefore a strong argument that large intermolecular separation observed in this direction is caused by a presence of thiadiazole central acceptor part in the molecule. It is generated by a balance of π-stacking and electrostatic interactions. The observed face-to-face location of acceptor units (thiadiazole) of two neighboring molecules leads to mutual repulsive interactions and finally to larger intermolecular distance along molecular rows. As a consequence, a nanometric-size cavity between the cores of two following molecules is formed in this direction. The more detailed discussion about influence of the central acceptor part on monolayer structure is presented in the next section.

Interesting feature of **T2** organization, observed even in large-area images, are characteristic linear imperfections existing in the monolayer (marked in image **(a)** by green arrows). They follow one direction and occur periodically after every fourth to seventh molecule in each row. Image at higher resolution (**Figure 4.2.2.1.1 (b)**), indicates that these defects correspond to additional shift of molecules in the monolayer along direction perpendicular to the orientation of molecular rows. The postulated reason of this molecular movement is a misfit between two organizations at the interface: the adsorbate molecules in the adlayer and carbon atoms on the HOPG substrate surface. In order to confirm those expectations correlated imaging of the monolayer near its boundary and of the uncovered HOPG substrate surface in the vicinity was required to directly determine relative positions of atoms and molecules in these two organizations. **Figure 4.2.2.1.2** shows results of such experiment. Part (**c**) presents image at atomic resolution of HOPG substrate surface which

enabled determination of three crystallographic axes (1-3) additionally marked by magenta, purple and blue lines.

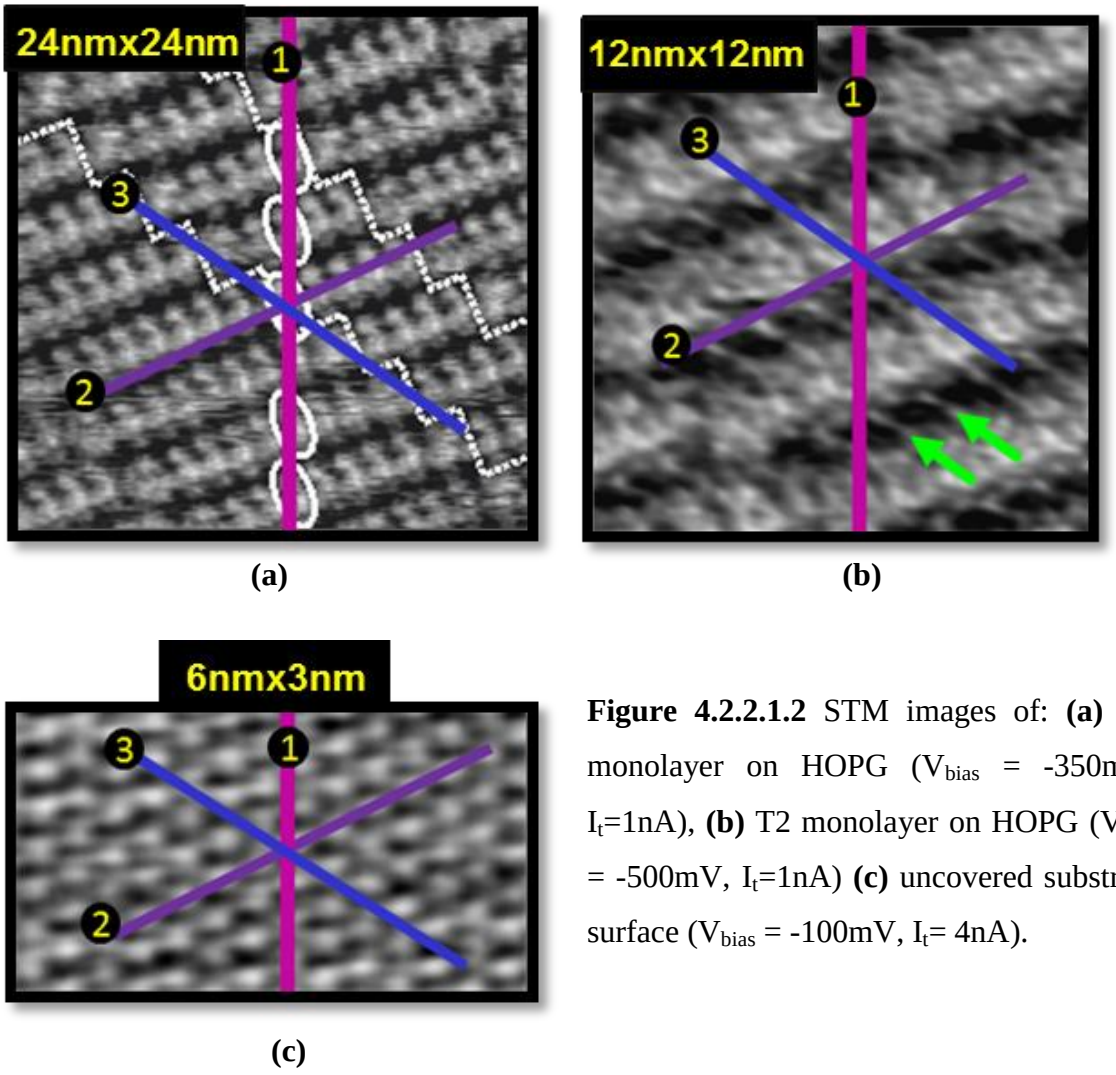

(a) **(b)**

(c)

Figure 4.2.2.1.2 STM images of: **(a) T2** monolayer on HOPG (V_{bias} = -350mV, I_t=1nA), **(b)** T2 monolayer on HOPG (V_{bias} = -500mV, I_t=1nA) **(c)** uncovered substrate surface (V_{bias} = -100mV, I_t= 4nA).

Comparison of the substrate orientation with the adsorbate organization in the adlayer (images **a** and **b**) reveals the misfit. The direction of rows is rotated by about 12° with respect to the substrate axis labeled in the images as (2) (purple line). It is expected, that observed misfit generates stress at the interface and is a driving force of already discussed linear imperfections in the monolayer organization. Moreover, it is worth to emphasize that the two other graphite axes (1) and (3) are, for their part, perfectly in accordance with the adsorbate layer geometry. Firstly, the organization of adsorbate molecules from adjacent parallel rows (marked for example by white ellipses in image **(a))** follows exactly the direction of the substrate axis (1) (magenta line). The second fit concerns the orientation of alkyl substituents in the monolayer. They can be visible as thin bright lines (marked for example by two green arrows) in the STM image **(b)** obtained with negatively polarized tip

(bias voltage -0.5 V). As it is expected from the monolayer structure, the substituents are located periodically in between bright parallel rows corresponding to the stacked molecular conjugated cores. One interesting observation concerns the orientation of these substituents. The images show that alkyl chains are adsorbed exactly along one graphite axis (in the presented image axis (3)). This preferential orientation is typical and frequently observed for linear hydrocarbons adsorbed on HOPG in the form of pure compounds[161-163] and alkyl substituents of larger molecules.[164-165]

Finally, it is worthwhile to analyze submolecular contrast in the STM images. As it is observed in the previously discussed images the **T2** molecule in a monolayer appears typically as a bright rectangular spot (for example: **Figure 4.2.2.1.2 (a-b)**). This higher tunneling signal is related to the central part of the molecule. The correlation is consistent since centrally located backbone of the investigated semiconductor is a conjugated part with higher electronic delocalization in comparison to terminal alkyl substituents. However the fine image contrast of this area as seen by STM depends on the applied bias voltage. **Figure 4.2.2.1.3** shows a set of four images of **T2** monolayer obtained for different bias from +0.5 to -1 V (tip polarity). The rectangular image of the molecule recorded for positive bias (image **a**) is dominated by centrally located bright spot. The correlation with the molecular topology indicates that this part corresponds to thiadiazole acceptor group in the conjugated molecular core. Let's remind that in these conditions with positively polarized tip the electrons tunnel from the substrate to the tip. Therefore, this observation means that the electron deficient part of the molecule constitutes the favored pathway for electrons to tunnel in this direction. The submolecular contrast changes when scanning is performed for negatively polarized tip. The decrease of bias from -0.35 to -1 V (images **b-d**) causes symmetrical extension of bright area to periphery of the molecular conjugated core. As a result, scanning with -0.5 V bias (image **c**) enables to distinguish signal from alkyl substituents interdigitated between adjacent rows of molecules. These changes finally lead to different image of the molecule observed for -1 V (image **d**). This last one is itself characterized by two well-focused dominant bright spots located at periphery of the molecular backbone with less bright central area (also compare corresponding zoom images **b'** and **d'**). To conclude, own results show experimentally evident changes in **T2** submolecular contrast in the monolayer caused by the bias voltage. A precise explanation of this dependency is a complex matter. It should take into account influence of several possible factors, like: complex electronic structure of the molecule which consists of

segments of different electronic affinity, internal charge transfer in the molecule, molecular topology in the adsorbate state, and expected nonuniformity of electron tunneling in the investigated substrate-molecule-tip system.

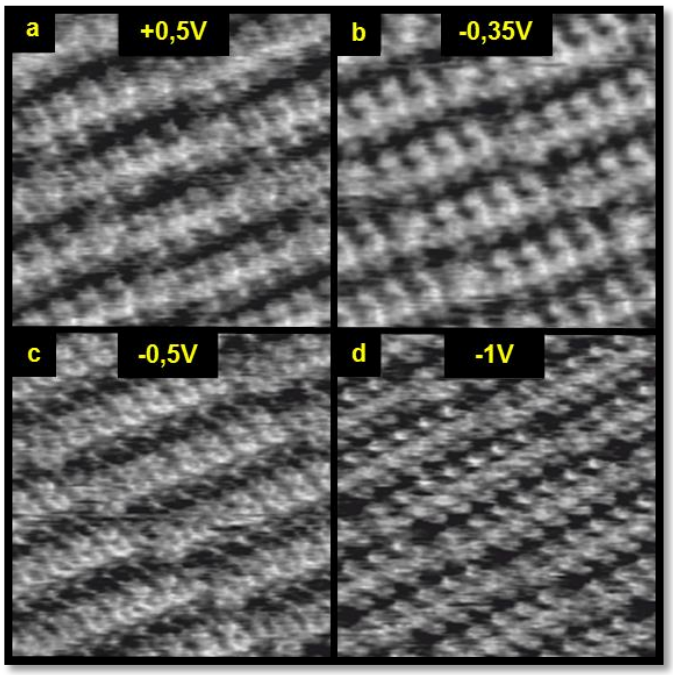

Figure 4.2.2.1.3. STM images of **T2** monolayer on HOPG obtained for different bias voltage: **(a)** 500mV, **(b)**- 350mV, **(c)** -500mV, and **(d)** -1V. Scanning area and parameters: (a-d) 15x15nm^2, and I_t=1nA.

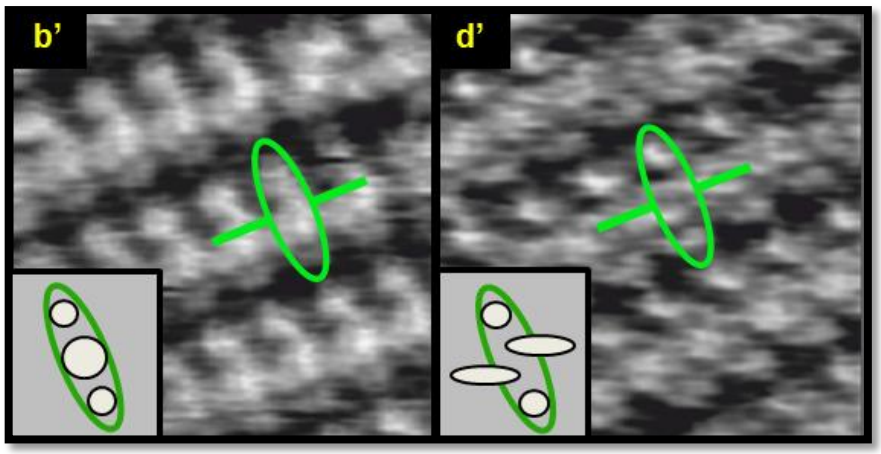

Figure 4.2.2.1.4. Parts **(b')** and **(d')** are zoom images of **(b)** and **(d)** from **Figure 4.2.2.1.3.**. Scanning area and parameters: (b' and d') 10x10nm^2, and I_t=1nA.

When comparing 2D and 3D molecular organization of **T2**, in fact, we can compare only the size along molecular longitudinal axis. Those distances, derived from powder 3D crystallites (2.37nm) turned out to be shorter than the corresponding distance in thin films (2.46nm) and significantly shorter than observed in the monolayer (3.1 nm). This indicates that packing of molecules along their longitudinal axis is denser in 3D than in 2D system.

4.2.2.2. Non-linear T3 molecule (chains in inner β position (C3)

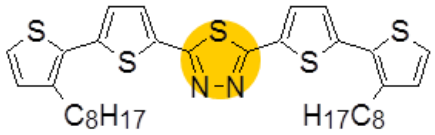

Figure 4.2.2.2.1 (a-b) shows representative STM images of **T3** monolayer, whereas proposed model of absorption geometry and the unit cell are presented in **Figure 4.2.2.2.1 (c,d)**. **T3** creates ordered monolayers on HOPG easily, covering whole surface of the substrate by large well-defined domains of at least one micrometer size. Similarly to **T2**, the two-fold symmetry of unit cell of **T3** isomer suggests stronger adsorbate-adsorbate interactions in comparison to the adsorbate-substrate ones.

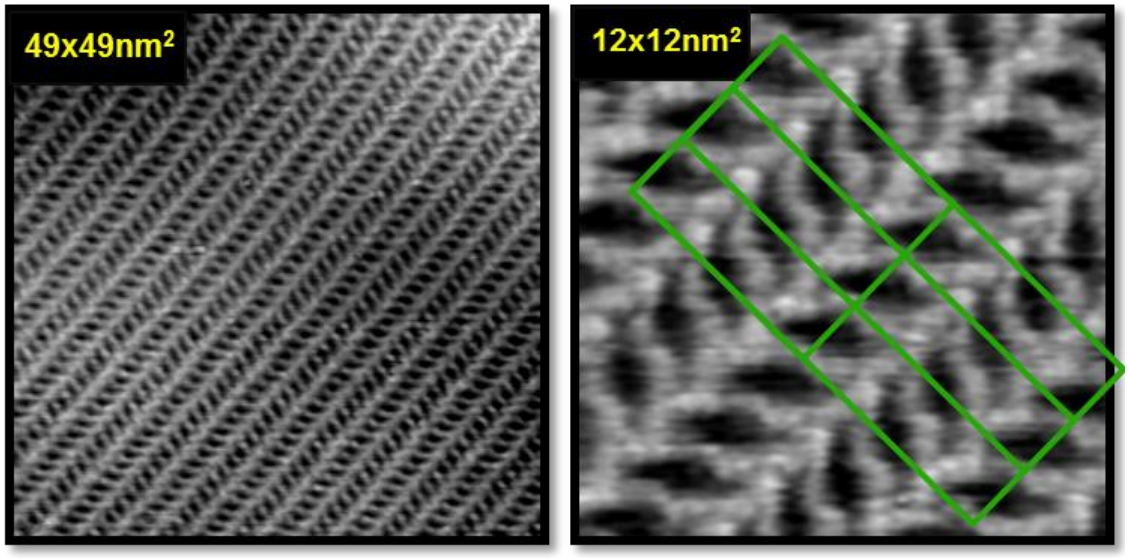

(a) **(b)**

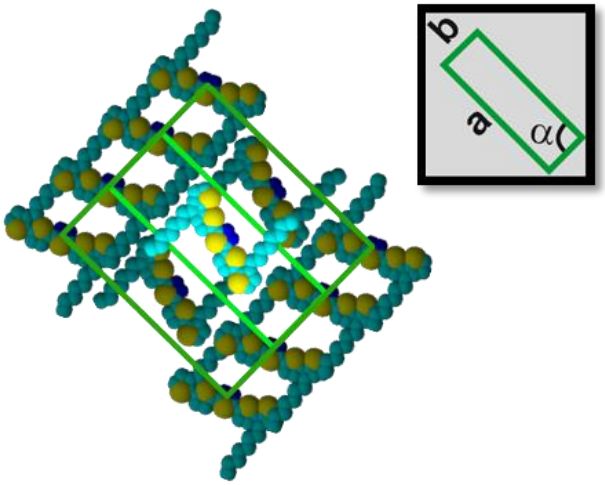

(c) **(d)**

Figure 4.2.2.2.1 (a-b) STM images, **(c)** postulated real space model of adsorption geometry and **(d)** unit cell of **T3** monolayer on HOPG (V_{bias}= -370mV, I_t = 0.3nA).

However, the different position of alkyl substituents between both molecules leads also to important dissimilarities in their submolecular organizations. The most spectacular one is the type of molecular organization. In contrast to regular assembly observed for **T2**, the **T3** molecules exhibit tendency to organize into very different, herringbone-type monolayer. The molecules from two adjacent rows are in this case alternatively oriented by ca. 120° with respect to each other. In this molecular arrangement the alkyl substituents do not interdigitate, they form parallel rows between rows of conjugated backbones. This is a similar behavior of the substituents as observed in the organization of this isomer in a single crystal. However, it is very different in comparison to observed in **T2** monolayer (in this case the alkyl chains mutually interdigitate).

Image of **T3** monolayer obtained at higher magnification **(b)** enables to determine parameters of the unit cell: ***a* = 3.9 nm, *b* = 1.4 nm, *α* = 87°.** The constant ***a*** corresponds to the distance between two rows of the same molecular arrangement in space (i.e. the same orientation with respect to the direction of formed rows). Half of this value (1.95 nm) is therefore related to the separation between molecular backbones in two adjacent rows. The corresponding distance in the structure of a single crystal is much smaller and equal 1.28 nm indicating much denser packing of **T3** in the bulk in comparison to the monolayer. The second parameter of the unit cell (***b)*** is related to separation between cores of adjacent molecules located in the same row. The measurements indicate that this separation is very similar for both isomers (1.4 nm for **T3** and 1.5nm for **T2**) confirming its independence of the alkyl chain position. It is important to remind that in both cases the separation, much larger than expected from the van der Waals size of both molecules, is a consequence of relative position of acceptor thiadiazole units of neighboring molecules in the monolayer and their mutual repulsive electrostatic interaction. In comparison with 3D organization, parameter ***b*** of the unit cell determined for **T3** monolayer is over 40% larger than corresponding constant (parameter **b**) of the unit cell in a single crystal (1.4 nm for monolayer with respect to 0.88 nm for 3D) again indicating denser packing of **T3** isomer in the bulk.

Figure 4.2.2.2.2 presents the results of imaging of **T3** monolayer during polarization switching of bias from +0.35 to -1V. Image **(a)** and part A-B of image **(c)** were obtained for positively polarized tip (i.e. imaging of occupied states). The submolecular contrast of the monolayer observed in these conditions is characterized by dominant bright spots located in the central part of each molecule. Hence, this area corresponds to thiadiazole

ring in the conjugated backbone of this molecule. As was previously discussed in the case of **T2**, it can be postulated that this acceptor group is the best mediator of electrons tunneling from the substrate to the tip. The image contrast changes with the bias polarization switching (to -1V). The amplification of the tunneling current in the central part of the molecule disappears in these new tunneling conditions (image **(b)** and part C-D of image **(c)**). It can therefore be concluded, that scanning with different polarizations of bias voltage enables to selectively distinguish in the STM image elements of molecular backbone of different electron affinity.

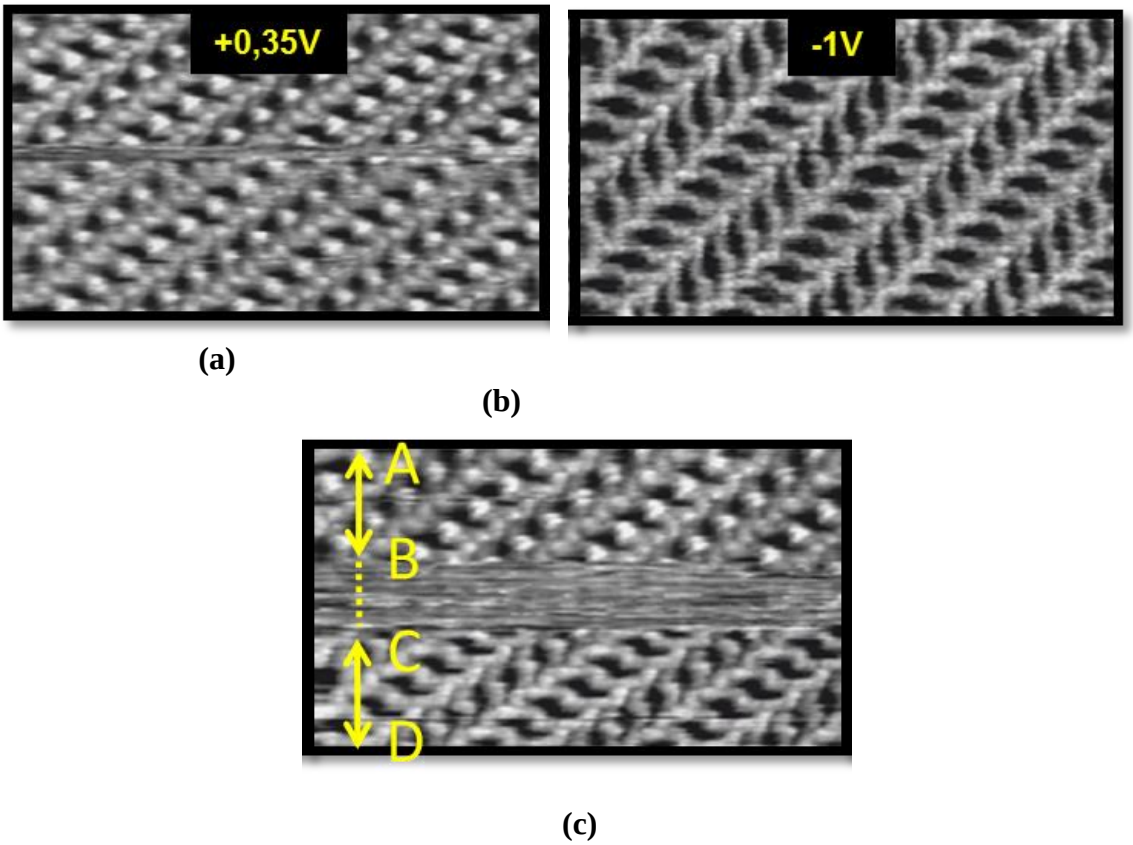

Figure 4.2.2.2.2 STM images of **T3** monolayer on HOPG obtained for different bias voltage: **(a)** 0.35 V**, (b) -**1 V, **(c)** image obtained with one step polarization switching from V_{bias}= + 0,35 V (areas indicated as A-B) to -1 V (C-D). Scanning area and parameters: **(a-c)** 24x13nm^2 and I_t =1nA.

Finally, it is interesting to compare 2D and 3D supramolecular organizations of **T3** isomer. This molecule organizes differently in the monolayer and in the bulk. The noted dissimilarities concern firstly the type of organization - regular in 3D and herringbone in 2D - and secondly its dimensions (significantly denser organization in 3D than in 2D).

Therefore, important question arises about driving force of the observed polymorphism of this molecule? As previously discussed, in optimal molecular conformation deduced from modeling of free molecule **T3** exhibits a nonplanar conformation. At the same time the image of the conjugated core in the monolayer is much more focused in comparison to **T2** analogue (compare images **Figure 4.2.2.1.1(b)** and **Figure 4.2.2.2.1(b)**), leading to thinner bright areas in STM images. This difference suggests, that **T3** does not lie flat on the HOPG surface, but rather adopt an edge-on configuration with a given tilt angle. As a result of complex matrix of interactions (including substrate-alkyl interactions compelling substituents to stay co-planar with the conjugated cores and stabilization achieved as a result of "mixed" substrate-molecule and alkyl-alkyl interactions) **T3** form monolayers which looks like corrugated iron. The non-planarity of this derivative is also particularly important when looking at the structural arrangement in the single crystal. The molecular torsion induces one π rotation of consecutive molecules in the crystal leading to their different alternative orientations in space (**Figure 4.2.1.5.1(c)**, more detailed discussion on this structure was described previously). Consequently, alkyl substituents are not contained in the same planes as stacked molecular backbones. This molecular arrangement results in a significantly dense packing. Concerning the 2D structure of **T3** monolayer, it is characterized by a weaker herringbone type packing, but with the alkyl substituents in the same plane of stacked molecular backbones. Therefore, the comparison of 2D and 3D organizations of this isomer clearly shows how the existence of the substrate forces changes in molecular arrangements to enable alkyl substituents to be located in similar or exactly the same horizontal plane as molecular backbones.

To summarize, in this chapter, structural organizations of five molecules (with the same thiophene-thiadiazole-thiophene DAD core) were compared. Molecules differed by the location of terminal octyl substituents (among five, three of them were structural isomers). A strong effect of substituent position on both, 2D and 3D organizations was discussed.
In the case of linear derivatives (nonsubstituted **T1** and α-substituted **T4**) lamellar-type arrangement occurs in a direction perpendicular to the substrate plane (in powder grains as well as in thin films). No ordered monolayers could be obtained for these derivatives. These findings are compatible with literature reports concerning preferential lamellar-type 3D organization[166] of other DAD semiconductors with terminal thiophene rings and with

alkyl substituents in α positon, as well as, with the lack of 2D organization of such molecules on HOPG.[157]

Nonlinear isomers (**T2** and **T3**) organize in both 2D and 3D. All three nonlinear compounds (**T2**, **T3** and **T5**) form typical 3D polycrystalline powders and lamellar-type films. The dimensions of the unit cells derived from 3D crystals turned out to be shorter than the corresponding ones in films (for all five compounds) and significantly shorter than corresponding distances in 2D unit cell (ordered monolayers were possible to obtain for both β substituted compounds). For this reason, the polymorphism of the studied molecules was acknowledged.

Depending on the position of alkyl substituents in the molecule and their arrangement in monolayer either herringbone type (**T3**) or regular (**T2**) organization have been observed. Different behavior of alkyl substituents in both structures was noted. In the herringbone organization they are oriented in one direction in the layer and form rows parallelly oriented to the rows of molecular backbones. In this arrangement the following chains mutually interacts however they do not interdigitate. In regular structure the substituents, located between consecutive molecules in the layer, are oriented and interdigitated in one direction. Similar arrangements of chains as in the monolayer were also observed in bulk (in **T2** powder and thin films, also in **T3** single crystal, and thin films). However, it must be highlighted that contrary to the monolayer the molecules in 3D systems are oriented nearly perpendicularly to the substrate plane.

The lack of the interdigitation of alkyl chains was proved to be characteristic for **T3** molecule in both 2D and 3D. This feature was already confirmed for 2D monolayers of other oligothiophenes alkylated in inner β position.[167-168] However, it must be pointed out, that for **T3** the alkyl substituents in 3D do not lie on the same plane as backbones of the molecules. The clearly observed polymorphism of this molecule shows how the presence of the substrate restrain the molecules in the 2D monolayer to align the alkyl groups parallel to the backbone plane.

Thiadiazole central acceptor part was proved to have strong effect on intermolecular separation in 2D. The dominant interactions between the central acceptor groups of adjacent molecules in the face to face configuration lead to an unexpectedly large intermolecular separation for investigated alkyl derivatives. As a consequence, ordered

monomolecular layers are characterized by stacking of low density with cavities of nanometric size which are formed between conjugated backbones of every pair of neighboring molecules. The behavior of those molecules in 3D is different. Molecules are differently oriented. Due to intermolecular shift observed in single crystal the thiadiazole acceptor group faces terminal thiophene group of adjacent molecule. As a consequence of this intermolecular shift corresponding intermolecular separation is much smaller.

Finally, no effect of the substrate on 3D organization was observed for investigated compounds. The change of solvent had no apparent effect also on their 2D structure on HOPG. Deposition method influences only the film thickness, not its molecular organization in the films. Only **T3** showed subtle solvent organization dependence on 3D thin films.

4.2.4. Effect of the central acceptor unit

As have been presented above, relatively loose molecular packing prevails in **T2** and **T3** monolayers. Both molecules adopt face to face configuration in 2D, hence, the repulsive forces between acceptor parts of adjacent molecules in one row are supposed to be responsible for large separation in *b*-direction. For comparison purpose, it was therefore instructive to perform investigations of new derivatives of **T2** and **T3** in which thiadiazole central acceptor parts was replaced by different acceptor unit. An even stronger acceptor, namely, tetrazine was proposed (**Figure 4.2.4.1** described as **TT2** and **TT3**).[169] The representative images of **TT2** and **TT3** monolayers along with the proposed models of adsorption geometry are presented in **Figure 4.2.4.2** and **Figure 4.2.4.3** respectively.

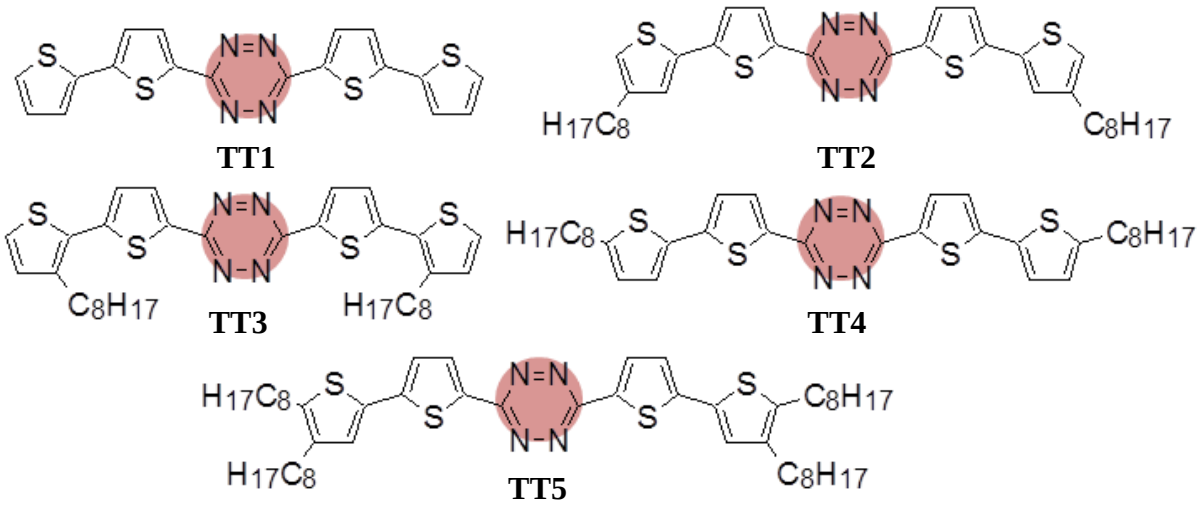

Figure 4.2.4.1 Investigated semiconductors.

In **TT2** isomer the alkyl chains are located in outer β position of terminal thiophene rings. The molecules are oriented in monolayer in one direction and mutually stacked in parallel molecular rows (see **Figure 4.2.4.2**). The parameters of unit cell determined for this isomer from STM images are ***a* = 2.6 nm**, ***b* = 0.85 nm**, ***α*=89°**. The ***a*** parameter corresponds to separation between molecular rows. It is much smaller than the length of a molecule. This relation in combination with proposed model of adsorption geometry indicates intedigitation of alkyl substituents in the layer. This is a common feature of 2D structural organizations of **TT2** and **T2** analogue.

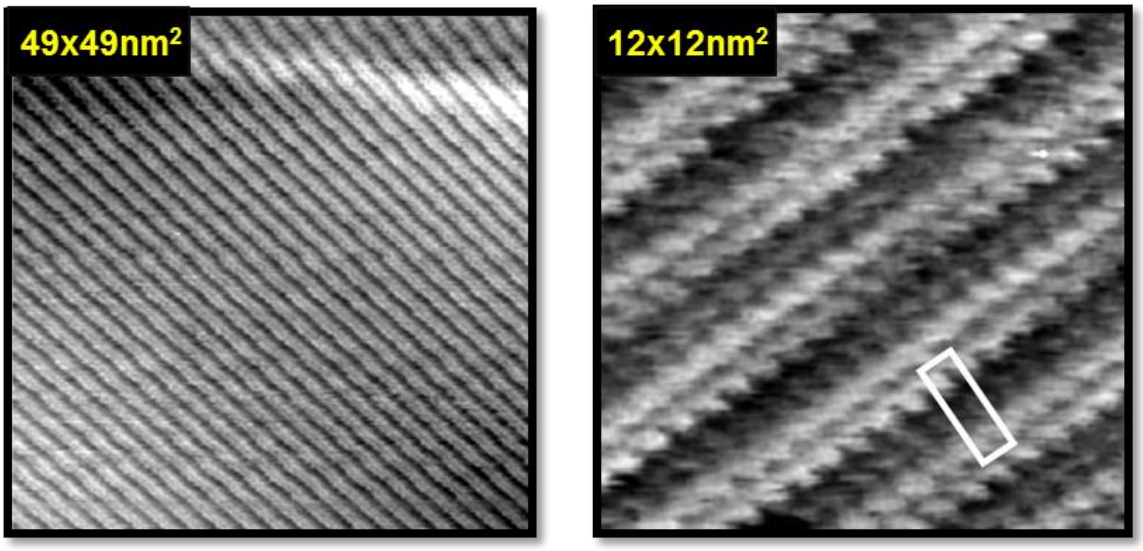

(a) **(b)**

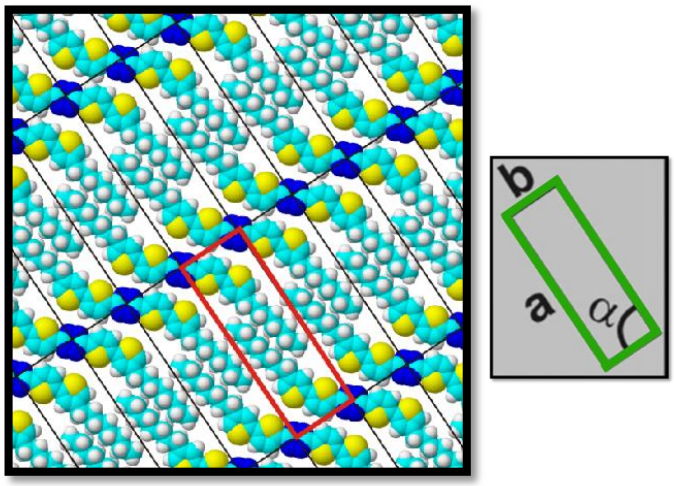

(c) **(d)**

Figure 4.2.4.2 (a-b) STM images, **(c)** postulated real space model of adsorption geometry and **(d)** unit cell of **TT2** monolayer on HOPG (V_{bias}= 1V, I_t =0.3 nA).

However there is also one important difference between organizations of both molecules which concerns intermolecular separation in one row (parameter ***b***). The determined distance of 0.85 nm for **TT2** is much smaller (over 40%) that separation noted for **T2** monolayer. This value is very close to the conjugated core width.

TT3 isomer is organized in similar way as **TT2**. The molecules are also oriented in one direction and mutually stacked in parallel molecular rows (**Figure 4.2.4.3**). Thus, contrary to the case discussed above of thiadiazole derivatives, the position of the alkyl substituent has a much less pronounced effect on the selfassembly pattern of the bithienyl tetrazine molecules. The unit cell dimensions of **TT3** monolayer are ***a* = 1.7 nm, *b* = 1 nm, *α* = 87°**.

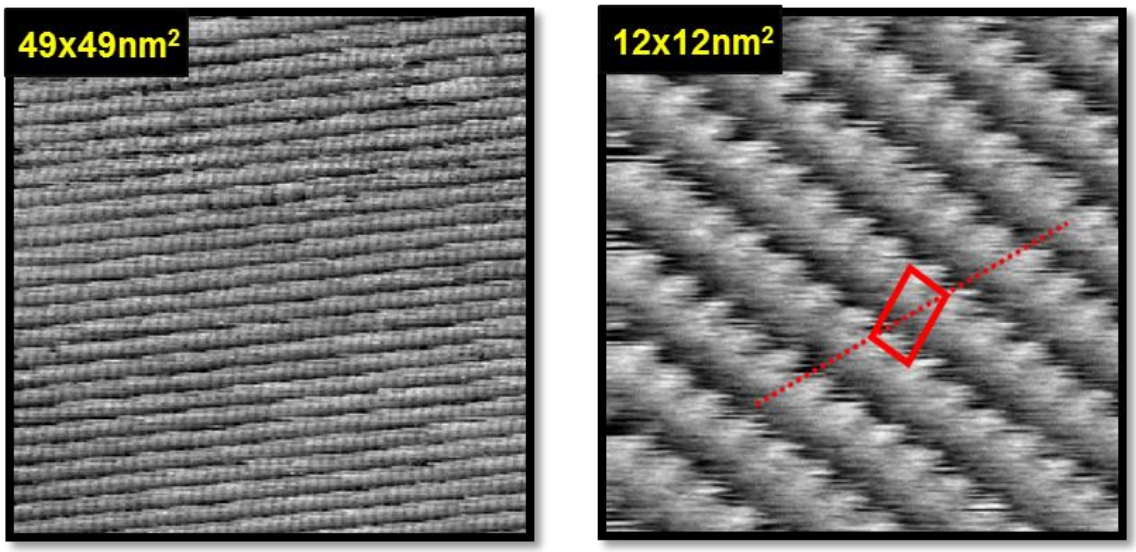

(a) **(b)**

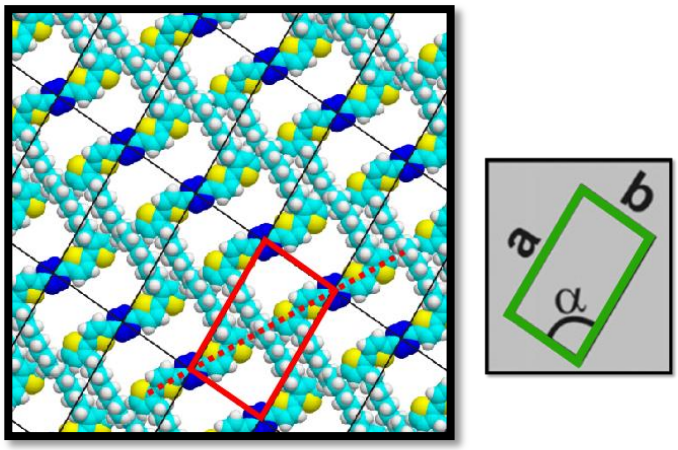

(c) **(d)**

Figure 4.2.4.3 (a-b) STM images, **(c)** postulated real space model of adsorption geometry and **(d)** unit cell of **TT3** monolayer on HOPG (V_{bias}=1 V, I_t =0.3 nA).

These crystallographic constants are different in comparison to **TT2** which results from different substituent position in these isomers. As expected, ***a*** parameter corresponding to the separation between molecular rows is much lower for **TT3** (by 34%) due to smaller effective length of this molecule. This value is in a good correlation with the length of the conjugated backbone of **TT3** isomer. The opposite effect is noted in the direction perpendicular to the longitudinal axis of the molecule. The separation between following molecules in one row is slightly larger for this isomer in comparison to **TT2**. This is a consequence of nearly perpendicular orientation of the substituents in the monolayer with respect to molecular axis. It is also important to mention that in the case of **TT3** monolayer the alkyl substituents do not interdigitate, they form parallel rows between the rows of conjugated backbones. Thus, in spite of different molecular arrangement in **TT3** and **T3** monolayers, the behavior of alkyl substituents is nearly the same.

To conclude, the observed main dissimilarity between organizations of the investigated molecules with different acceptor units is intermolecular separation along molecular rows (parameter ***b*** of the unit cell). The unexpectedly smaller separation noted for molecules with stronger acceptor tetrazine is caused by stronger repulsive intermolecular interactions generated by this group in the monolayer in comparison to thiadiazole ones. This is a reason why **TT2** and **TT3** molecules do not adopt face to face configuration in the layer, but they prefer to be mutually shifted with respect to each other along their longitudinal axis. In this way, the central tetrazine group of each molecule faces thiophene ring of the adjacent molecule in the layer and vice versa. As a consequence, the monolayer of tetrazine derivatives is characterized by the domination of attractive donor-acceptor electrostatic interactions instead of repulsive acceptor-acceptor ones, as it is expected in the case of thiadiazole derivatives. The indirect result of this difference is 2D organization and much denser packing of monolayers consisting DAD semiconductors with stronger acceptor unit. The relation between effective area of a single molecule in the layer determined for four molecules under consideration confirms this conclusion (4.63 nm^2 and 2.72 nm^2 for **T2** and **T3** and much smaller values 2.2 nm^2 and 1.7 nm^2 for **TT2, TT3** respectively).

Kurach et al[166] reported studies of 3D organization of molecules from **TT** series presented in **Figure 4.2.4.1** as **TT1**, **TT2**, **TT4** and **TT5** performed by means of X-ray diffraction**..** Single crystal measurements performed for non-substituted dithienyl-tetrazine derivative (**TT1**) shown shift from face-to-face configuration along molecular longitudinal axis. This is well correlated to the observations of molecular arrangement in monolayers of substituted **TT2** and **TT3**. Different molecular organization observed in own studies for thiadiazole evidently indicates strong influence of acceptor group on molecular organization of this type of molecules in both 2D and 3D.

Unfortunately, for substituted analogues (**TT2**, **TT4** and **TT5**), the authors discuss only 3D powder measurements hence no information about ***b*** parameter could be extracted. However, concerning ***a*** parameter (longest unit cell dimension determined from position of the first peak of diffraction profiles) no significant differences were determined for these substituted derivatives in comparison to non-substituted **TT1**. Own results concerning powders of corresponding molecules with different acceptor group (thiadiazole) lead to similar conclusion This indicates deep interdigitation of alkyl substituents in 3D powder structure of both families of DAD molecules.

Moreover, the powder profile of **TT4** molecule is of the same type as obtained for its thiadiazole analogue **T4**. Both of them show preferential orientation of powder grains exhibiting lamella type structure in which molecules stand upright in the lamellae. Such orientation of powder grains deposited from simple alcohol suspension is not common. This observation indicates that the position of the alkyl substituents and the final shape of this type of DAD semiconductor affect not only submolecular organization but also the macroscopic arrangement of crystal grains. According to own results, **T1** also exhibits such behavior of its powder grains. It is possible, that **TT1,** tetrazine analogue of **T1,** creates "oriented powder" as well, and consequently, that "macroscopic orientation" feature is characteristic to all linear DAD molecules. However, **TT1** powder profile presented in[166] was calculated from single crystal data and I cannot confirm this assumption.

Finally, in the undertaken studies of the role of acceptor group on submolecular organization of DAD type semiconductors it is interesting to discuss behavior of related donor-donor semiconductors without central acceptor part i.e. alkyl derivatives of thiophenes or oligothiophenes. Fukunaga et al[170] performed STM studies of organization at liquid-graphite interface of monothiophene functionalized in α-position with a dodecyl alkyl chain. The thiophene molecules were found to be lying head-to-head, with thiophene rings oriented diagonally on the graphite surface and stacked in face-to-face positions. The observed in own studies preferential face-to-face configuration of DAD semiconductor with weaker acceptor part (thiadiazole) on HOPG is therefore correlates with this tendency of pure thiophene organization.

At this point it is also worth to compare intermolecular separation (***b*** parameter of the unit cell) reported for 2D organization of alkyl derivatives of oligothiophenes. This separation varies typically for oligothiophenes between 0.9 to 1.1 nm (for example, for monolayers of α substituted oligothiophenes imaged on MoS_2 it is equal: trithiophene substituted by octyl chains – 1.13±0.5nm[155], terthiophene substituted by hexyl chains – 1.13±0.8nm or 0.94±0.5nm (two different structures)[155] and 1.2±0.1nm,[158] tetrathiophene substituted by dodecyl chains – 1.15±0.05nm,[155] moreover β substituted (outer position) pentathiophene on Ag (III) – 0.65 nm,[171] β (inner position) pentyl disubstituted pentathiophene – 1.0 nm[155,168]). It is therefore evident that unusually high intermolecular separation of 1.3 and 1.4 nm observed for **T2** and **T3** monolayers is a consequence of the presence of thiadiazole acceptor unit in the conjugated backbones of these DAD semiconductors.

4.2.5. Effect of the alkyl chain length

The results discussed in the previous chapters exhibit dissimilarities in supramolecular organization of investigated thiadiazole-thiophene semiconductors. The particular differences are observed in organization of **T3** in comparison to other investigated linear and nonlinear isomers. The spectacular example are different types of monolayers, herringbone and regular, formed by two nonlinear isomers: **T3** and **T2** respectively. In this situation interesting question arises; how herringbone organization, typical for **T3** molecule, depends on the alkyl substituents length. To answer this question, two new compounds (**T6** and **T8**) were synthesized and investigated in the same manner as previously discussed for other isomers. They are analogues of **T3** with different length of alkyl chains: butyl and dodecyl, respectively (**Figure 4.2.5.1**). The dimensions of optimized central part and terminal chains of the investigated semiconductors are presented on **Figure 4.2.5.2.**

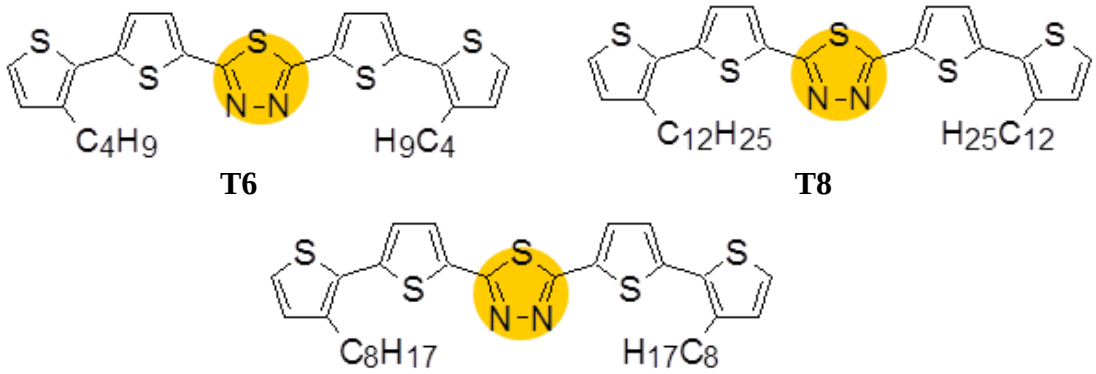

Figure 4.2.5.1. Investigated semiconductors.

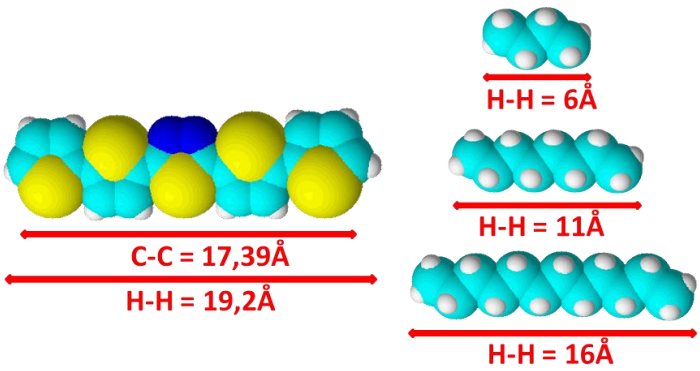

Figure 4.2.5.2. Sizes of parts of investigated semiconductors.

Diffractograms of **T6** and **T8** powders are presented in **Figure 4.2.5.3** (**T6**) and **Figure 4.2.5.4** (**T8**).

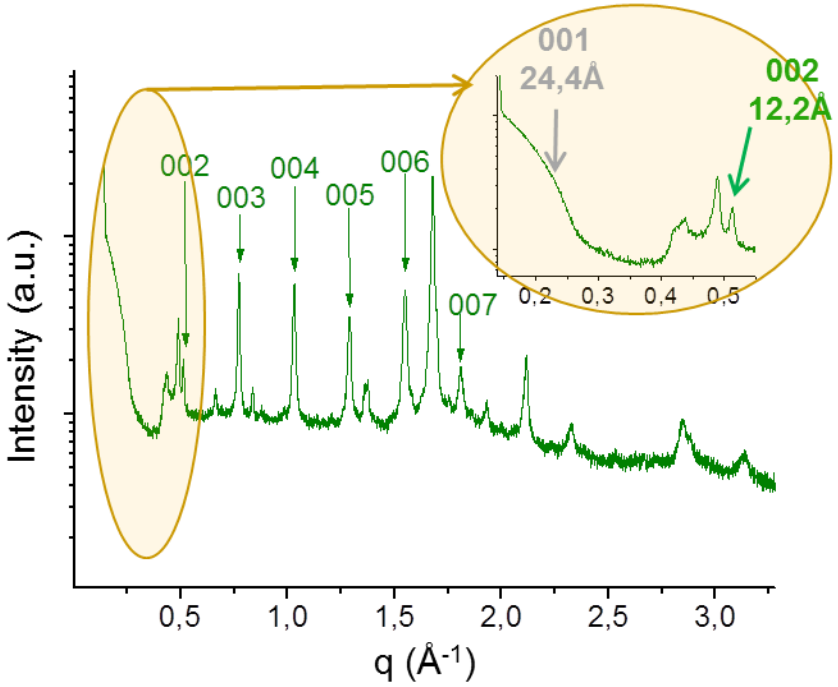

Figure 4.2.5.3 Powder diffractograms of **T6**. Low q range is shown in detail as an inset.

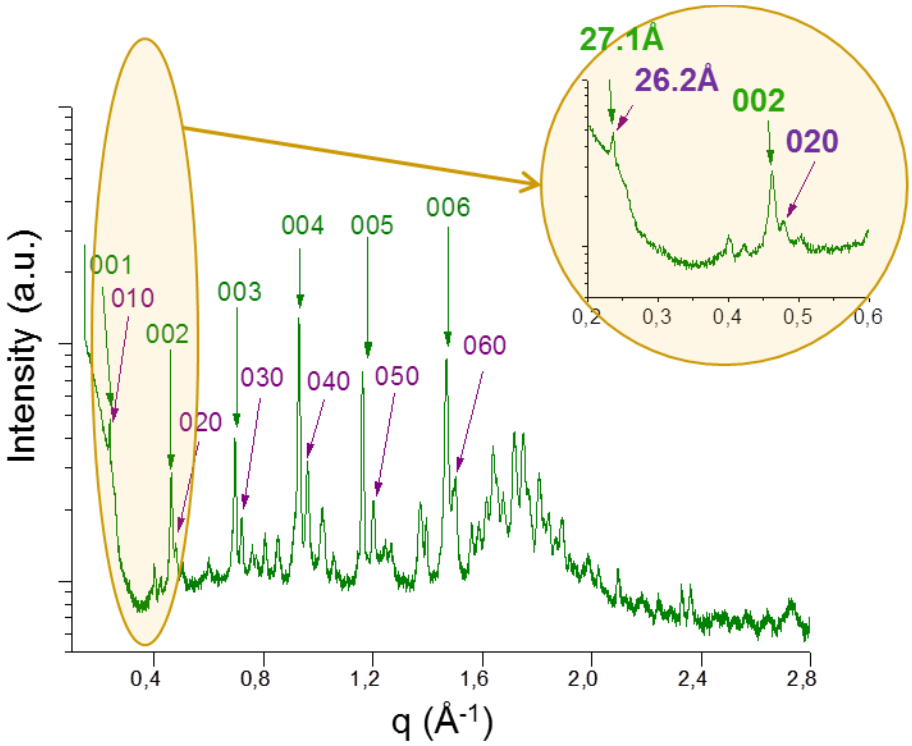

Figure 4.2.5.4 Powder diffractograms of **T8**. Low q range is shown in detail as an inset

Powder profiles of both compounds are characteristic of 3D low symmetry structure with peaks originating from different crystallographic planes. However, for both, the characteristic sets of well distinguishable reflections that might be indexed as a members of families can be distinguished. They suggest predominant orientations of powder grains deposited on the substrate from simple alcohol suspension.

The first distinguishable reflection from 001 family in **T6** powder profile is situated at q equal to 0.515 $Å^{-1}$ which corresponds to a period of 12.2 Å. Considering the position of other peaks of the same family, it is most probable that this signal does not correspond to the first order (001) reflection. This location is more consistent with position of calculated second order peak of this family. The expected position of the 001 reflection (related to q=0.258 $Å^{-1}$ and period 24.4 Å) is marked by gray arrow. In principle, it should be seen on the diffraction profile when using this diffraction geometry. Attempts to separate it have not been successful, probably because of the artifact shadow effect present in the diffractometer at this time.

In **T8** powder diffractogram two different families of reflections can be easily indexed. The 001 and 010 periods equal to 27.1 Å and 26.2 Å can be distinguished indicating that 3D organization of crystalline grains may exhibit two long parameters for the unit cell, which could be either monoclinic or orthorhombic. The sizes of crystallites, determined from 004 and 040 peaks by means of Sherrer formula are 80 and 70 nm, respectively. For comparison, the corresponding dimension of **T6** grains determined from 002' reflection is 60 nm. Let's remind, that the same value was also obtained for grains of **T3** powder. Hence, the dimensions of grains in powder are consistent for all the molecules from the discussed series.

It is worth to notice in addition, that the position of the 001 reflection corresponding to intermolecular separation along molecular axis (24.4 Å for **T6,** as well as, 27.1Å **for T8**) is much larger than observed for **T3** (15.9 Å). On the other hand, those distances are fitting well with the equivalent distances of other substituted molecules of **T** series (28.2 Å for **T4**, 24.6 Å for **T2** and 27.3 Å for **T5**) suggesting truly divergent packing mode of **T3** in comparison to all its analogues. This conclusion will be further supported by 2D studies of monolayers. **T3** exhibits different supramolecular organization (including molecular 3D orientation) in monolayers in comparison to **T6** and **T8**. **T3** monolayer is not really flat

and the molecule is partly out of plane resulting in “corrugated iron structure”. This is not the case for **T6** and **T8** for which the whole molecules are in contact with HOPG substrate.

Two diffractograms of **T6** and **T8** thin films are presented below in **Figure 4.2.5.5** and **Figure 4.2.5.6**, respectively.

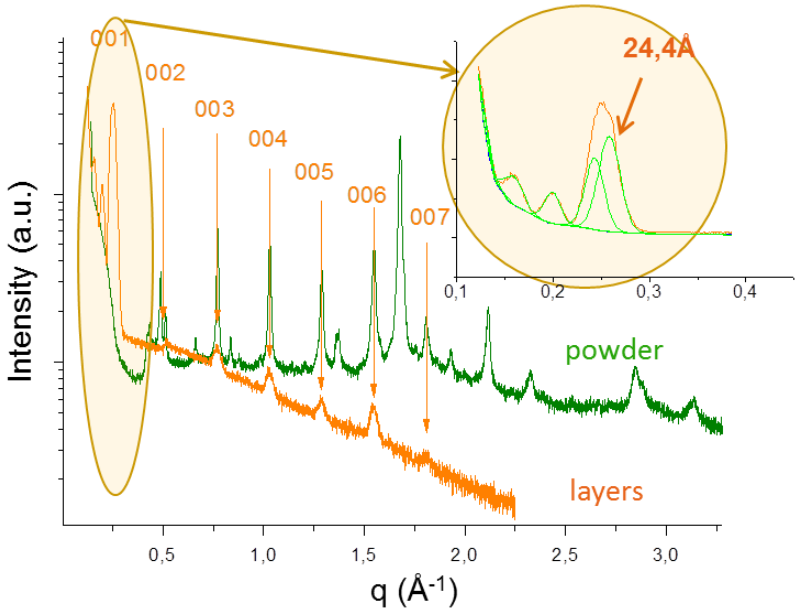

Figure 4.2.5.5 Powder and thin-layer diffractograms of **T6.** Low q range is shown in detail as an inset. Green curves are decoupled 001 peak and Kiessieg fringe.

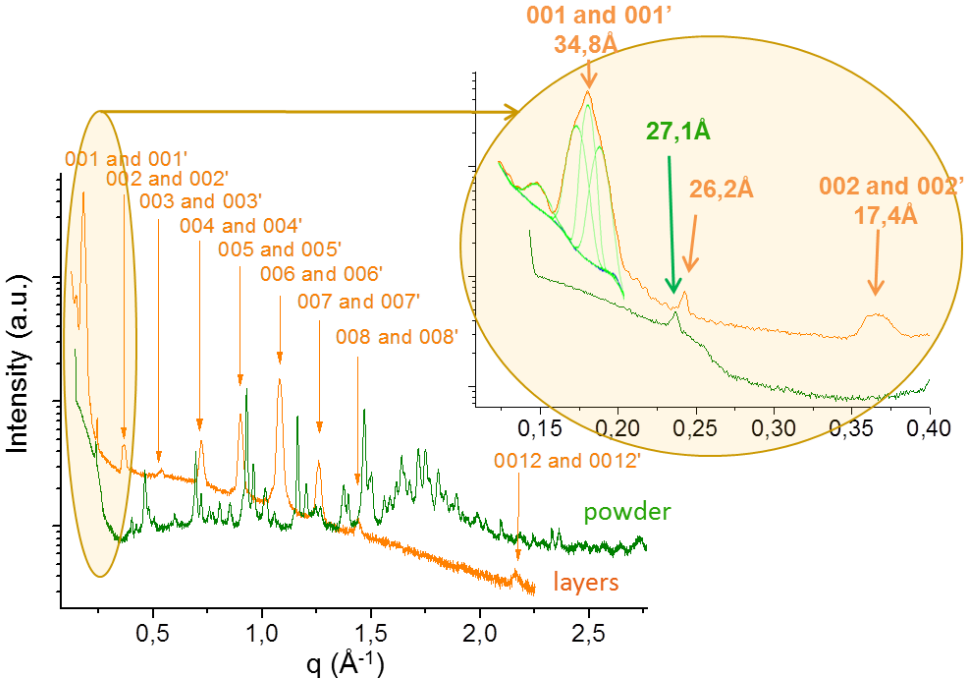

Figure 4.2.5.6 Powder and thin-layer diffractograms of **T8.** Low q range is shown in detail as an inset. Green curves are decoupled 001, 001’peaks and Kiessieg fringe

No apparent effect of the type of solvent or substrate choice on thin films organization was observed for these derivatives. The representative films were prepared by spincoating from 10g/ml chloroforme solution on Si wafer covered with thermal SiO_2 layer. The thickness of the layers estimated by Kiessig fringes positions was approximately 15 nm and 30 nm for **T6** and **T8,** respectively.

Despite the small thickness, a very well-defined layered-type organization is present in thin films of both discussed compounds. The diffraction profile of **T6** reveals a family of reflections in which peaks up to 7^{th} order might be indexed. Main, first order peak of this family (001) is situated at q corresponding to period 24.4 Å. Computer analysis allowed separation of fused Kiessig peak and 001 reflection (marked in the inset of **Figure 4.2.5.5** by a green lines), however with some inaccuracies. Therefore the abovementioned values should be taken as approximate dimensions. Nevertheless, this results suggest very well-organized film of **T6**, consisting of less than ten layers of molecules arranged more or less perpendicularly along their longitudinal axis versus the substrate plane. It is important to note, that positions of other reflections of 001 family in layers coincide with 001 family in powder. We can therefore conclude that the molecules crystallizes with the same orientation. Yet, substrate enforces specific orientation of formed crystallites which are oriented in the layer in such a way that the 001 plane in contact with the substrate surface.

T8 thin films also reveal well-ordered family of reflections with 001 peak around 35 Å in which peaks up to 12^{th} order might be indexed. This result indicate that **T8** layers are organized in oriented lamellar structure but with a different period than those recognized in the powder profile. This is a typical example of molecule for which the stacking mode obtained on the substrate significantly differs from that one found in the 3D system, as suggested by the powder profile. However, given the "dual" nature of the powder grains, the question arose whether it is truly single family? Omega scans allowed to address this problem. The measurements performed for 001 and 006 reflections revealed coexistence of two reflections in each 2θ point, proving coexistence of two families instead of one. However, despite my best efforts, they are inseparable. Therefore, the crystallite size determined from 001 and 006 reflections (approximately 7 nm) is the average value from both families.

Regarding the general trends, both molecules, as well as others previously discussed, are packed in films in such a way, that their molecular longitudinal axis is arranged perpendicularly (or with small tilt angle) to the substrate. That is implied by low q position of both 001 reflections in thin films. In addition, **T8** organization reflects general trend,

that longitudinal stacking mode is denser in powder grains (27 Å) than in the films (34.8 Å). By contrast, this trend is not reflected for **T6**. The behavior of this derivative resembles rather unsubstituted **T1** since they both appear to display one preferred model of assembly, or to be more precise, the same periodicity in films and powder grains. Most probable explanation of this phenomena is a supposition that the butyl chains are yet too small to influence organization. As a consequence **T6** final structure is governed by DAD central part. Attraction between small, butyl chains is too weak to have the impact on the submolecular structure.

That again brings us to the delicate balance between different parts influence and to the question posed at the beginning of this section: why **T3** organization is so different in comparison to all its substitution isomers as well as analogues with different alkyl chain length? Fortunately, this matter could be investigated further by STM studies of monolayers.

Both β-substituted molecules form well-ordered monolayers of flat laying molecules when they are deposited on HOPG by dropcasting method. STM images of representative **T6** and **T8** monolayers are presented in **Figures 4.2.2.7**, and **4.2.2.8**, respectively.

In both cases the monolayers are characterized by large, well packed domains of the size of few hundred nanometers or larger. Each domain consists of parallel rows of molecules oriented in one direction. It has been confirmed for isomer with longest substituents (**T8**), that adjacent domains are rotated against each other by angle different than 60 degrees. This observation can indicate relatively weak influence of the substrate topology on the monolayer formation. It is unexpected observation, because the longer the alkyl chain the stronger interaction it develops to the substrate, typically following one of its axes. The parameters of unit cells determined from STM images for monolayers of both isomers are: ***a* = 2.8 nm**, ***b* = 2.3 nm**, ***α* = 70º (T6)** and ***a* = 3.6 nm**, ***b* = 2.5 nm**, ***α* = 64º (T8**). Let's remind, that some of those values are very similar to observed in 3D cells (2,4 nm for **T6**, 2.71 nm and 3.48 nm for **T8,** in powder and layers, respectively).

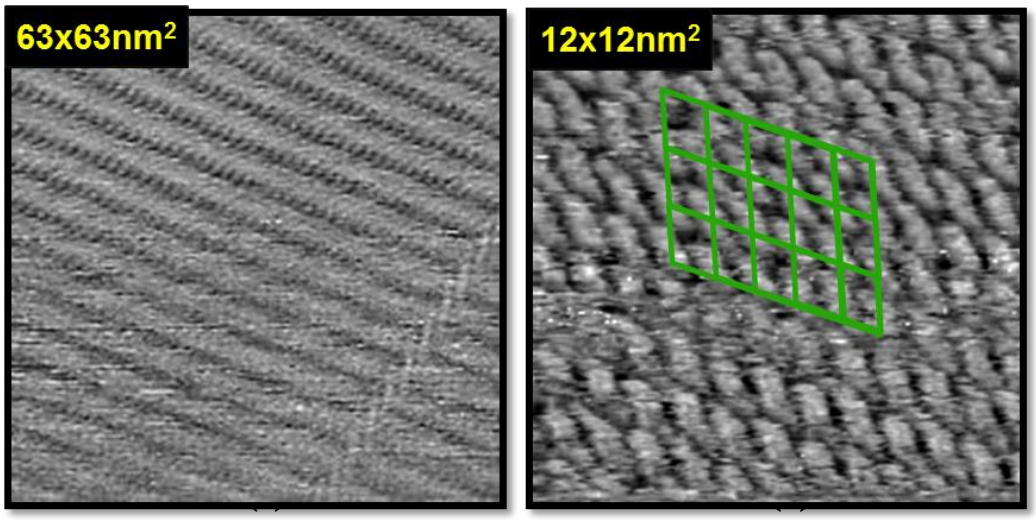

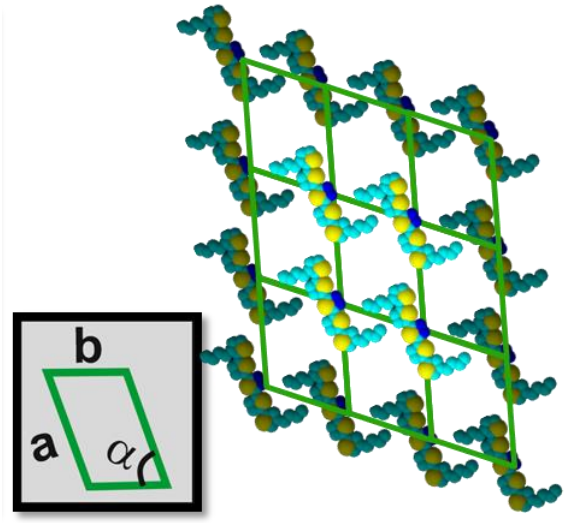

(c) **(d)**

Figure 4.2.2.7 (a-b) STM images**, (c)** unit cell and **(d)** postulated real space model of adsorption geometry of **T6** monolayer on HOPG (V_{bias}=-1V, I_t =1nA).

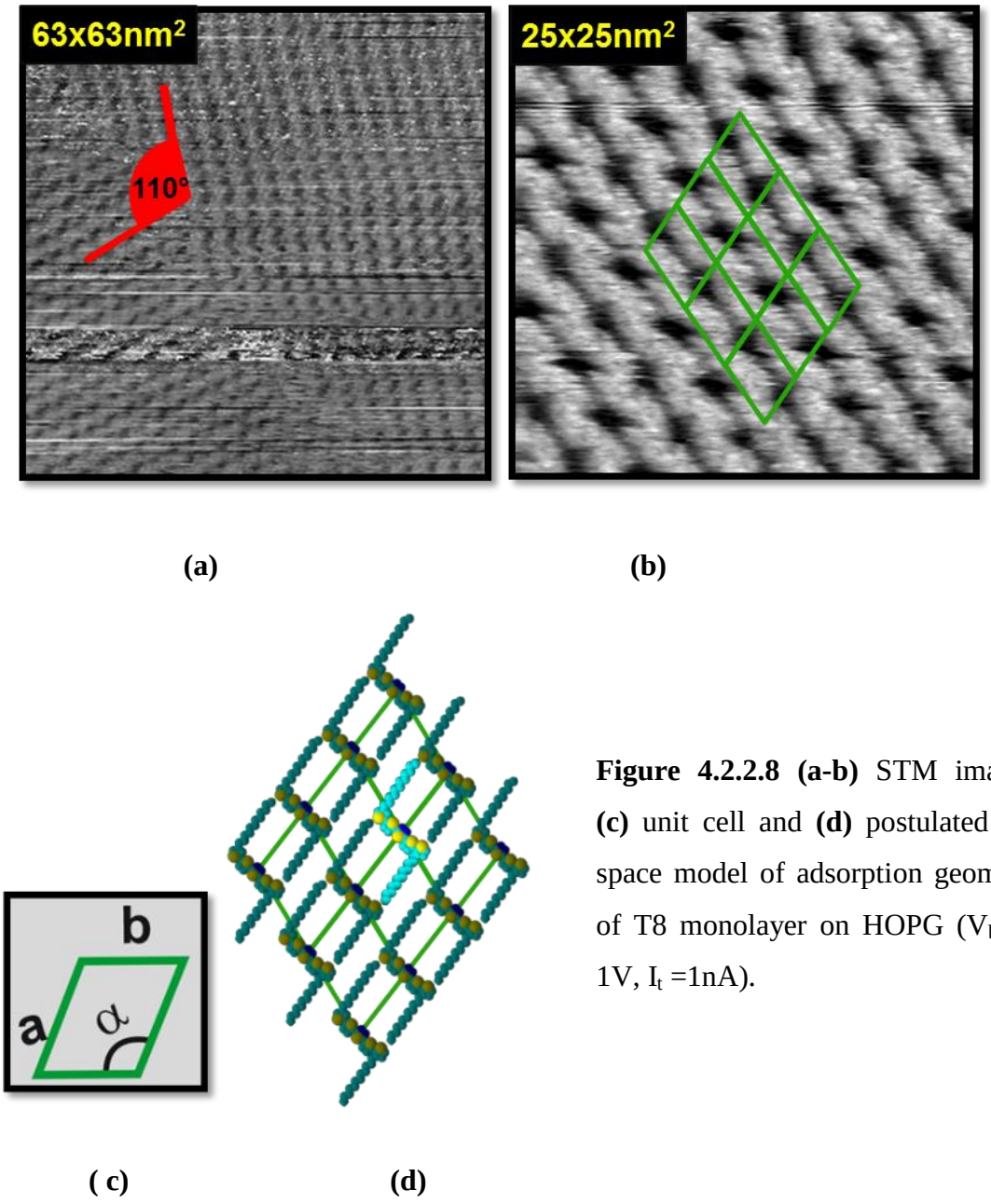

Figure 4.2.2.8 (a-b) STM images**, (c)** unit cell and **(d)** postulated real space model of adsorption geometry of T8 monolayer on HOPG (V_{bias}=-1V, I_t =1nA).

In comparison, it is worth to remind the unit cell of **T3** is again very different It corresponds to herring-bone organization with two different orientations of following molecules in the layer. As a consequence the unit cell consists of 2 molecules (instead of 1 molecule as were observed for **T6** and **T8**). The crystallographic constants of **T3** monolayer are: **3.9 nm / 1.4 nm / 87º.** Postulated real space models of all three semiconductors are compared in **Figure 5.2.2.9.**

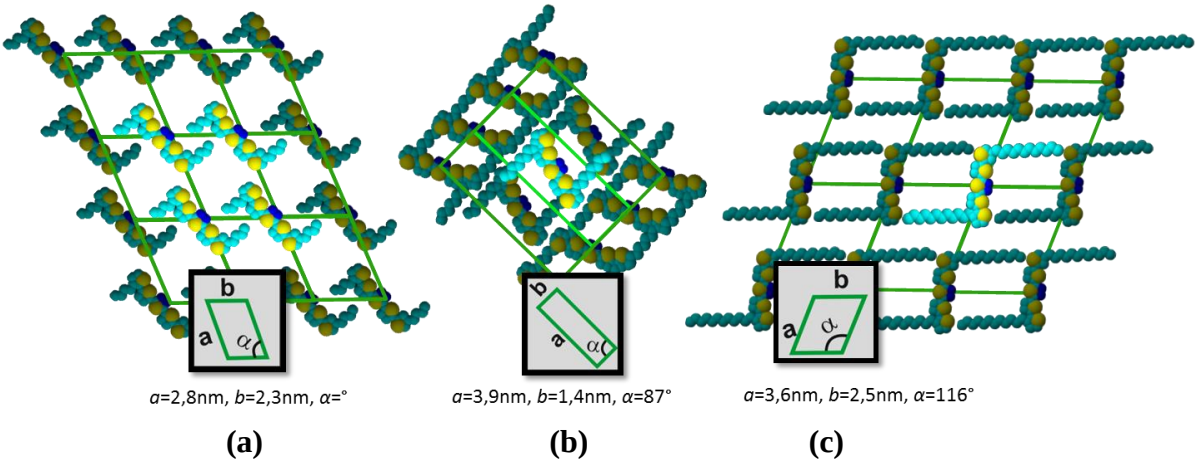

Figure 4.2.2.9 Postulated real space models of **(a) T6, (b) T3, (c) T8** monolayers on HOPG.

The comparison of their unit cells parameters turns to three general conclusions. The first one concerns shape of the unit cell. The type of organization is evidently reflected in α angle. Herring-bone organization of **T3** leads to nearly rectangular unit cell which is diacritical in comparison to the shape of unit cells formed by other two isomers. The second conclusion deals with the density of molecular packing in the monolayer. It is evident from microscopic observations that monolayer of **T6** isomer with shortest alkyl chain is characterized by relatively loose molecular organization. This feature can be a consequence of influence of electrostatic interactions between acceptor (thiadiazole) units of neighboring molecules in the layer. The overall influence of this repulsive interaction on supramolecular organization should be amplified more effective for derivatives with shorter alkyl substituents. The third finding concerns the behavior of alkyl substituents in the monolayer. For all three isomers these substituents are oriented perpendicularly to the molecular longitudinal axis and located in parallel rows between rows of backbones of neighboring molecules in the monolayer. As a consequence of this position the alkyl chains cannot interdigitate. This seems to be a characteristic feature of monolayers formed by all investigated DAD semiconductors (**TT3** as well) with terminal alkyl chains in inner *β* position.

Finally it is interesting to discuss driving force of observed changes in supramolecular organization induced by the size of alkyl substituents. Alkyl derivatives of pure thiophene (without acceptor unit) have been studied by Baüerle et al. [165] This group imaged a series

of tetrathiophenes with alkyl substituents (dodecyl, hexyl and pentyl) in the inner β-position. The obtained results indicated crucial role of attraction between alkyl chains and their interdigitation in the formation of the final structures. Yet, in contrast to pure oligothiophenes, the evolution of molecular organizations of thiadiazole-thiophene DAD semiconductors can be discussed in even more complex way. Particularly, in the light of competition between two opposite kinds of intermolecular interactions coexisting in the monolayer, namely: interactions between conjugated cores with long range repulsive electrostatic forces between thiadiazole acceptor units and attractive forces between alkyl substituents. As it is expected the relation between these two interactions changes with the alkyl chains length. Two mechanisms of this relation can be taken into consideration. First of all, the increase (decrease) of the substituents size in the molecule simply increases (decreases) the strength of their mutual interactions in the monolayer. The second mechanism is a consequence of the alkyl substituents location in the monolayer observed for all isomers from the series. As was stated above, they are situated inside molecular rows between backbones of neighboring molecules. Consequently, the intermolecular separation in this direction is related to the size of these groups. In this way alkyl separators have indirect effect on the strength of mutual interaction between backbones of following molecules in the monolayer. Taking into account these findings a domination of the interaction between molecular cores in monolayers of isomers with shortest alkyl substituents (**T6**) can be expected. As a consequence of strong in this case repulsive forces between acceptor groups the mutual shift of neighboring molecules along their longitudinal axis is generated in the monolayer to minimize the layer energy. The situation is qualitatively similar to that one previously observed in monolayer of molecules with stronger acceptor – tetrazine. Accordingly, the increase of alkyl substituents length enhances mutual interactions between alkyl chains and reduces effect of interactions between molecular cores. Hence, the submolecular organization evolves from that one in which molecules are located asymmetrically with shift (**T6**) to parallel face-to-face molecular arrangement (**T8**).

These two extreme situations correspond to the domination of one type of interactions in the monolayer. The interesting case concerns the isomer **T3** with alkyl substituents of medium size. As was already discussed the monolayer of this molecule is characterized by very different structure. This indicates that observed in this case herring-bone type organization with two alternate molecular orientations is a consequence of weak balance between two interactions mentioned above comparable in strength.

5. Conclusions

X-Ray Diffraction studies and comparative “real space” surface imaging at molecular resolution carried out by scanning tunneling microscopy made possible to determine correlation between chemical structure of organic semiconductors under investigation and their supramolecular organization. Based on experimental results, an attempt was made to propose and to discuss distribution of supramolecular interactions in the investigated structures in order to obtain conclusions of broader cognitive context.

Objectives of undertaken studies were sixteen new semiconductors of complex electronic structures (donor-acceptor type) from two families, namely: arylene bisimide derivatives containing triarylamine (4 compounds) or alkoxyphenyl (3 compounds) N-substituents and dithiophene derivatives with central electron-acceptor unit consisting of thiadiazole (7 compounds) or tetrazine (2 compounds) ring. It was expected that some of the investigated semiconductors exhibit n-type conductivity or very attractive ambipolar behavior. The studies included supramolecular organizations in both: 2D monolayers deposited on HOPG and in various 3D systems (thin layers on different substrates, single crystals and powders).

For each type of semiconductor a series of derivatives differing by important elements of molecular structure was comparably analyzed. This enabled to distinguish and clearly determine influence of certain structural features (extension of the conjugated unit, type, location and size of terminal substituents) as well as of presence of the substrate on self-organization of these compounds. In addition, comparison of obtained information with literature data concerning electrical properties of thin layers made possible for arylene bisimides to extend discussion on the influence of supramolecular organization on efficiency and type of electrical conductivity.

In this summary the postulated conclusions are listed in the form of three independent parts each concerning one type of the investigated semiconductors.

1. Arylene bisimides functionalized with triarylamine

1.1. Microscopic observations indicate that 2D organization of this kind of semiconductors on HOPG substrate is governed by coexistence and competition between two kinds of intermolecular interactions, namely: **(i)** direct forces between planar conjugated cores (arylene units) of neighboring molecules leading them to stack, and **(ii)** interactions between non-planar triphenylamine substituents. The latter can be treated as a factor which hinder interaction of aromatic cores, and as a consequence, supramolecular ordering. Hence, an increase of the size of conjugated backbone changes the balance between these two forces and leads to evolution of 2D molecular organization. It evolves from fully amorphous films, characteristic for pure triphenylamines and substituted derivative with smaller core (benzene, **S1**), via ordered organization with well-defined rhomboidal unit cell (for naphthalene derivative, **S2**) resulting from balance between both interactions comparable in strength, up to strong tendency of molecules to form one-dimensional clusters (for perylene derivative, **S3**). Consequently, the largest **S3** derivatives are stacked in the solution and adsorbed in the form of pre-organized clusters.

1.2. STM experiment involving tip polarization change during scanning of a single image allowed to distinguish, in a single molecule, parts of different electronic affinity. That experiment confirmed theoretical DFT calculations.

1.3. Similarly to the case of monolayers, thin layers of smallest derivative (**S1**) were found to be completely amorphous. This conclusion fits well with literature findings which indicate that thin films of molecules in which triphenylamine moieties are dominant are known to be glass-like, amorphous. The weak signals corresponding to molecular ordering were detectable in selected films of larger derivatives (**S2** and **S3**). Moreover, results indicate that organization of these molecules depends on the preparation conditions.

1.4. Combined STM and XRD studies acknowledged polymorphism of the investigated molecules in this series. The derivatives which exhibit ordering in monolayers (**S2** and S**3)** hardly organize in thin films and vice-versa (**S1**). In the case of derivatives which

exhibit some trace of ordering in thin films their powder organizations were different (surprisingly, the smaller intermolecular separations were observed in films then in powders).

1.5. HOMO and LUMO levels delivered from electrochemical measurements and DFT calculations indicate that semiconductors from this series (**S1**-**S3**) can be considered as materials capable for conductivity by both holes (p-type) and electrons (n-type). The lack of ambipolar behavior of these derivatives is directly related to their supramolecular organization. The presence of three-dimensional triphenylamine N-substituents prevents organization of molecules in the layers which selectively hinders electron mobility. As a consequence the formed layers exhibit holes conductivity (p-type) via triarylamine substituents which is less dependent on molecular organization. This example clearly shows how important is the supramolecular organization to the type of conductivity of organic electroactive layers.

1.6. Comparison of two derivatives with symmetrical (**S2**) and asymmetrical (**As2**) distribution of triarylamine substituents provides information about influence of molecular symmetry on supramolecular organization. Corresponding self-assemblies are significantly different for both molecules. The monolayer of asymmetric derivative (**As2**) is much denser than observed for symmetrical one (**S2**). Moreover the molecular orders are characterized by different symmetry: rectangular and hexagonal, respectively. The asymmetrical derivative also exhibits much stronger tendency to self-organize in 3D systems (powder and thin films) in comparison to symmetrical analogue.

1.7. Although both compounds (**S2**, **As2**) are spectroscopically similar and are characterized by almost identical electrochemical behavior, only asymmetrical molecule exhibits ambipolar properties in field effect transistors (symmetrical one is p-type semiconductor). This is a further confirmation that a wider extent of supramolecular ordering in layers of such donor-acceptor molecules is essential for obtaining ambipolar behavior.

2. Arylene bisimides functionalized with alkoxyphenyl N-substituents

2.1. All three semiconductors studied in this series (**NBI-4n-OBuPh**, **NBI-4n-OHexPh**, **NBI-4n-OOcPh**) exhibit a strong tendency to create organized layers. On all used substrates these semiconductors are oriented more or less perpendicular to the substrate plane. This molecular preference is probably the reason why these semiconductors do not form in gas (air) atmosphere monolayers on HOPG of flat lying molecules.

2.2. 3D supramolecular organization of the molecules becomes more extended with increasing chain length. As is expected, the periodicity in layers increases with alkyl chain length. Moreover, this dependence is observed in detail in single crystals in which molecular organization evolves with the substituent size from herringbone type characterized by two molecular orientations to regular organization with one exactly the same molecular arrangement.

2.3. The molecular packing in thin layers exhibits some similarities to the organizations in single crystals. However, comparison shows difference in periodicities in both organizations. Interesting effect of film thickness was noted for derivative with shortest substituent (**NBI-4n-OHePh**). For this semiconductor, a second phase characterized by higher molecular tilt is observed in films thicker than 50 nm.

2.4. Strong tendency of these naphthalene derivatives to organize in 3D systems may suggests good n-type conductivity of the formed layers. This prediction was confirmed in literature. As have been reported, the OFETs fabricated with these semiconductors exhibit good electrical transport parameters even when they operate unprotected in air. The best charge carriers mobility and the highest ON/OFF ratio was obtained for transistor with active layer of **NBI-4n-OOcPh** i.e. the largest molecule which exhibits highest tendency for regular organization.

3. Thiophene based donor-acceptor-donor derivatives

3.1. Studies of thiophene-based derivatives of donor-acceptor-donor type indicate that supramolecular organization of such complex in electronic structure molecules is a hard to predict process which has to consider coexistence and competition between mutual interactions between segments of neighboring molecules of different electron affinity.

3.2. Comparison of results obtained for analogous derivatives differing only in acceptor unit: thiadiazole (**T2**, **T3**) or tetrazine (**TT2**, **TT3**) evidently confirmed important role of this structural segment of the molecule on the type of supramolecular organization. Two different structural situations in monolayers were found for the derivatives with these two acceptor units. Introduction of thiadiazole ring into a thiophene oligomer lead to unexpected increase of the intermolecular stacking distance. Observed 2D organizations were characterized by ordered cavities of nanometric size between each pair of neighboring molecules. This is a direct effect of the relative location in the layer of the thiadiazole acceptor groups and their mutual repulsive acceptor-acceptor interaction. Significantly different behavior was noted for the corresponding derivative with stronger acceptor – tetrazine. Due to stronger and dominating electrostatic interactions an intermolecular shift is additionally generated in the ordered monolayers. As a consequence tetrazine groups face in the monolayer thiophene rings of the neighboring molecule. Monolayers of tetrazine derivatives are therefore unexpectedly much more densely packed.

3.3. Position of alkyl substituents in this kind of molecules is a next important factor influencing molecular self-assembly. A detailed study suggests that important factor influencing supramolecular organization of investigated DAD semiconductors is molecular linearity (the presence, or its absence, of steric hindrance caused by substituents in β position). The molecules can be divided into two classes. In the case of linear thiadiazole-thiophene derivatives (nonsubstituted **T1** and α-substituted **T4**) lamella-type arrangement occurs in a direction perpendicular to the substrate plane (in powder grains as well as in thin films). Moreover, those two molecules form powders characterized by unusual, preferential orientation of powder grains observed even in microscopic scale. As a consequence of this strong tendency of organization the ordered

monolayers of flat lying molecules had not been observed for these semiconductors. The second class concerns non-linear derivatives (**T2**, **T3** and **T5)**. They formed typical 3D crystals in powders and oriented layers in thin films. Only **T2** and **T3** organize in both: 2D and 3D systems. Very different regular (**T2**) or herringbone-type (**T3**) monolayer organizations have been noted. This effect is not such pronounced in monolayers of tetrazine-thiophene derivatives due to occurred in this case much stronger and dominant interactions between molecular cores. Self-assembly patterns of **T5** proved that **(i)** steric hindrance induced by alkyl substituents in β position causes the lack of macroscopic organization of powder grains and **(ii)** 2D formation of the monolayers is not only governed by presence of substituent in β position (although it is a necessary condition), but also substituent in α position prevents this organization.

3.4. All investigated thiadiazole-thiophene compounds organize in 3D systems. They form powder crystallites and lamella-type films with preferential orientation of molecules perpendicular to the substrate plane. Intercellular distances derived from 3D crystals turned out to be shorter than the corresponding separation in films (for all five compounds) and significantly shorter, then in 2D unit cell (as was stated above ordered monolayers were possible to obtain only for β substituted compounds). Two different types of mutual interactions between alkyl substituents have been distinguished depending on molecular structure. Because of a particular periodicity in powders and films, most likely behavior of alkyl chains in solid state is their mutual intedigitation (for **T2**, **T4** and **T5)**. This situation is different for **T3** derivative, for which a lack of intedigitation is postulated. Such conclusion is supported by a single crystal measurements and by 2D studies of **T2** and **T3** monolayers on HOPG. In the cases of monolayers a different behavior of alkyl substituents in herringbone and regular structures is noted. In the herringbone organization these substituents mutually interacts however they do not interdigitate. Contrary, in regular structure they are oriented and mutually interdigitated in two directions. The lack of interdigitation of alkyl chains was proved to be characteristic in both 2D and 3D systems only for thiadiazole-thiophene derivative functionalized in β inner position (**T3**). However, it must be pointed out, that alkyl substituents of this molecule take different arrangement in both systems. As was experimentally confirmed by measurements of single crystals, contrary to the monolayers, they do not lie in the same plane as molecular backbones. The clearly

observed polymorphism shows in this case how the presence of the substrate restrain the molecules in the 2D monolayer to align the alkyl groups parallel to the backbone plane

3.5. Careful analysis of supramolecular assemblies of three thiadiazole-thiophene derivatives substituted in inner β position by alkyl chains of different length allowed to distinguish effects of two competitive interactions influencing final organization, that is **(i)** repulsive interactions between thiadiazole acceptor parts of conjugated cores and **(ii)** attractive interactions between alkyl substituents. In principle, the strength of the first interactions do not change in a series of compounds consisting substituents of different length. However, due to location of these substituents in β inner position and their characteristic arrangements in the monolayer (i.e. perpendicular to the long axis of the molecule) the increase of substituent length enhances both: the strength of interactions between substituents and the separation between the molecular backbones (in this way the latter one indirectly affects also the effective strength of the repulsive forces between acceptor parts of neighboring molecules in the layer). As chains are forced to be in the same plane as molecular backbones in 2D system, the microscopic examination of monolayers allowed to observe supramolecular effect of the competition between both interactions. The interesting conclusion concerns **T3** derivative for which both interactions are comparable in strength and, as a consequence, the supramolecular organization is different from all its analogous (either substitution isomers or derivatives with alkyl substituents of different length). This derivative develops herringbone packing in monolayers. In monolayers, contrary to all others, the molecules does not lie flat on the substrate surface but rather adopts edge-on position (and form "corrugated iron" structure). These conclusions were supported also by 3D diffraction measurements of powders and films of this series of thiadiazole-thiophene derivatives.

3.6. Finally, no effect of the substrate on 3D organization was observed for the whole family of investigated compounds. The change of solvent (or even deposition method for **T3**) had no apparent effect also on their 2D organization on HOPG. Deposition method influences only the film thickness, not molecular organization in the films. Only **T3** showed subtle solvent organization dependence in 3D thin film.

6. References

1. Organic Electronics for a Better Tomorrow: Innovation, Accessibility, Sustainability A White Paper from the Chemical Sciences and Society Summit (CS3) San Francisco, California, United States September 2012
2. H. Akamatu, H. Inokucii, Y. Matsunaga; *Bulletin of the Chemical Society of Japan*, **1956,** *29, (2)*, 213-218
3. H. Shirakawa, E.J. Louis, A.G. MacDiarmid, C.K. Chiang, A.J. Heeger, *J Chem Soc Chem Comm*, **1977**, 579-580,
4. *The Nobel Prize in Chemistry, 2000: advanced informations*
5. P.Bujak, I. Kulszewicz-Bajer, M. Zagorska, V. Maurel, I. Wielgus , A. Pron, *Chem. Soc. Rev.*, **2013**, *42*, 8895-8999
6. L. Maggini, D. Bonifazi, Chem. *Soc. Rev.*, **2012, 41,** 211–241
7. S. H. Kim, K. Hong, W. Xie, K. H. Lee, S. P. Zhang, T. P. Lodge , C. D. Frisbie, *Adv. Mater.*, **2013,** *25*, 1822-1846.
8. M. C. Gather, A. Kohnen, K. Meerholz, *Adv. Mater.*, **2011,** ***23 (2)***, *233*-248
9. S. R. Cowan, N. Baneji, W. L. Leong, A. J. Heeger, *Adv. Funct. Mater.*, **2012*, 22 (6),*** 1116-1128
10. P. Lin, F. Yan, *Adv. Mater.*, **2012,** *24*, 34-51
11. R. D. McCullough, R.D. Lowe, *J.Chem. Soc.Chem Commun.*, **1992**,*1*, 70-72
12. H. Sirringhaus, P.J. Brown, R.H. Friend, M.M. Nielsen, K. Bechgard, B.M. Langeveld-Voss, A.J.H. Spiering, R.A.J. Jansen, E.W. Meijer, P. Herwig, D.M. Leeuw *Nature*, **1999**, *401*, 685-688
13. R.J. Kline, M.D. McGhee, E.N. Kadnikova, J. Liu, J.M. Frechet, *Adv. Mater*, **2003**, *15*, 1519–1522
14. R.J. Kline, M.D. McGhee, E.N. Kadnikova, J. Liu, J.M. Frechet, M.F. Toney, *Macromolecules* ,**2005**, *38*, 3312–3319
15. A. Zen, J. Pflaum, S. Hirshmann, W. Zhuang, F. Jaiser, U. Asawapirom, J.P. Rabe, U. Sherf, D. Neher, *Adv. Funct. Mater* ,**2004**, *14*, 757–764
16. G.M. Wang, J. Swensen, D. Moses, A.J. Heger, *J. App. Phys.*, **2003**, *93*, 6137–6141
17. G.R. Hutchinson, M.A. Ratner, T.J Marks, *J. Am. Chem. Soc.*,**2005**, *127*, 2339–2350
18. H. Ishakawa, X. Xu, A. Kobayashi, M. Satoh, M. Suzuki, E. Hasegaa, *J. Phys. D: Appl. Phys.*,**1992**, *25*, 897–900
19. T. Jaroch, M. Knor, R. Nowakowski, M. Zagorska, A. Proń, *Phys. Chem. Chem. Phys*., **2008**, *10*, 6182-6189
20. P. Moreno-Gracia, M. Gulcur, D. Manrique, T. Pope, W. Hong, V. Kaliginedi, C. Huang, A.S. Batasanov, M.R. Bryce, C. Lambert, T. Wandalowski *J.Am.Chem. Soc.*, **2013**, *135*, 12228-12240
21. O.D. Jurchescu, J. Baas, *Applied Physics Letters*, **2004**, *84*, 3061-3063

22. Y. Yuan, G. Giri, A. L. Ayzner, A. P. Zoombelt, S. C. Mannsfeld, J. Chen, D. Nordlund, M. F. Toney,J. Huang, Z. Bao, *Nat. Commun.*, **2014**, *5*, 3005, 1-9
23. A. Proń, P. Gawryś, M. Zagórska, D. Djurado, R. Demadrille**,** *Chem. Soc. Rev.* **2010**, *39*, 2577-3632
24. Y.J. Cheng, S.H. Yang, C.S. Hsu, *Chem. Rev.*, **2009**, *109*, 586-5923
25. H. Wu, L. Ying, W. Yang, Y. Cao, *Chem. Soc. Rev.*, **2009**, *38*, 3391-3400
26. R.H. Hadfield, *Nat. Photon.*, **2009**, *3*, 696-705
27. A.A. Argun, P.H. Aubert, B.C. Thompson, I. Schwendeman, C.L. Gaupp, J. Hwang, N.J. Pinto, D.B. Tanner, A.G. MacDiarmid, J.R. Reynolds, *Chem. Mater.*, **2004**, *16*, 4401-4412
28. S.W. Thomas III, G.D. Joly, T.M. Swager, *Chem. Rev.*, **2007**, *107*, 1339-1386
29. D.E. Tallman, G.M. Spinks, A.J. Dominis, G.G. Wallace, *J. Solid State Electrochem.* **2002**, *6*, 73-84
30. G.M. Spinks, A.J. Dominis, G.G. Wallace, D.E. Tallman, *J. Solid State Electrochem.* **2002**, *6*, 85-100
31. B. Gangadasu, S. Palaniappan, V.J. Rao, *Synlett*, **2004**, *7*, 1285-1287
32. D. Di Pietro, Fazzi, T.B. Kehoe, H. Sirringhaus. *J Am Chem Soc.* **2012**, *134(36)*, 14877-14889
33. H. T. Nicolai, M. Kuik, G. A. H. Wetzelaer, B. de Boer, C. Campbell, C. Risko, J. L. Brédas & P. W. M. Blom *Nature Materials*, **2012**, *11*, 882–887
34. B. A. Jones, A. Facchetti, M. R. Wasielewski, T. J. Marks *J. Am. Chem. Soc.*, ***2007***, *129*, *15259-15278*
35. A. Pron, P. Rannou *Prog. Polym. Sci.* **2002**, *27*, 135-190
36. R. Schmidt, J. Oh, Y. Sun, M. Deppisch, A. Krause, K. Radacki, H. Braunschweig, M. Könemann, P. Erk, Z. Bao, F. Würthner, *J. Am. Chem. Soc*., **2009**, *131*, 6215-6228
37. H. E. Katz , A. J. Lovinger , J. Johnson , C. Kloc , T. Siegrist , W. Li ,Y.-Y. Lin , A. Dodabalapur , *Natur,e* **2000** , *404* , 478-481
38. J. G. Laquindanum , H. E. Katz , A. Dodabalapur , A. J. Lovinger, *J. Am. Chem. Soc.* **1996** , *118* , 11331-1132
39. S. Ando, R. Murakami, J. Nishida, H. Tada, Y. Inoue, S. Tokito, Y. Yamashita, J. Am. Chem. Soc., **2005**, *127*, 14996-14997
40. M. Yoon, S. A. DiBenedetto, A. Facchetti, T. J. Marks, J. Am. Chem. Soc., **2005**, *127*, 1348-1349
41. A. Proń, R. R. Reghu, R. Rybakiewicz, H. Cebulski, D. Djurado, J.H. Grazulevicius, M.Zagórska, I. Kulszewicz-Bajer, J.M. Verhilac *J. Phys. Chem. C*, **2011**, *115 (30)*, 15008–15017
42. R. Dabirian, V. Palermo, A. Liscio, E. Schwartz, M.B.J. Otten, C.E. Finlayson, E. Treossi, R.H. Friend, G. Calestani, K. Müllen, R.J.M. Nolte, A. E. Rowan, P. Samori *J. Am. Chem. Soc.* **2009**, *131*, 7055–7063
43. N.S. Sariciftci, Z.L. Smilowitz, A.J. Heeger, F. Wudl *Science* **1992**, *258*, 1474–1476.
44. J.H. Burroughes, D.D. Bradley, A.R. Brown, R.N. Marks, K. MacKay, R.H. Friend, P.L. Burns, A.B. Holmes *Nature* **1990**,*347*, 539–541.
45. Y. Wu, P. Liu, S. Gardner, B.S. Ong, *Chem. Mater*., **2005** , *17*, 221-223
46. B. S. Ong, Y. L. Wu, P. Liu, S. Gardner, *J. Am. Chem. Soc*, **2004**, *126*, 3378-3379
47. H. Xu, I. Jun, J. Mai, T. Xiao, X. Lu, N. Zhao *Phys.Chem.C*, **2014**, *118*, 5600−5605
48. T.A. Chen, X.M. Wu, R.D. Rieke, *J. Am. Chem. Soc*.,**1995**, *117*, 233–244

49. Y. Kim, S. Cook, S. Tuladhar, S.A. Choulis, J. Nelson, J.R. Durrant, D.D. Bradley, M. Giles, I. McCullough, C.S. Ha, M. Ree, M. *Nat. Mater.*, **2006**, *5*, 197-203
50. M. M. Durban, P. D. Kazarinoff, C. K. Luscombe, *Macromolecules*, **2010**, *43*, 6348-6352
51. R. Schmidt , J. H. Oh , Y. S. Sun , M. Deppisch , A.-M. Krause , K. Radacki , H. Braunschweig , M. Könemann , P. Erk , Z. Bao , F. Würthner , *J. Am. Chem. Soc.* **2009** , *131* , 6215-6228
52. C. Qing, Z. Xu, C. Ting, W. Dong; Q. Hua-Lei, W. Zhao-Hui, W. Li-Jun *Surface Science*, **2010,** *604*, 2078–2083
53. W.H. Lee, J.A. Lim, D.H. Kim, J.H. Cho, Y.Jang, Y. Kim, J.I. Ham, K. Cho, *Adv. Funct. Mater*. **2008**, *18*, 560-565
54. W. Junhua, L. Yibao, M. Zhun, L. Tingcheng, H. Wei, H. Chin. *J. Chem.* **2010**, 28, 1821−1828
55. M.M. Payne, S.R. Parkin, J.E. Anthony, C.C. Kuo, T.N. Jackson, *J. Am. Chem. Soc.* **2005**, 127, 4986-4987
56. Y. Wang, Q. Huang, H. Li, Z. Liu *Asian J. Org. Chem.* **2014**, *3*, 134 – 139
57. M. Surin, P. Sonar, A.C. Grimsdale, K. Mullen, S. De Feyter, S. Habuchi, S. Sarzi, M. Van der Auweraer, F.C. De Schryver, M. Cavallini, J.F. Moulin, F. Biscarini, C. Femoni, R. Lazzaroni, P,Leclere *J. Mater. Chem*., **2007**, *17*, 728–735
58. Q. Shuai, H. T. Black, A. Dadvand, D. F. Perepichka *J. Mater. Chem. C*, **2014**, *2*, 3972–3979
59. S. Tatemichi , M. Ichikawa , T. Koyama , Y. Taniguchi , *Appl. Phys. Lett.*, **2006**, *89*, 112108 - 112111
60. B. A. Jones , A. Facchetti , M. R. Wasielewski , T. J. Marks , *Adv. Funct.Mater.* **2008**, *18*, 1329-1339
61. J. Xue, S.R. Forrest, *Appl. Phys. Lett.* **2001**, *79*, 3714-3716
62. A.L. Briseno, S.C. Mannsfeld, C. Reese, J.M. Hancock, Y. Xiong, S.A. Jenekhe, Z. Bao, Y. Xia, *Nano Lett.*, **2007**, *7*, 2847–2853
63. V. Palermo, A. Liscio, D. Gentilini, F. Nolde, K. Mullen, P. Samori. *Small*, **2006**, *3*, 161–167
64. G. De Luca, A. Liscio, P. Maccagnani, F. Nolde, V. Palermo, K. Mullen, P. Samori, *Adv. Funct. Mat.*, **2007**, *17*, 3791–3798
65. K. Balakrishnan, A. Datar, T. Naddo, J. Huang, R. Oitker, M. Ye, J. Zhao, L. Zang *J. Am. Chem. Soc.* **2006**, *128*, 7390-7398
66. M. Brinkmann, E. Gonthier, S. Bogen, K. Tremel, S. Ludwigs, M. Hufnagel, M. Sommer, *ACS Nano*, **2012**, *6*, 10319-10326
67. C. Tanase, P.W.M. Blom, D.M. De Leeuw, E.J. Meijer, *Phys. Status Solidi A* **2004**, *201***,** 1236–1245
68. R. J. Kline, M. D. McGehee, M. F. Toney, *Nature Materials*, **2006**, 5, 222 - 228
69. R. Nowakowski, C. Seidel, H. Fuchs, *Phys. Rev. B*, **2001**, *63*, 195418 (1-10)
70. R. Nowakowski C. Seidel, H. Fuchs *Surface Science* , **2004**,5*62*, 53–64
71. M. Knor, R. Nowakowski, A. Maranda-Niedbała, P. Gawryś, M. Zagórska, A. Proń, *Surface. Science*, **2013**, 607, 61–67
72. J. Rivnay, R. Steyrleuthner, L. H. Jimison, A. Casadei, Z. Chen, M. F. Toney, A. Facchetti, D. Neher, A. Salleo, *Macromolecules*, **2011**, 44, 5246-5255

73. B. J. Murray, J. E. Kaeding, W. T. Gruenbaum, P. M. Borsenberger, *Jpn. J. Appl. Phys.*, **1996**, *35*, 5384-*5388*
74. S. Y. Lee, T. Yasuda, H. Nomura, C. Adachi *Appl. Phys. Lett.*, **2012**, *101*, 093306 (1-4)
75. Y. T. Tao, Q. Wang, Y. Shang, C. L. Yang, L. Ao, J. G. Qin, D. G. Ma, Z. G. Shuai, *Chem. Commun.* **2009**, 77-79
76. Y. T. Tao , Q. Wang , L. Ao, C. Zhong, J. G. Qin , C. L. Yang , D. G. Ma , *J. Mater. Chem.* **2010** , *20* , 1759-1765
77. Y. T. Tao , Q. Wang , C. L. Yang , C. Zhong , J. G. Qin , D. G. Ma , *Adv.Funct Mater.* **2010** , *20*, 2923-2928
78. J. Kim, K.J. Baeg, D. Khim, D.T. James, J.S. Kim, B. Lim, J.M. Yun, H.G. Jeong, P.S.K. Amegadze, Y.Y. Noh, D.Y. Kim, *Chem.Mater.***2013**, *25*, 1572−1583
79. J. Qu, N.G. Pschirer, D. Liu, A. Stefan, F.C. De Schryver, K. Mullen, *Chem. Eur. J.*, **2004**, *10*, 528-537
80. J. Feng, Y. Zhang, C. Zhao, R. Li, W. Xu, X. Li, J. Jiang, *Chem. Eur. J.*, **2008**, *14*, 7000-7010
81. C. Thalacker, C. Roger, F. Wurthner, *J. Org. Chem.*, **2006**, *71*, 8098-8105
82. M. J. Ahrens, M.J. Tauber, M.R. Wasielewski, *J. Org. Chem.* **2006**, *71*, 2107-2114
83. Z. An, S.A. Odom, R.F. Kelley, C. Huang, X. Zhang, S. Barlow, L.A. Padilha, J. Fu, S. Webster, D.J. Hagan, E.W. Van Stryland, M.R. Wasielewski, S.R. Marder, *J. Phys. Chem. A* **2009**, *113*, 5585-5593
84. H. E. Katz, A. J. Lovinger, J. Johnson, C. Kloc, T. Siegrist,W. Li, Y. Y. Lin, A. Dodabalapur, *Nature*, **2000**, *404*, 478-481
85. H. E. Katz, J. Johnson, A. J. Lovinger, W. J. Li, *J. Am. Chem.Soc.*, **2000**, *122*, 7787-7792
86. M. M. Shi, H.-Z. Chen, J.Z. Sun, J. Ye, M. Wang, *Chem. Commun.*, **2003**, 1710-1711
87. H. Z. Chen, M. M. Ling, X. Mo, M. M. Shi, M. Wang, Z. Bao, *Chem. Mater.*, **2007**, *19*, 816-824
88. R. Rybakiewicz, D. Djurado, H. Cybulski, E. Dobrzynska, I. Kulszewicz-Bajer, D. Boudinet, J.-M. Verilhac, M. Zagorska, A. Pron, *Synth. Met.*, **2011**, *161*, 1600-1610
89. R. Rybakiewicz, J. Zapala, D. Djurado, R. Nowakowski,P. Toman, J. Poeger, J.-M. Verilhac, M. Zagorska, A. Pron, *Phys. Chem. Chem. Phys.*, **2013**, *15*, 1578-1587
90. Z. Chen, A. Lohr, C. R. Saha-Moller, F. Wurthner, *Chem. Soc. Rev.*, **2009**, *38*, 564-584
91. L. Heinz, J. Wolfgang, Angew. *Chem. Int. Ed.* **1998**, *37*, 3340-3350
92. W. S. Horne, N. Ashkenasy, M. R.Ghadiri, *Chem.Eur. J.*, **2005**, *11*, 1137-1144
93. S. K. Lee, Y. Zu, A. Herrmann, Y. Geerts, K. Mullen, A. J. Bard, *J. Am. Chem. Soc.*, **1999**, *121*, 3513-3520.
94. L. Schmidt-Mende, A. Fechtenkotter, K. Mullen, E. Moons, R.H. Friend, J.D. MacKenzie, *Science*, **2001**, *293*, 1119-1120
95. H. Wang, T.E. Kaiser, S. Uernura, F. Wurthner, *Chem. Commun.*, **2008,** 1181-1183
96. T.E. Kaiser, V. Stepanenko, F. Wurthner, *J. Am. Chem. Soc.* 131, **2009,** 6719-6732
97. H.L. Qian, C.M. Liu, Z.H. Wang, D.B. Zhu, *Chem. Commun.*, **2006**, 4587-4589
98. J. E. Anthony, A. Facchetti, M. Heeney, S. R. Marder, X. Zhan, *Adv. Mater.*, **2010**, *22*, 3876-3892
99. N. Sokolov, M. E. Roberts, O. B. Johnson, Y. Cao, Z. Bao,*Adv. Mater.*, **2010**, *22*, 2349-2353

100. X. Zhan, A. Facchetti, S. Barlow, T. J. Marks, M. A. Ratner, M. R. Wasielewski, *Adv. Mater.*, **2011**, *23*, 268-284
101. F. Wurthner, M. Stolte, *Chem. Commun.*, **2011**, *47*, 5109-5115
102. C. Huang, S. Barlow, S. R. Marder, *J. Org. Chem.*, **2011**, *76*, 2386-2407
103. Y. Kim, J. Hong, J. Hak Oh, C. Yang, Chem. Mater., **2013**, *25*, 3251-5259
104. W. Gu, W. Hu, J. Yao, H. Fu, Chem. Mater., **2013**, *25*, 2178-2183
105. T. Lana-Villarreal, J. M. Campina, N. Guijarro, R. Ǵomez, *Phys. Chem. Chem. Phys.*, **2011**, *13*, 4013–4021
106. C. Quinton, V. Alain-Rizzo, C. Dumas-Verdes, F. Miomandre,G. Clavier, P. Audebert, *RSC Adv*., **2014**,*4*, 34332-34342
107. A.R. Murphy, J.M Frechet, *Chem. Rev.* **2007**, *107*, 1066−1096
108. S. Allard, M. Forster, B. Souharce, H. Thiem, U. Scherf, *Angew. Chem., Int. Ed.* **2008**, *47*, 4070−4098
109. A. Mishra, C.Q. Ma, P. Baeuerle, *Chem. Rev.* **2009**, *109*, 1141−1176
110. T. Otsubo, Y. Aso, K. Takimiya, *J. Mater. Chem.* **2002**, *12*, 2565−2575
111. J. Roncali, *Acc. Chem. Res.* **2009**, *42*, 1719− 1730
112. X. Sun, Y. Zhou, W. Wu, Y. Liu, W. Tian, G. Yu, W. Qiu, S. Chen, D. Zhu, D *J. Phys. Chem. B* **2006**, *110*, 7702−7707.
113. T. Noda, H. Ogawa, N. Noma, Y. Shirota, J. Mater. Chem. **1999**, 9, 2177−2181
114. M. Mazzeo, V. Vitale, F. Della Sala, M. Anni, G. Barbarella, L.Favaretto, G. Sotgiu, R. Cingolani, G.Gigli, Adv. Mater. **2005**, 17, 34−39
115. D. Fichou, S. Delysse, J.M. Nunzi, *Adv. Mater.* **1997**, *9*, 1178−1181
116. M. Nagawa, R. Hibino, S. Hotta, H. Yanagi, M. Ichikawa, T. Koyama, Y.Taniguchi, *Appl. Phys. Lett.* **2002**, *80*, 544−546
117. D. Pisignano, M. Anni, G. Gigli, R. Cingolani, M. Zavelani-Rossi, G. Lanzani, G. Barbarella, L. Facaretto *Appl. Phys. Lett.* **2002**, *81*, 3534−3536.
118. Y. Kim, J. Do, E. Kim, G. Clavier, L. Galmiche, L. Audebert, *J. Electroanal. Chem.* **2009**, *632*, 201−205.
119. M. Lebrini, M. Lagrenee, M. Traisnel, L. Gengembre, H. Vezin, F. Bentiss, *Appl. Surf. Sci.* **2007**, *253*, 9267−9276.
120. M. Lebrini, M. Lagrenee, H. Vezin, L. Gengembre, F. Bentiss, *Corros. Sci.* **2005**, *47*, 485−505.
121. L. Burgi, M. Turbiez, R. Pfeiffer, F. Bienewald, H. Kirner, C.Winnewisser *Adv. Mater.* **2008**, *20*, 2217–2224.
122. A.S. Fisyuk, R. Demadrille, C. Querner, M. Zagorska, J.L. Bleuse, A. Pron, *New J. Chem.* **2005**, *29*, 707−713.
123. K. Ajay Kumar, G. Vasanth Kumar, N. Renuka *Int J PharmTech Res*, **2013**,*5(1)*,239-248
124. Y. Yamashita, K. On, M. Tomur, S. Tanak, *Tetrahedron*, **1997**, *53 (29)*, 10169-10178
125. S.M. Weinreb, R. Staib, *Tetrahedron*, **1982**, *38*, 3087-3128
126. D.L. Boger, *Tetrahedron* **1983**, *39*, 2869-2939
127. D.L. Boger,.*Chemtracts: Org. Chem*., **1996**, *9*, 149-189

128. W. Jinxia, W. Hailong, X. Shuping, X. Weiqing *J. Phys. Chem. A*, **2015**, *119* (8), 1303–1308
129. Z. Chen, V. Stepanenko, V. Dehm, P. Prins, L. D. A. Siebbeles, J. Seibt, P. Marquetand, V. Engel. F. Würthner *Chemistry - A European Journal*, **2007**, *13* (2), 436–449
130. F.Wurthner, C. Thalacker, S. Diele, C. Tschierske, *Chem. Eur. J.*,**2001**,*7*, 2245–2253
131. S. Yabin, D. Chong'an, Y. Xiaodi, L. Shouping, X. Wei, L.Yunqi, Y. Lianming, S. Zhigang, Z. Deqing, Z. Daoben *J. Am. Chem. Soc.*, **2006**, *128* (50), 15940–15941
132. U. Hisayuki, N. Daisuke, N. Hideyuki, S. Yasuhiko *J. Mater. Chem.*, **2002**,*12*, 2612-2619
133. U. Hisayuki, N. Daisuke, N. Hideyuki, S. Yasuhiko *Chem. Mater*. **2003**,*15*,4021-4027
134. L. Lien, H. Hui-Lin, C. Szu-Ying, Y. Tri-Rung *J. Phys. Chem. C*, **2008**, *112* (*5)* 1694–1699
135. J. Jung, K. Lee, Jia Sun, A. G. Andreou, H. E. Katz *Adv. Funct. Mater.***2010**, *20*, 2930–2944
136. J. Jun, S. Jia, L. Taegweon, A. Sarjeant, H. E. Katz *Chem. Mater.*, **2009**, *21* (1), 94–101
137. M. Ichikawa *Organic Electronics*, **2013**, *14* 516–522
138. Qi-Dai, F. Hong-Hua, X. Bin, Y. Jie, X. Hong, C. Fei-Peng, T. Wen-Jing, *Appl. Phys. Lett*. **2009**, *94*, 2011-2013
139. M.A. Muth, *J. Phys. Chem. C*, **2014**, *118*, 92−102
140. I. Tszydel, M. Kucinska, T. Marszalek, R. Rybakiewicz, A. Nosal, J. Jung, M. Gazicki-Lipman, C. Pitsalidis, C. Gravalidis, S. Logothetidis, M. Zagorska, J. Ulanski, *Adv. Funct. Mater.*, **2012**, *22*, 3840-3844
141. W. Zhang, J. Smith, R. Hamilton, M. Heeney, J. Kirkpatrick, K. Song, S.E. Watkins, T. Anthopoulos, I. McCulloch, *J. Am. Chem. Soc*., **2009**, 131, 10814-10815
142. T. Jaroch, R. Nowakowski, M. Zagórska, A. Proń, *JPCC*, **2010**, *14* (33), 13967-13974
143. K. Glockler, C. Seidel, A. Soukopp, M. Sokolowski, E. Umbach, M. Bohringer, R. Berndt, W.-D. Schneider, *Surf. Sci.*, **1998**, *405*, 1-20
144. Y. Kaneda, M. E. Stawasz, D. L. Sampson, B. A. Parkinson, *Langmuir*, **2001**, 17, 6185-6195
145. R. Rybakiewicz, I. Tszydel, J. Zapala, L. Skorka, D. Wamil, D. Djurado, J. Pécaut, J. Ulanski, M. Zagorska, A. Pron *RSC Adv.*, **2014**,*4*, 14089-14100
146. E. Kurach, K. Kotwica, J. Zapala, M. Knor, R. Nowakowski, D. Djurado, P. Toman, J. Pfleger, M. Zagorska, A. Pron J. *Phys. Chem. C*, **2013**, *117* (*29*), 15316–15326
147. F. van Bolhuis, H. Wynberg, E. E. Havinga, E. W. Meijer, E. G. J. Starring, *Synth. Met*. **1989**, *30*, 381 - 389
148. L. Antolini, G. Horowitz, F. Kouki, F. Garnier, *Adv. Mater.* **1998**, *10*, 382-385
149. G. Horowitz, B. Bachet, A. Yassar, P. Lang, F. Demanze, J. L. Fave, F. Garnier, Chem. Mater. **1995**, 7, 1337-1341
150. G. Barbarella, M. Zambianchi, A. Bongini, L. Antolini, *Adv. Mater.* **1994**, *6*, 561-564
151. S. Hotta, J. Waragai, *J. Mater. Chem.* **1991**, *1*, 835-842
152. P. A. Chaloner, S. R. Gunatunga, P. B. Hitchcock, *J. Chem. Soc. Perkin Trans.* **1997**, *2*, 1597-1604
153. J.H. Liao, M. Benz, E. LeGoff, M. G. Kanatzidis, *Adv. Mater.* **1994**, *6*, 135-138
154. K. Herrema, J. Wildeman, F. van Bolhuis, G. Hadziioannou, *Synth. Met.* **1993**, *60*, 239-248
155. R. Azumi, G. Gotz, P. Bauerle, *Synth. Met.* **1999**, *101*, 569-572.

156. P. Buerle, T. Fischer, B. Bidlingmeier, A. Stabel, J. P. Rabe, *Angew. Chem., Int. Ed. Engl.*, **1995**, *34*, 303-307

157. A. Stabel, J. P. Rabe, *Synth. Met.* **1994**, 67, 47-53.

158. N. Afsharimani, A. Minoia, C. Volcke, M. Surin, R. Lazzaroni, J.Balandier, C. Niebel, Y. H. Geerts, B. Nysten *J. Phys. Chem. C* **2013**, *117*, 21743−21751

159. T. Jaroch, R. Nowakowski, M. Zagórska *J. Phys. Chem. C,* **2010**, *114* (*33*) 13967-13974

160. T. Yokoyama, S. Kurata, S. Tanaka *J. Phys. Chem. C* **2008**, *112*, 12590−12593

161. G.C. McGonigal, R.H. Bernhardt, D.J. Thomson, *Appl. Phys. Lett.* **1990**, *57*, 28−30

162. J.P. Rabe, S. Buchholz, *Makromol. Chem., Macromol. Symp.* **1991**, *50*, 261−268

163. A. Wawkuschewski, H.J. Cantow, S.N. Magonov, *Langimur* **1993**, 9, 2778−2781

164. T. Kirschbaum, R. Azumi, E. Mena-Osteritz, P. Bäuerle, *New J. Chem.* 1999, *23*, 241−250

165. R. Azumi, G. Götz, T. Debaerdemaeker, P. Bäuerle, *Chem.Eur. J.* **2000**, *6*, 735−74

166. E. Kurach, D. Djurado, J. Rimarčik, A. Kornet, M. Wlostowski, V. Lukeš, J. Pécaut, M. Zagorska, A.Pron *Phys. Chem. Chem. Phys., **2011**,13,* 2690-2700

167. O. Guskova, E. Mena-Osteritz, E. Schillinger, P. G. Khalatur, P. Ba1uerle, A. R. Khokhlov, *J. Phys. Chem. C* **2007**, *111*, 7165-7174

168. H. Muller, J. Petersen, R. Strohmaier, B. Gompj, W. Eisenmenger, M. S. Vollmer, F. Effenberger *Adv. Mater.* **1996**,*8*, 733-737

169. Zapala, M. Knor, T. Jaroch, A. Maranda-Niedbala, E. Kurach, K. Kotwica, R. Nowakowski, M. Zagorska, A. Pron. *Langmuir.* **2013,** *29*(47), 14503-14511

170. T. Fukunaga, K. Harada, W. Takashima, K. Kaneto, *Jpn. J. Appl. Phys.* **1997**, *36*, 4466-4467

171. A. Soukopp, K. Glockler, P. Bauerle, M.Sokolowski, E. Umbach *Adv. Mater.* **1996**,8, 902-906

172. D.P.E. Smith, J.K.H. Horber, G. Binnig, H. Nejoh *Nature*, **1990**, *344*, 641−644

173. L. Gross, N. Moll, F. Mohn, A. Curioni, G. Meyer, F. Hanke, M. Persson *Phys. Rev. Lett.*, **2011**, *107*, 086101(1-4)